Sensor and Simulation Note

Note 177

May 1973

Application of the Singularity Expansion Method
to the Analysis of Impedance Loaded Linear Antennas

F. M. Tesche
The Dikewood Corporation
Albuquerque, New Mexico 87106

Abstract

This note extends the previous work done in the area of SEM analysis of
linear wire antennas and scatterers so as to include impedance loading of
the structure. In addition, the concept of a far-field natural mode is
introduced and related to the natural current modes. Four particular
antennas are analyzed, one being unloaded and the other three having
special forms of resistance loading. The current and far field modes,
natural frequencies and coupling coefficients are defined for each case,
and the step excited time domain radiated fields are presented.

Acknowledgement

I would like to thank the following people who at one time or another pro-
vided ideas and advice during the course of this research.

Table of Contents

I. Introduction

One type of EMP simulator consists of a linear antenna which is center fed by a pulse generator. In order to shape the waveform of the radiated electromagnetic pulse, it is possible to add some lossy material along the antenna to dampen out the oscillations in time which normally occur in transient excited perfectly conducting antennas. This note begins a study of this class of EMP simulators by the Singularity Expansion Method (SEM). This technique basically describes the radiating behavior of the antenna (loaded or unloaded) in terms of natural frequencies for the exterior boundary value problem and their corresponding residues. Once these quantities have been determined, the general transmitting and receiving problem for the linear wire in question can be easily constructed. This technique has been discussed and illustrated in Refs. 2, 3, 7, 11, 12, 13, 14, and 19.

Other investigators have considered the analysis of this class of EMP simulators. Merewether[15,16] has presented the integral equation solution for currents on an antenna having lumped resistive elements. Wu, King and Shen[18,22] have investigated the behavior of an antenna having a resistive load which varies inversely as the distance from the ends of the wire, by using an approximate integral equation analysis. Baum[1] and Wright and Prewitt[21] have all considered transmission line models for the loaded antenna and the loaded, infinitely long radiating antenna has been analyzed by Lee and Latham[4,5,6] among others.

The present note is, then, a continuation of the work begun by the above investigators. In Section II the formulation for impedance loaded linear antennas is discussed and the definitions of the natural frequencies, modes and coupling coefficients are reviewed in a format consistent with a previous note.[19] Section III deals with the far-field natural modes and how the construction of the time domain response of the radiated field is obtained.

4

As an example of this technique applied to radiating antennas, four cases are discussed at length: Section IV treats the unloaded radiating antenna, Section V deals with the uniformly loaded wire, Section VI discusses the linearly loaded wire, and the special loading proportional to $(h - |z|)^{-1}$ is investigated in Section VII.

As will be seen, this last class of loading is the most suitable for EMP simulation purposes, as the end reflections of the current on the wire are considerably reduced.

diameter d
radius a

z = h

Impedance Load of
Λ (z) ohms/L

L

Source of
V_o volts

z = -h
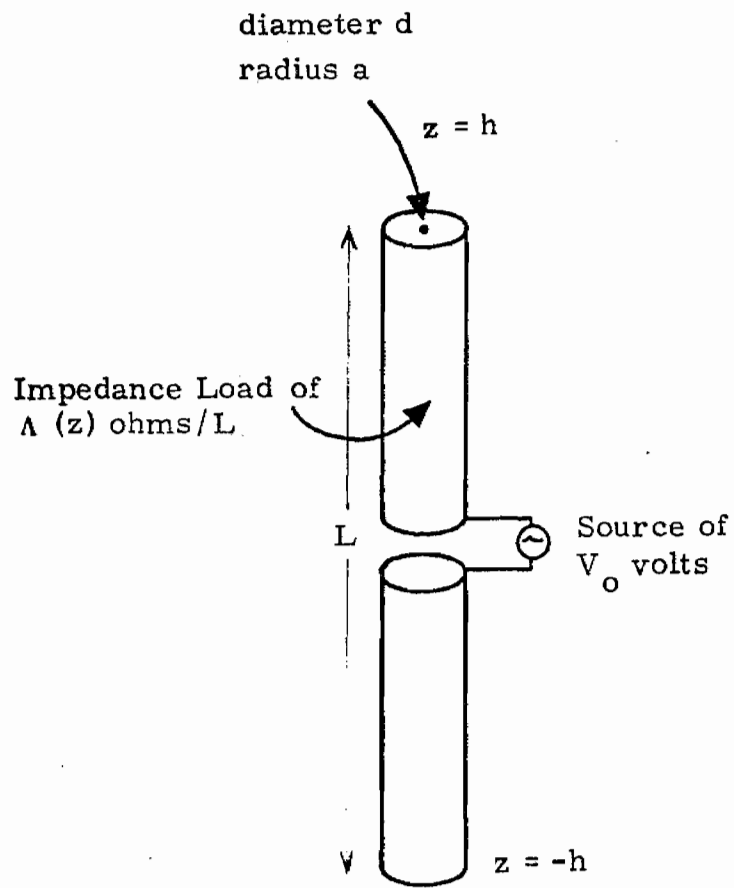
Figure 1. Linear impedance loaded EMP simulator.

II. Integral Equation for the Loaded Antenna

Consider a thin, linear antenna of length L = 2h and radius a (or diameter d) which is fed from a finite source gap located at the midpoint of the structure. It is assumed that the antenna is loaded by an impedance loading function Λ which is, in the general case, dependent upon both position and frequency. Figure 1 shows the geometry of this problem.

To understand the radiating properties of this antenna (for both transient and steady state signals) it is first necessary to determine the behavior of the currents on the wire which are excited by the voltage source on the antenna. Assuming that the wire is thin enough so that only the axial current need be considered, it is possible to find these currents by solving a Pocklington type integro-differential equation as described in Ref. (19). Using the complex frequency $s = j\omega + \sigma$ and assuming a temporal variation of e^{st}, the relation for the tangential component of the electric field scattered by the unknown wire current I is written as

$$s\epsilon_o E^{sca}(z, s) = \int_{-h}^{h} I(z', s) \left(\frac{d^2}{dz^2} - \frac{s^2}{c^2} \right) K(z, z'; s) \, dz' \tag{1}$$

The Kernel K is the exact kernel and is given by

$$K(z, z'; s) = \frac{1}{2\pi a} \int_0^{2\pi} \frac{e^{-sR/C}}{4\pi R} \, a \, d\phi \tag{2}$$

where $R = \left[(z-z')^2 + 4a^2 \sin^2(\phi/2) \right]^{1/2}$.

Using an impedance loading function, it is assumed that the total tangential electric field and the current on the wire surface are related by

$$E^{tot}(z, s) = \Lambda(z, s) I(z, s) \tag{3}$$

Noting that $E^{inc} + E^{sca} = E^{tot}$, with E^{inc} being the incident tangential electric field produced by the source gap, Eqs. (1) and (3) become

$$E^{inc}(z,s) = \Lambda(z,s)I(z,s) - \frac{1}{s\epsilon_o} \int_{-h}^{h} I(z',s)\left(\frac{d^2}{dz^2} - \frac{s^2}{c^2}\right)K(z,z';s)dz' \qquad (4)$$

It has been verified that the incident field produced by the source gap is, to a good degree of approximation, zero outside of the gap and equal to $V_o(s)/\Delta$ in the gap, where the parameter Δ denotes the size of the gap.

As pointed out by Baum,[3] the integral equation in (4) can have non-trivial solutions at certain complex frequencies, s_α, for $E^{inc} = 0$. If $E^{inc} \neq 0$, the solution then diverges. The current which exists for no forcing function at a singular point s_α, has been referred to as a natural current mode, and is a solution to the homogeneous version of Eq. (4) which has the form

$$\mathcal{L}_\alpha M_\alpha(z) = 0 \qquad (5)$$

where the operator $\mathcal{L}_\alpha$ is defined as

$$\mathcal{L}_\alpha( ) = \Lambda(z,s_\alpha)( ) - \frac{1}{s_\alpha \epsilon_o}\left(\frac{d^2}{dz^2} - \frac{s^2}{c^2}\right)\int_{-h}^{h} ( )K(z,z';s_\alpha)dz' . \qquad (6)$$

$M_\alpha(z)$ is the natural current mode which has an arbitrary magnitude. The natural mode M_α is, in general, a complex quantity. For convenience, it is possible to normalize M_α such that its peak value is purely real and has the value of unity. Hence, the magnitude of M_α will be chosen to be

8

$$\left(M_\alpha(z) \right)_{max} = 1 . \tag{7}$$

In a similar manner, a coupling vector $C_\alpha(z)$ can be defined from the adjoint operator $\pounds_\alpha^+$ as

$$\pounds_\alpha^+ C_\alpha(z) = 0 . \tag{8}$$

For the symmetric operator as obtained from the electric field integral equation formulation, the mode and coupling functions are identical,

$$C_\alpha(z) = M_\alpha(z) \tag{9}$$

where C_α has been normalized in the same fashion as M_α.

The solution for the current in Eq. (4) then takes on the form

$$I(z,s) = \sum_\alpha \beta_\alpha \frac{\eta_\alpha(s) M_\alpha(z)}{s - s_\alpha} \tag{10}$$

for assumed simple poles. The sum is over all poles in the complex s plane. The term η_α is the coupling coefficient and determines how much of each mode is excited by the incident or driving field. This coefficient has the form

$$\eta_\alpha(s) = \int_{-h}^{h} C_\alpha(z) E^{inc}(z,s) \, dz . \tag{11}$$

The factor β_α is a normalizing factor given by Baum as

$$\beta_\alpha = \left[\int_{-h}^{h} C_\alpha(z) \frac{d}{ds} \pounds_\alpha(M_\alpha(z)) \, dz \right]^{-1} \tag{12}$$

As mentioned by Baum, there is another representation for $I(z,s)$ which is of the form

$$I(z,s) = \sum_{\alpha} \beta_{\alpha} \frac{\eta_{\alpha}(s_{\alpha}) M_{\alpha}(z)}{s - s_{\alpha}} + F_e(z,s) \tag{13}$$

where η is no longer a function of s and F_e is an entire function of s. The entire function does not contribute to the time domain response through a pole contribution, but may give an early time contribution due to singularities at infinity. This remains to be verified numerically.

The time domain response of the current can be evaluated by performing the integral

$$I(z,t) = \frac{1}{2\pi j} \int_{\sigma_0 - j\infty}^{\sigma_0 + j\infty} I(z,s) e^{st} ds \tag{14}$$

or, by closing the integral at infinity, and using Cauchy's integral theorem,

$$I(z,t) = \sum_{\alpha} \beta_{\alpha} \eta_{\alpha}(s_{\alpha}) M_{\alpha}(z) e^{s_{\alpha} t} U(z,t) + \text{waveform singularity response.} \tag{15}$$

$U(z,t)$ is a Heaviside step function used to insure causality and is discussed later. Here, an additional term has been included to account for the possibility of the structure responding to a singularity in the incident waveform. For the step excited linear antenna, there is a waveform pole at $s_{\alpha} = 0$, but the current on the linear wire antenna does not respond to this particular pole, so this term can be omitted.

The numerical solution of Eq. (4) is obtained by first casting it into matrix form by using the method of moments, and then determining the natural resonances of the structure by searching for those frequencies (complex in general) for which a unique solution exists with no forcing function. The resulting matrix equation has the form

10

$$\left(\left[\overline{\overline{Z(s)}}\right] + \left[\overline{\overline{Z_L(s)}}\right]\right)\left[\overline{I(s)}\right] = \left[\overline{V(s)}\right] \tag{16}$$

with the matrix $\left[\overline{\overline{Z(s)}}\right]$ resulting from the last portion of Eq. (14) and $\left[\overline{\overline{Z_L}}\right]$ being a matrix depending on the parameter Λ. For a simple pulse expansion for the current, $\left[\overline{\overline{Z_L}}\right]$ is a diagonal matrix.

Denoting the sum of the matrices $\left[\overline{\overline{Z}}\right]$ and $\left[\overline{\overline{Z_L}}\right]$ as $\left[\overline{\overline{Z_T}}\right]$, Eq. (16) takes on the form

$$\left[\overline{\overline{Z_T(s)}}\right]\left[\overline{I(s)}\right] = \left[\overline{V(s)}\right] \tag{17}$$

and the analysis then proceeds exactly as in the case of the unloaded wire scatterer.[19] The natural frequencies are defined as those s_α such that

$$\det\left[\overline{\overline{Z_T(s_\alpha)}}\right] = 0 . \tag{18}$$

The natural current modes $\left[\overline{M_\alpha}\right]$ are the non-trivial solutions to

$$\left[\overline{\overline{Z_T(s_\alpha)}}\right]\left[\overline{M_\alpha}\right] = 0 , \tag{19}$$

and the coupling vector $\left[\overline{C_\alpha}\right]$ is the solution to the transpose equation

$$\left[\overline{\overline{Z_T(s_\alpha)}}\right]^T\left[\overline{C_\alpha}\right] = 0 . \tag{20}$$

For this integral equation, $\left[\overline{\overline{Z_T}}\right]$ is symmetric, so

$$\left[\overline{C_\alpha}\right] = \left[\overline{M_\alpha}\right] . \tag{21}$$

From these quantities, the frequency domain representation of the wire current is

$$\left[\overline{I(s)}\right] = \sum_\alpha \beta_\alpha \frac{\left[\overline{M_\alpha}\right]\left[\overline{C_\alpha}\right]^T}{(s - s_\alpha)} \left[\overline{V(s_\alpha)}\right] + \left[\overline{F_e(s)}\right] \tag{22}$$

where $\left[\overline{F_e(s)}\right]$ is the entire function of s.

Transforming to the time domain, the time dependent antenna current is given as

$$\left[\overline{i(t)}\right] = \sum_{poles} \beta_\alpha \left[\overline{M_\alpha}\right]\left[\overline{C_\alpha}\right]^T \left[\overline{\overline{U(t)}}\right]\left[\overline{V(s_\alpha)}\right] e^{s_\alpha t} + \begin{array}{l}\text{possible response} \\ \text{of antenna at pole} \\ \text{of V(s)}\end{array} \tag{23}$$

As explained in Ref. (19), the unit Heaviside matrix serves to enforce causality in the case of a scattering problem. In the antenna problem where a small source gap is turned on at t = 0 and there is no other incident field on the wire, it may be assumed that all of the contributions of the forcing vector $\left[\overline{V(s_\alpha)}\right]$ occur simultaneously, so that the Heaviside matrix is simply the identity matrix.

For a step function in time of magnitude V_o for the excitation voltage, the forcing vector has the form $\left[\overline{V(s)}\right] = \left[\overline{V_o}\right]/s$, where the vector $\left[\overline{V_o}\right]$ describes how the driving voltage is distributed over the antenna surface. For example, using a point-match solution of the integral equation (1) and with the voltage source in the jth cell or zone on the antenna, the n dimensional vector $\left[\overline{V_o}\right]$ has the components $\left(V_o\right)_i = 0$ i = 1...n; $i \neq j$ $\left(V_o\right)_j = V_o$.

Since the driving function $\left[\overline{V(s)}\right]$ has a pole at s = 0, it is also necessary to evaluate the antenna response for this frequency. As discussed in Ref. (19), for currents on a linear structure, this contribution is zero, so Eq. (23) becomes

$$\left[\overline{i(t)}\right] = \sum_{poles} \beta_\alpha \left[\overline{C_\alpha}\right]\left[\overline{C_\alpha}\right]^T \frac{\left[\overline{V_o}\right]}{s_\alpha} e^{s_\alpha t} \tag{24}$$

for a step excited linear antenna. Note that since the poles occur in complex conjugate pairs or with only a real part, the resulting summation for $[\overline{i(t)}]$ is a real function.

12

Because the system matrix $[\overline{\overline{Z}}_T]$ depends on both the functional form of the loading and the magnitude of such loading, it is expected that both the locations of the natural frequencies and the forms of the natural modes will be a function of the loading parameters. This is observed in Sections V, VI, and VII.

III. Natural Far Field Modes

In the past work relating to SEM, investigators have considered the distributions of currents and charges on the surface of an obstacle as evaluated at a natural frequency to be defined as a natural mode of the obstacle. In an analogous manner, one may consider the radiation problem and define the natural radiated modes to be those electric and magnetic fields tangential to the sphere at infinity which are produced by the natural current and charge modes on the obstacle. As in the near field modes, these radiated modes are defined only at the natural frequencies, s_α.

To develop the expressions for the far field natural modes, the case of the thin-wire will be presented first so as to illustrate the method and the definitions. The results can be expressed in the more general notation used in Ref. (3) and will be reported in a future note by Baum.

Consider the antenna shown in Figure 2. It is assumed that the current $I(z)$ flowing on the antenna wire has been previously determined by the use of SEM. It is well known that the $\hat{\theta}$ component of the electric field at a point $\bar{r}_i$ produced by a $\hat{z}$ directed current of moment $I\,dz$ is

$$dE_\theta(\bar{r}_i;s) = \frac{I\,dz}{4\pi\epsilon_o}\,\sin\theta_i\,e^{-sr_i/c}\left[\frac{s}{c^2 r_i} + \frac{1}{cr_i^2} + \frac{1}{sr_i^3}\right] \tag{25}$$

where again the complex frequency $s = (\sigma + j\omega)$ has been employed.

In the far field, it is noted that the $1/r_i^2$ and $1/r_i^3$ terms contribute negligibly to the expression. Keeping only the $1/r_i$ term and integrating over the known current distribution, the total radiated field is given by

$$E_\theta(\bar{r}_i,s) = \frac{1}{4\pi\epsilon_o}\int_{-h}^{h} I(z',s)\sin\theta_i\,e^{-sr_i/c}\,\frac{s}{c^2 r_i}\,dz' \quad . \tag{26}$$

14
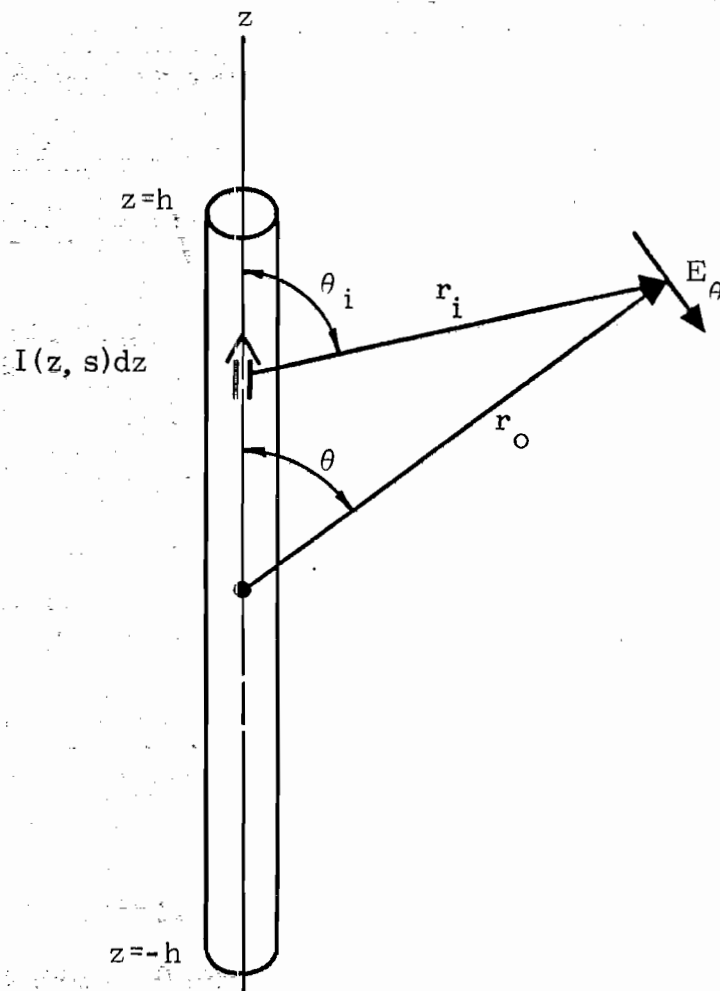
Figure 2. Electric field radiated by current
element Idz flowing on wire antenna.

Rigorously speaking, both θ_i and r_i are functions of z', but by making the customary approximations

$$r_i \simeq r_o \quad \text{(for } r_i \text{ not in the exponential)}$$

$$\theta_i \simeq \theta_o$$

$$r_i \simeq r_o - z'\cos\theta_o \quad \text{(for } r_i \text{ in the exponential)}$$

Eq. (26) then takes the following form

$$r_o E_\theta(r_o, s) = \frac{Z_o \sin\theta_o}{4\pi} e^{-sr_o/c} \frac{s}{c} \int_{-h}^{h} I(z', s) e^{\frac{s}{c}z'\cos\theta_o} dz'. \tag{27}$$

Noting that the continuous representation the current is given by Eq. (10) as

$$I(z, s) = \sum_{\alpha \text{ poles}} \beta_\alpha \frac{\eta(s) M_\alpha(z)}{s - s_\alpha} \tag{28}$$

where the coupling coefficient η is defined by Eq. (11). Eq. (27) then becomes

$$r_o E_\theta(r, s) = \frac{Z_o \sin\theta_o\, e^{-sr_o/c}}{4\pi} \frac{s}{c} \sum_\alpha \frac{\beta_\alpha \eta(s)}{s - s_\alpha} \int_{-h}^{h} C_\alpha(z') e^{\frac{s}{c}z'\cos\theta_o} dz'$$

$$+ \text{ possible entire function of (s) .} \tag{29}$$

As in the frequency domain representation for the wire current, this equation has singularities at $s = s_\alpha$. As a result, the time-domain response can be evaluated by the Cauchy theorem. Thus

$$r_o E_\theta(\theta_o, t) = \frac{Z_o \sin\theta_o}{4\pi} \sum_\alpha \beta_\alpha \frac{s_\alpha}{c} \eta(s_\alpha) \int_{-h}^{h} C_\alpha(z') e^{\frac{s_\alpha}{c}z'\cos\theta_o} dz'\, e^{s_\alpha(t - r_o/c)}$$

$$\cdot\, U(t - r_o/c) \tag{30}$$

16

where it has been assumed that the effect of the entire function on the integral at infinity can be neglected.

It is possible to define a normalized natural electric field mode $e_\alpha(\theta_o)$ by

$$\beta_\alpha^{(F)} e_\alpha(\theta_o) \equiv \frac{1}{L} \int_{-h}^{h} C_\alpha(z') e^{\frac{s_\alpha}{c} z' \cos\theta_o} dz' \tag{31}$$

where $L = 2h$. The constant $\beta_\alpha^{(F)}$ is such that $\left(e_\alpha(\theta_o)\right)_{max} = 1$, and the natural mode (also coupling vector in this formulation) has been similarly normalized so $\left(C_\alpha(z)\right)_{max} = 1$. With this definition, the time domain response for the radiated field becomes

$$r_o E_\theta(\theta_o, t) = \frac{Z_o \sin\theta_o}{4\pi} \sum_\alpha \beta_\alpha \beta_\alpha^{(F)} \left(\frac{s_\alpha L}{c}\right) \eta_\alpha(s_\alpha) e_\alpha(\theta_o) e^{s_\alpha(t - r_o/c)} U(t - r_o/c) \tag{32}$$

which is of the same basic form as the time domain expression for the current.

Putting this last relation in discrete vector notation like that used in Ref. (19), and assuming a step excitation voltage, the radiated field becomes

$$[\overline{r_o E_\theta(t)}] = \frac{Z_o \sin\theta_o}{4\pi} \sum_\alpha \beta_\alpha \beta_\alpha^{(F)} \left(\frac{s_\alpha L}{c}\right) \left([\overline{C_\alpha}]^T \frac{[\overline{V_o}]}{s_\alpha}\right) [\overline{e_\alpha}] e^{s_\alpha(t - r_o/c)} \tag{33}$$

for $(t - r_o/c) > 0$.

IV. Numerical Results: The Unloaded Antenna

The following section treats the analysis of the thin-wire antenna having an a/h ratio of .01. The pole locations, current mode vectors and coupling vectors are the same as those presented in IN 102 where the thin scatterer was treated, but the coupling coefficients and, therefore, the time domain results are different. In addition, the far field quantities are presented here. In all cases to be considered, enough data will be presented so that the time domain responses of the structures can be computed for any driving source.

As a result of searching the complex s plane for the singularities of Eq. (4) with $\Lambda(z, s) = 0$, a number of natural resonances for this structure have been found as indicated in Figure 3. As done previously, the numerical search procedure was a Newton-Rhapson method. For this relatively simple structure, this searching procedure proved to be efficient, but for other, more complex obstacles, it has been quite difficult to find all of the poles within a particular region. One method which has been employed by Shumpert is to actually plot contours of constant determinant of the system matrix in the complex s plane. Although this is relatively costly in terms of computer time, it is a sure way to determine all of the pole locations. Figure 4 shows the contour plots for the dashed region in Figure 3.

Since the poles occur in layers, the parameter α has been replaced by the parameters ℓ and n, ℓ referring to the layer number and n to the pole within any layer. In addition, the poles occur in complex conjugate pairs, which is not indicated in Figure 3.

After solving the homogeneous integral equation of the natural frequencies, the natural current modes can be determined. Figures 5 through 9 show the real and imaginary parts of the normalized natural current modes (and the normalized coupling vectors) for various n and ℓ values.

Once the natural current mode is determined, the natural far field mode $e_{\ell, n}(\theta)$ can be determined by a simple operation on the current mode,

18
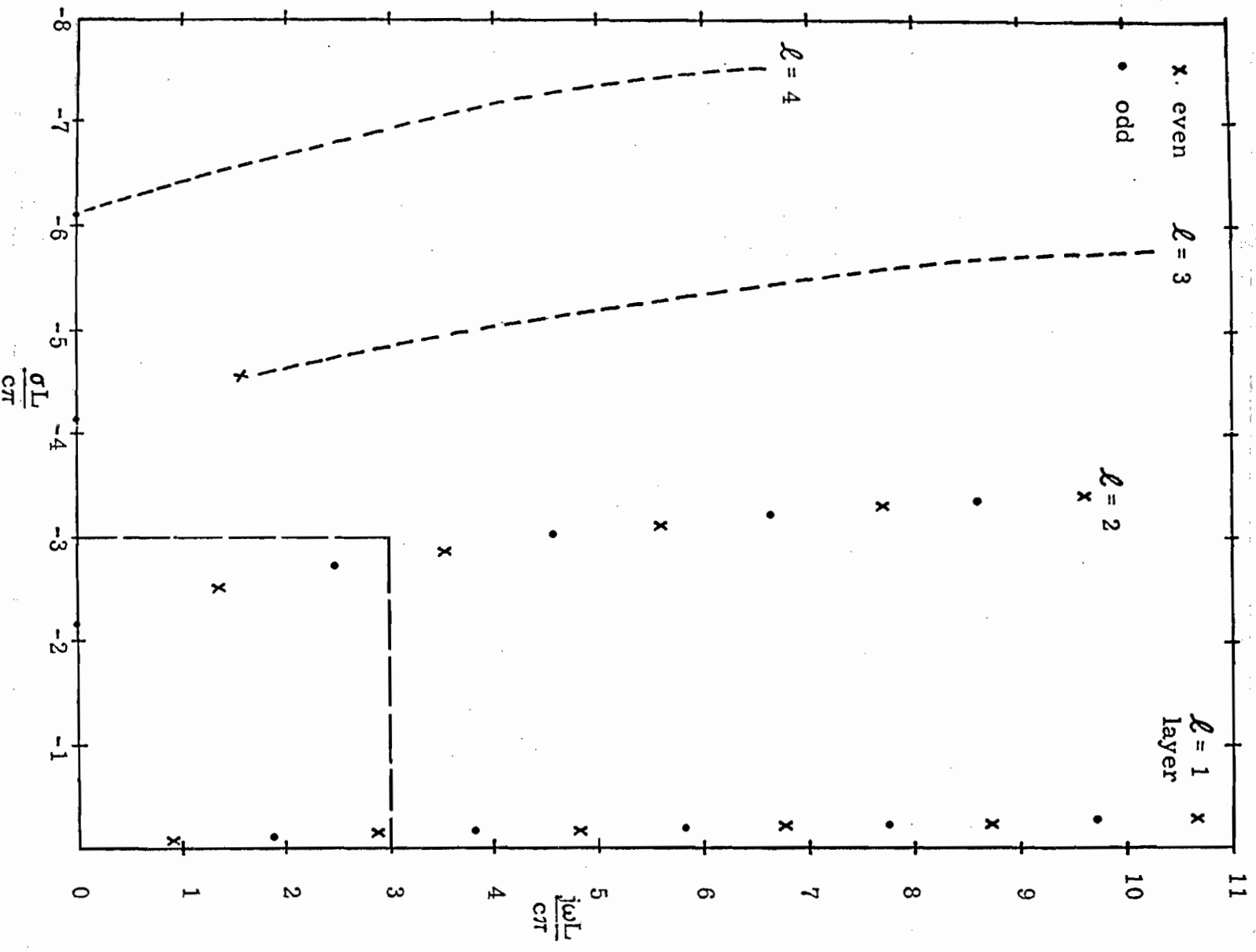
Figure 3. Pole locations in the complex frequency plane for the thin-wire of a/h = .01.

19
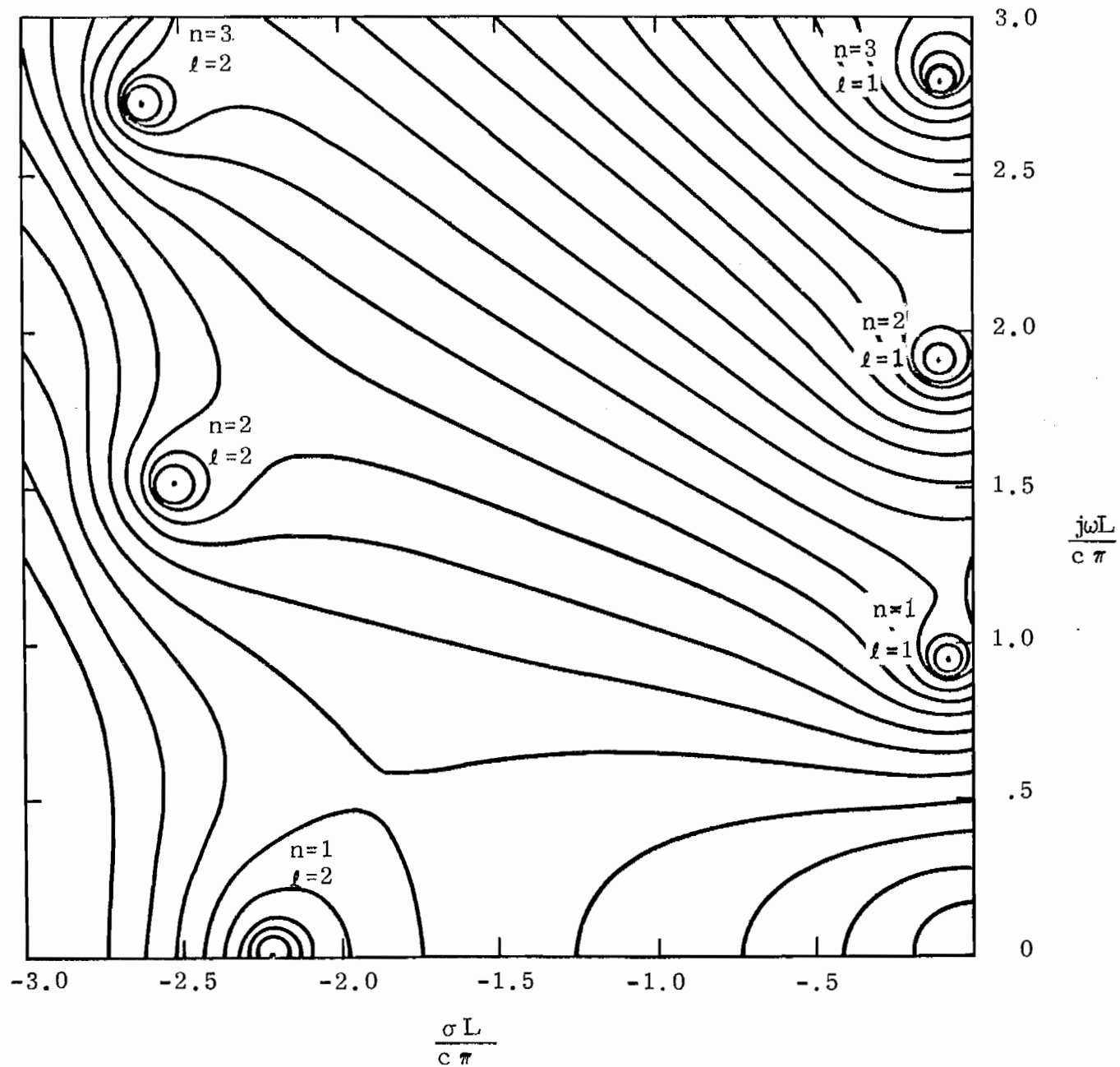
Figure 4. Contour plot of the constant determinent surface for the thin-wire, showing the first three poles in layers $\ell = 1$ and 2. (Courtesy of T. Shumpert.)
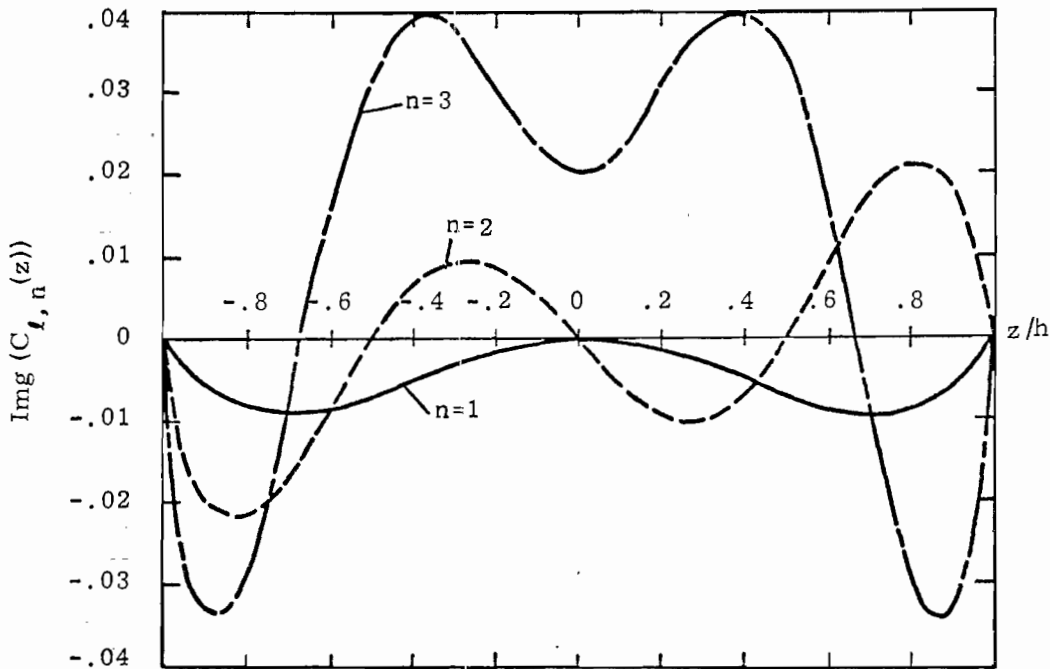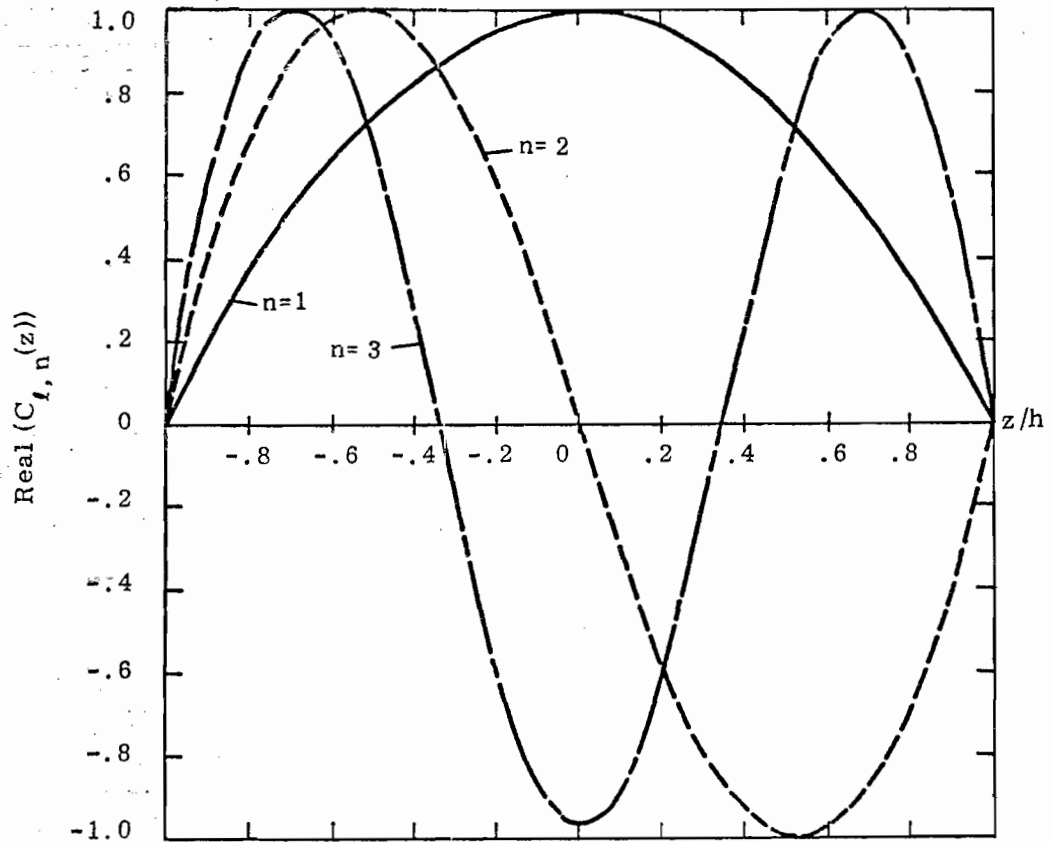
Figure 5. Real and imaginary parts of the natural current
mode (and the coupling vector) for the $\ell = 1$
layer poles of the unloaded antenna, $a/h = .01$.

21
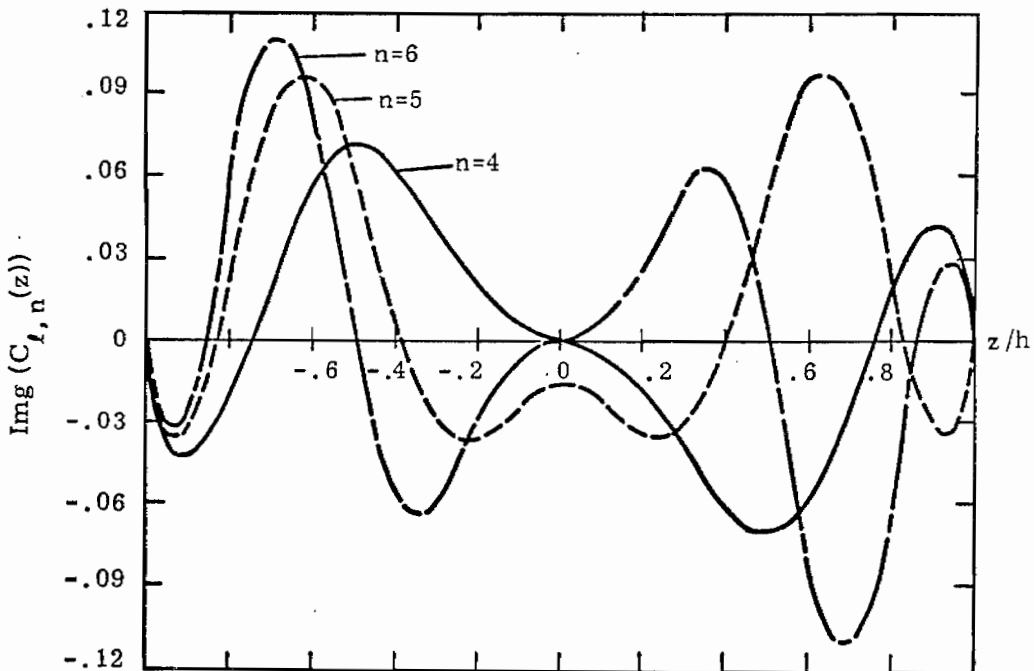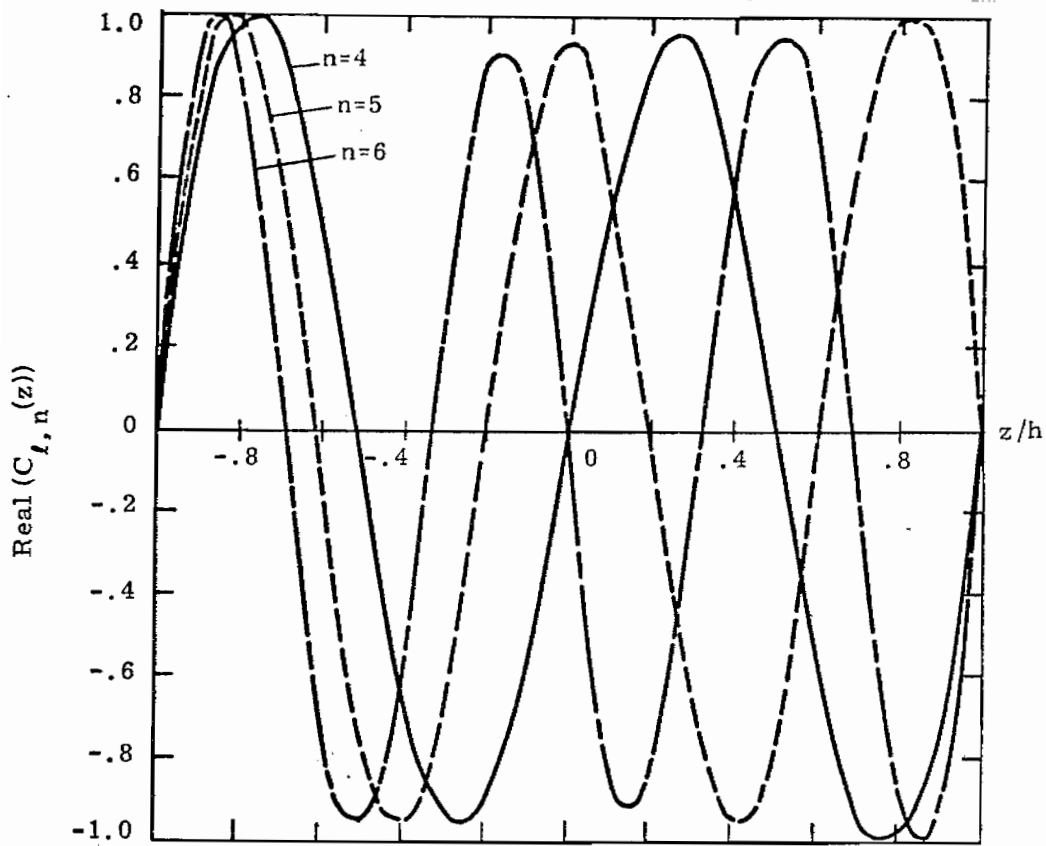
Figure 6. Real and imaginary parts of the natural current mode (and the coupling vector) for the $\ell = 1$ layer poles of the unloaded antenna, a/h = .01.
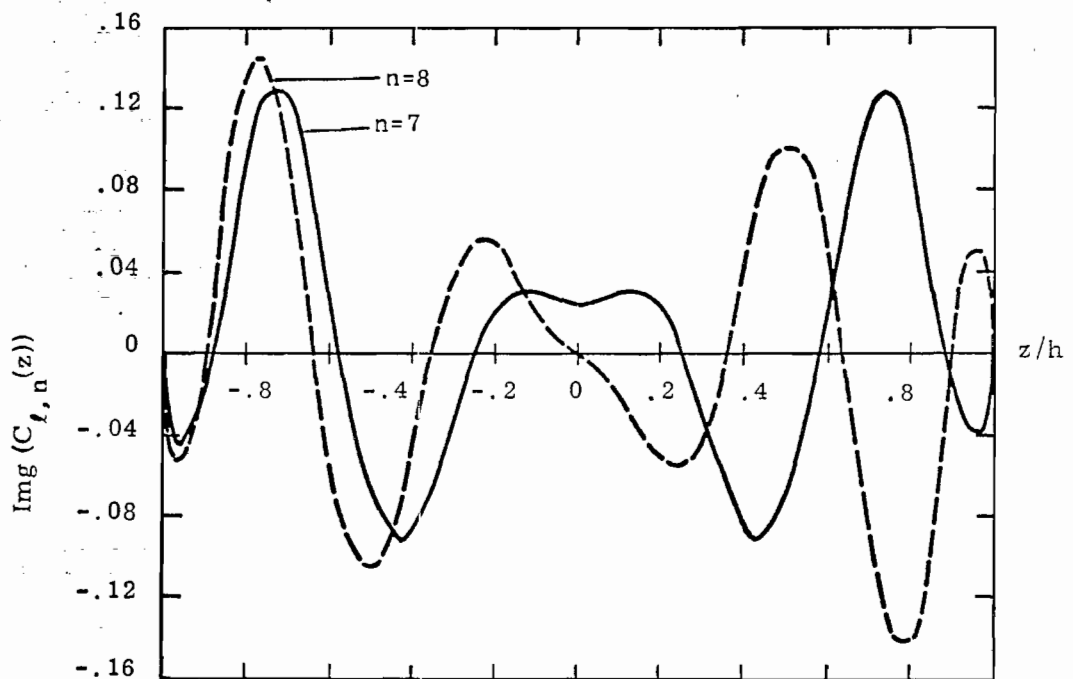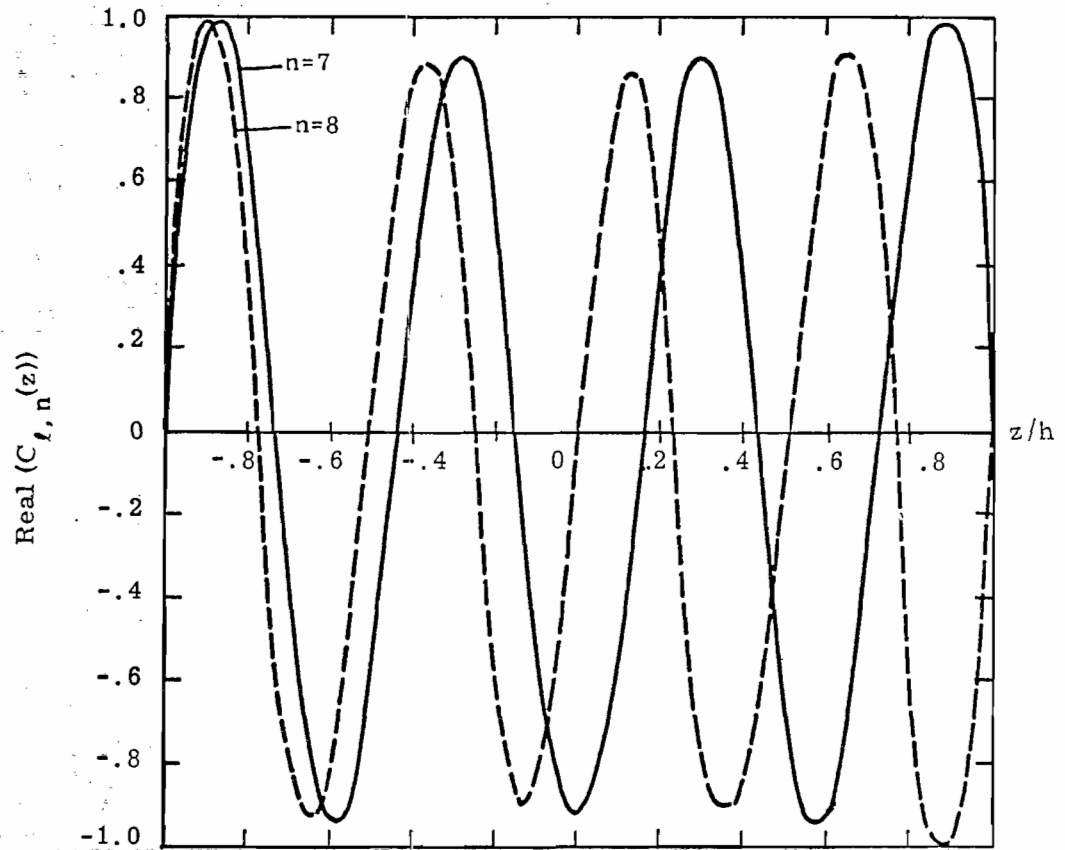
Figure 7. Real and imaginary parts of the natural current mode (and the coupling vector) for the $\ell = 1$ layer poles of the unloaded antenna, $a/h = .01$.

23
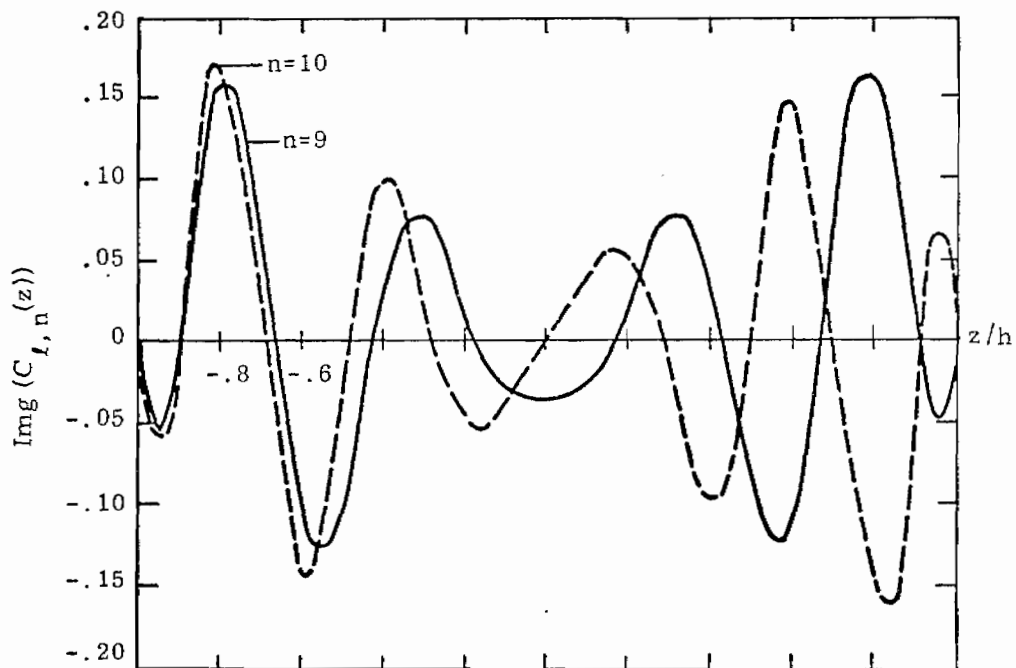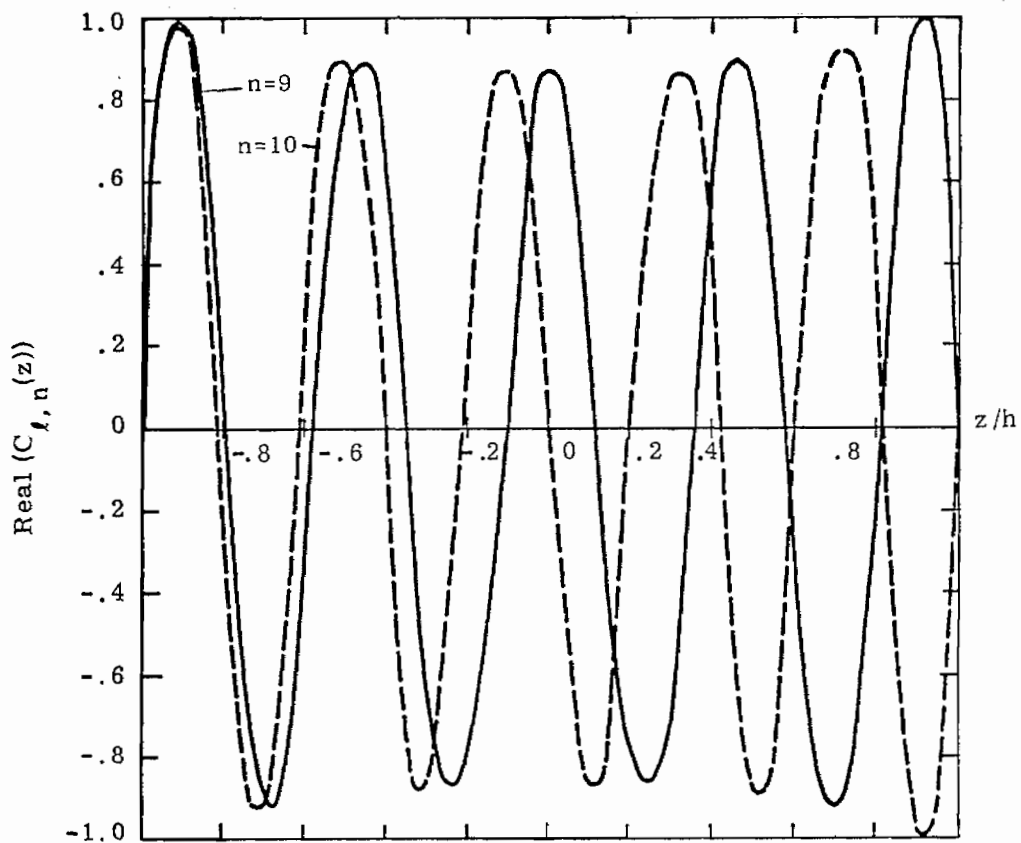
Figure 8. Real and imaginary parts of the natural current mode (and the coupling vector) for the $\ell = 1$ layer poles of the unloaded antenna, $a/h = .01$.

24
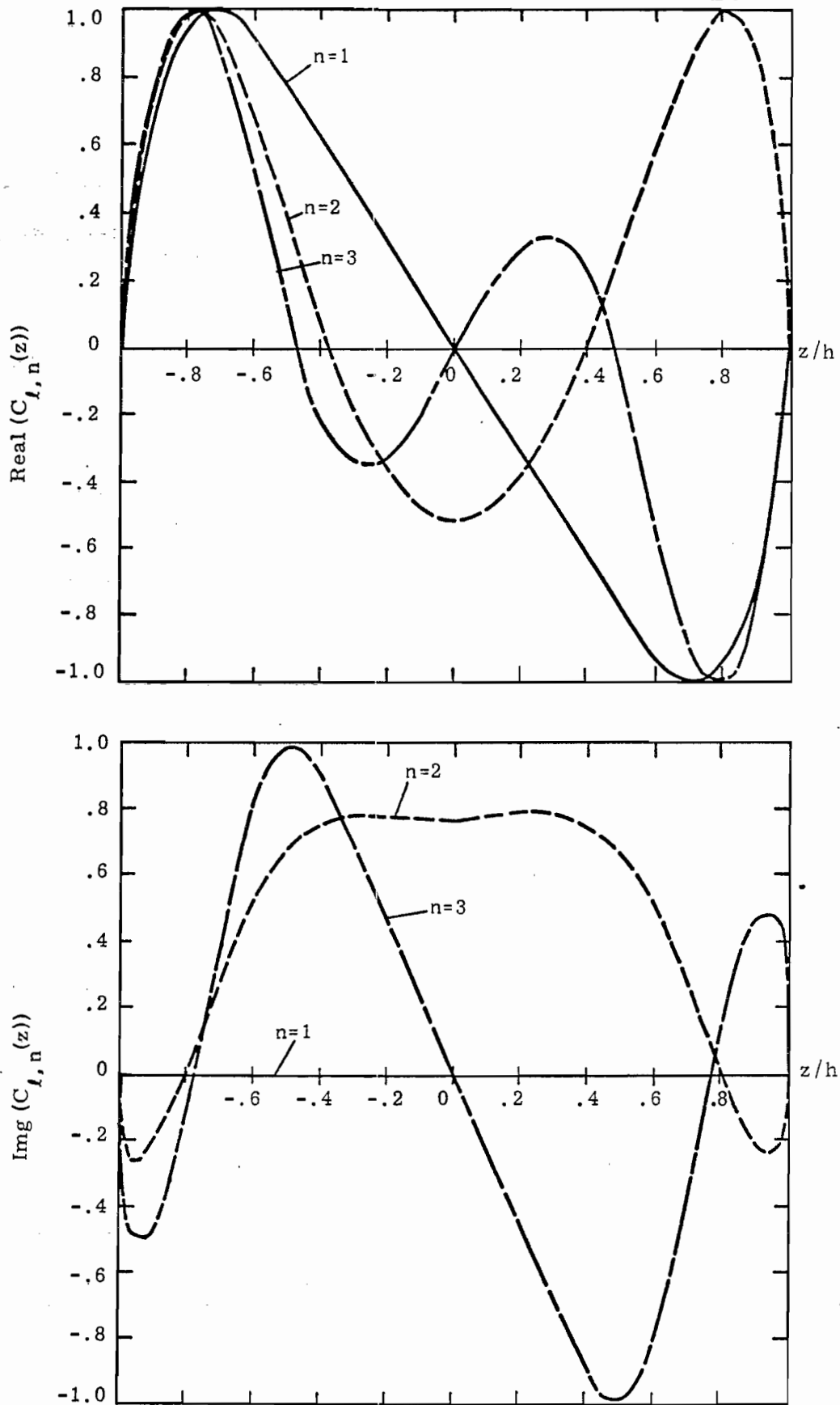
Figure 9. Real and imaginary parts of the natural current
mode (and the coupling vector) for the $\ell = 2$ layer
poles of the unloaded antenna, a/h = .01.

as indicated in Eq. (31). In Figures 10 through 13, the magnitudes of the normalized far field modes are plotted in polar form. Note that only half of the polar plot is given, as the field is symmetric about the antenna axis t = 0. More precise plots of the real and imaginary parts of these far-field modes are given in Figures 14 through 18 for various values of n and ℓ.

Aside from the natural modes and pole locations, it is necessary to have the values for the normalization factors β_α and $\beta_\alpha^{(F)}$ in order to compute the time domain responses for the antenna current or the radiated fields from Eqs. (24) and (33). Table I presents these coefficients, along with the natural frequencies and coupling coefficients. The coupling coefficients for the center fed antenna having a source of width Δ are computed for a step wave in time and have been defined as

$$\eta(s_\alpha) = \int_{-\Delta/2}^{\Delta/2} C_\alpha(z') \frac{E^{inc}(z')}{s_\alpha} dz' , \qquad (34)$$

where the incident field $E^{inc} = V_o/\Delta$. For the problem at hand, this coupling coefficient is defined for a gap of total width $\Delta = .1 L$ where L is the total antenna length.

In addition to the above, the decay times for each of the natural modes are presented. This is given the symbol τ_α and is defined as the time such that the contribution of each pole falls to 1/e of its value at $\tau = 0$. As expected, the larger the index n or ℓ, the faster the contributions attenuate in time.

Using the quantities presented above, it is now possible to determine the behavior of the antenna in the time and frequency domains. The delta function spectrum for the current at the input of the antenna was calculated by Eq. (22) and is presented in Figure 19, along with the corresponding quantity as determined from the direct integral solution. Notice that the agreement is rather poor, even though poles in the second layer have been included in the sum. For this analysis the eighteen poles given in Table I have been used.

26
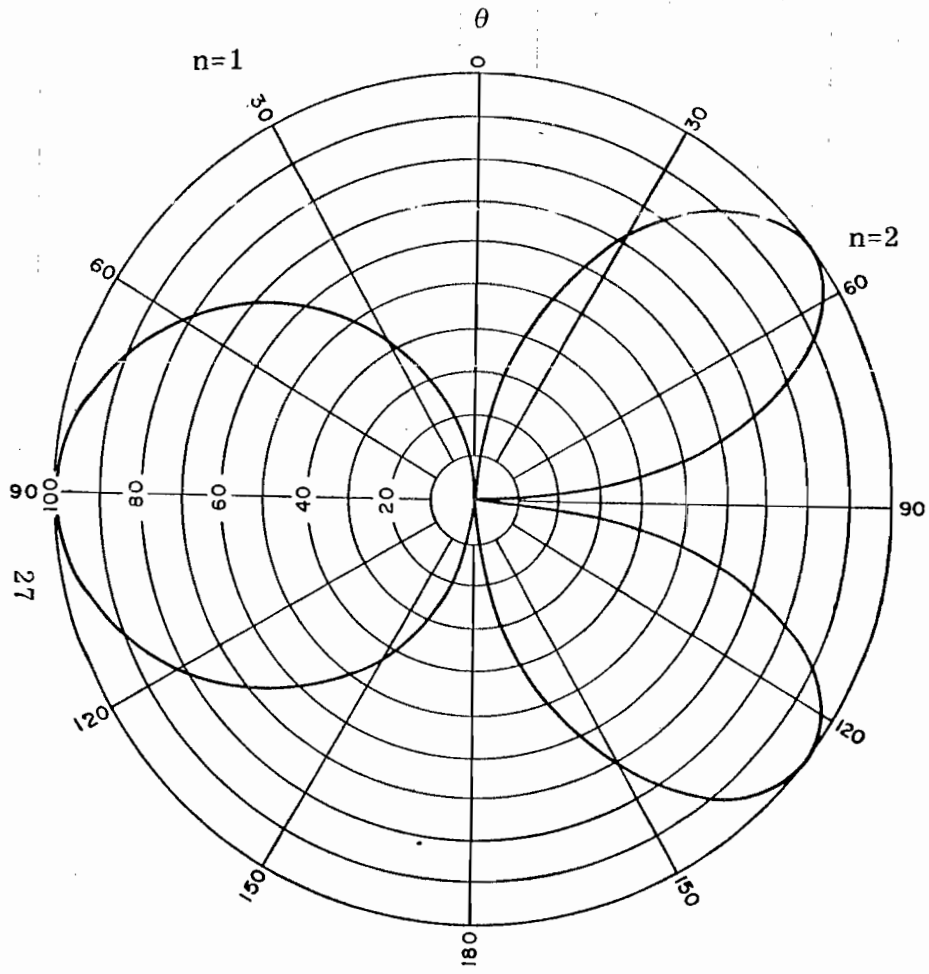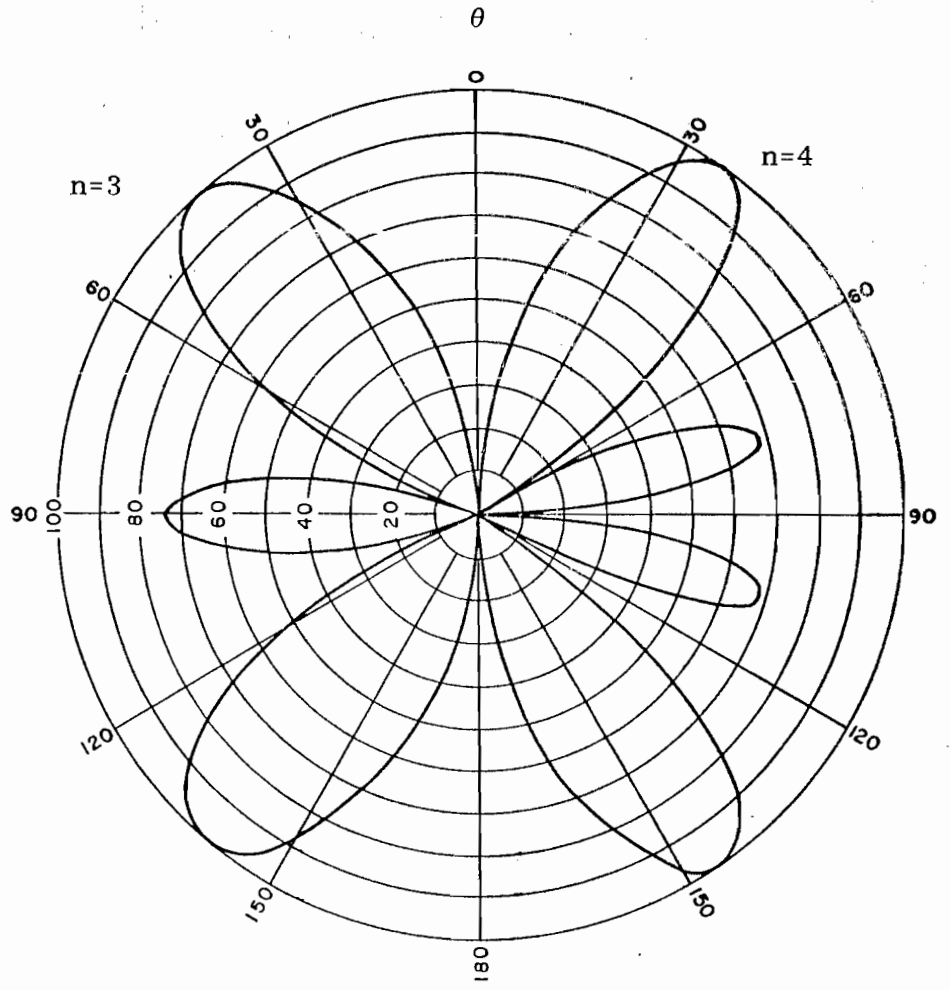
Figure 10. Polar plots of the magnitude of the normalized far field mode $e_{\textit{l}, \text{n}}(\theta)$ for $\textit{l}=1$ poles of an unloaded antenna.

27
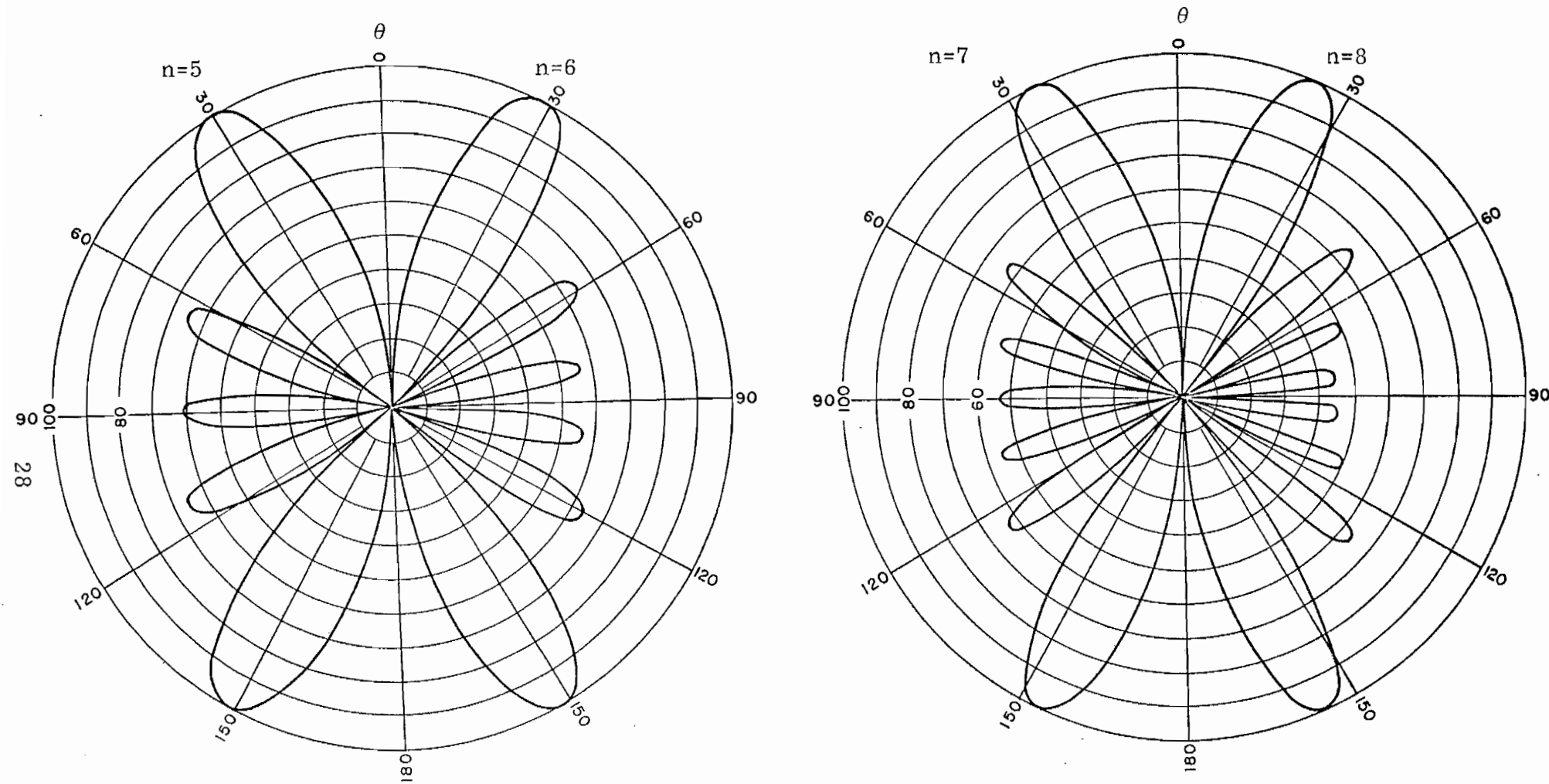
Figure 11.   Polar plots of the magnitude of the normalized far field modes $e_{\ell,n}(\theta)$ for $\ell = 1$ poles of an unloaded antenna.
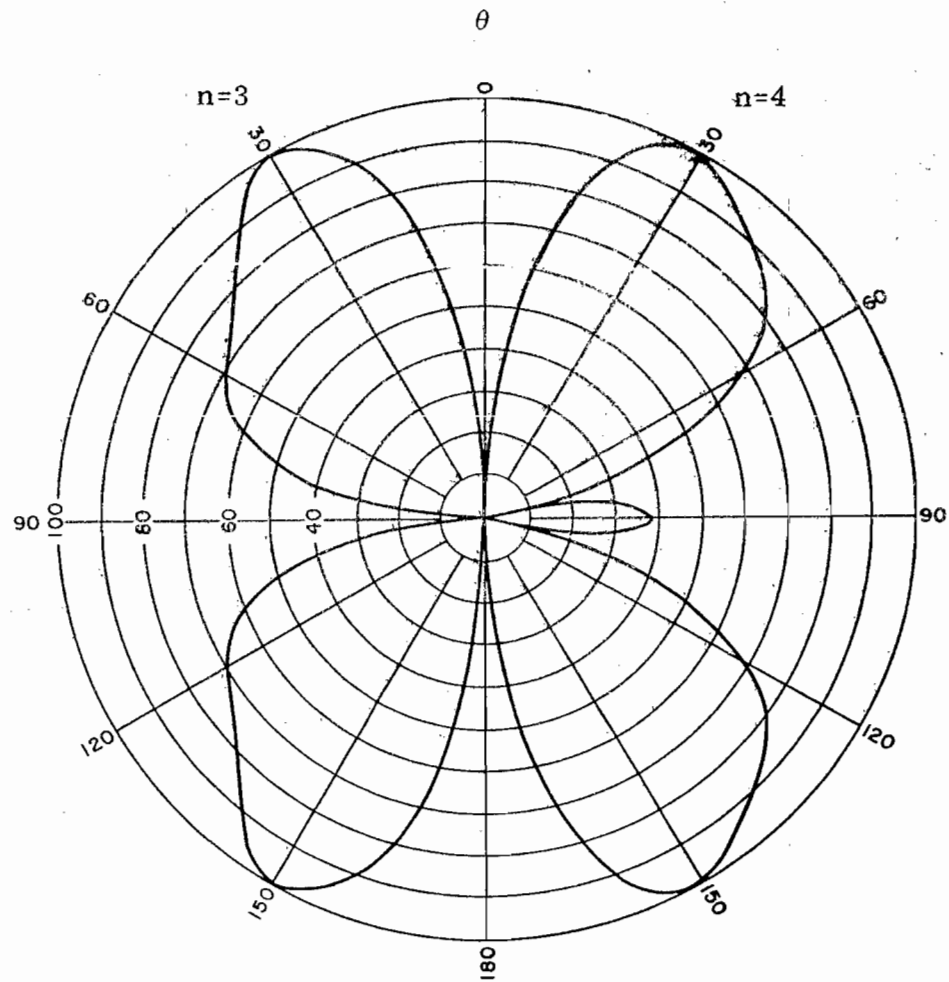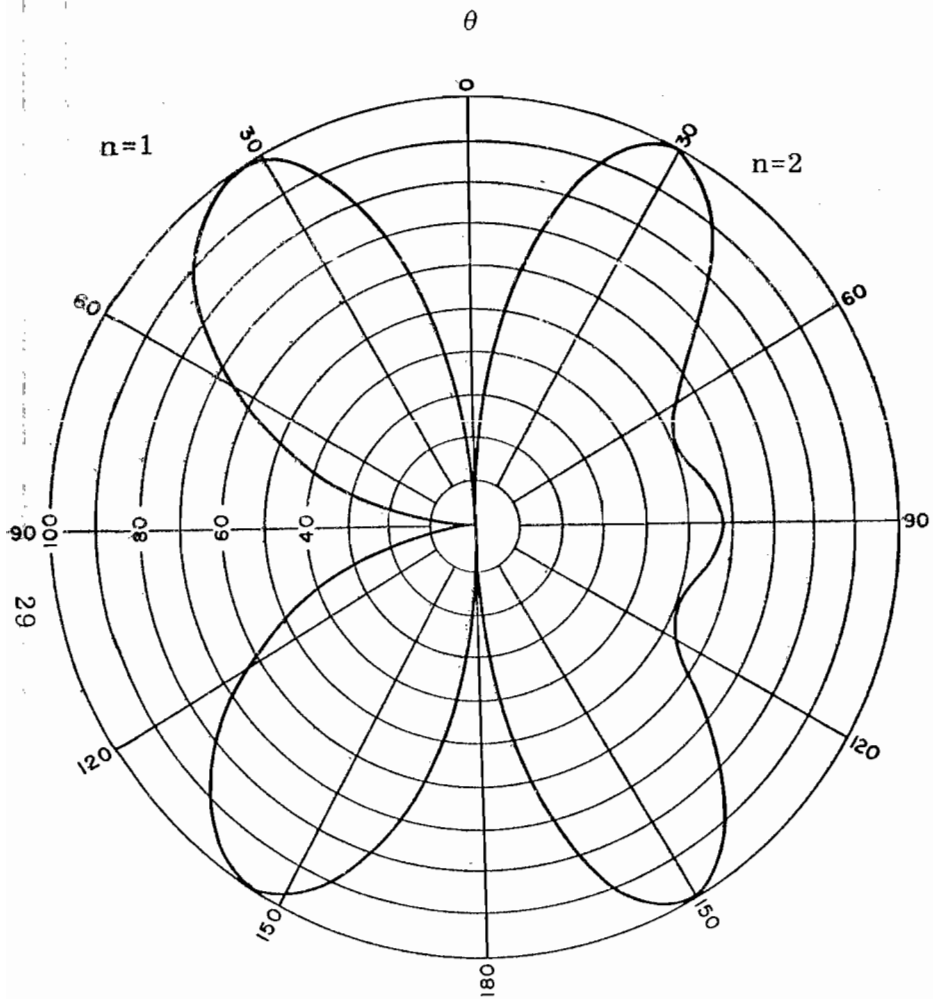
Figure 12. Polar plots of the magnitude of the normalized far field modes $e_{\ell,n}(\theta)$ for the $\ell = 2$ poles of an unloaded antenna.
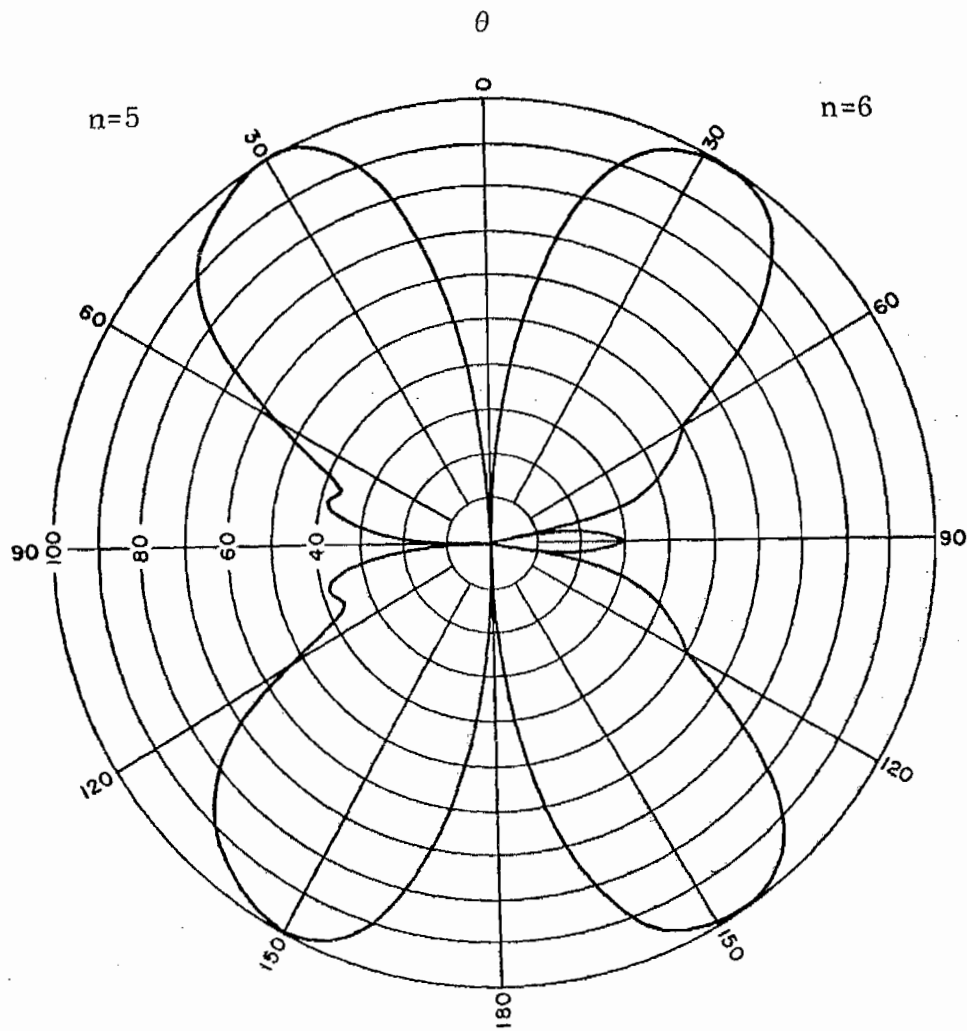
Figure 13. Polar Plots of the magnitude of the normalized far field modes $e_{\ell, n}(\theta)$ for the $\ell = 2$ poles of an unloaded antenna.
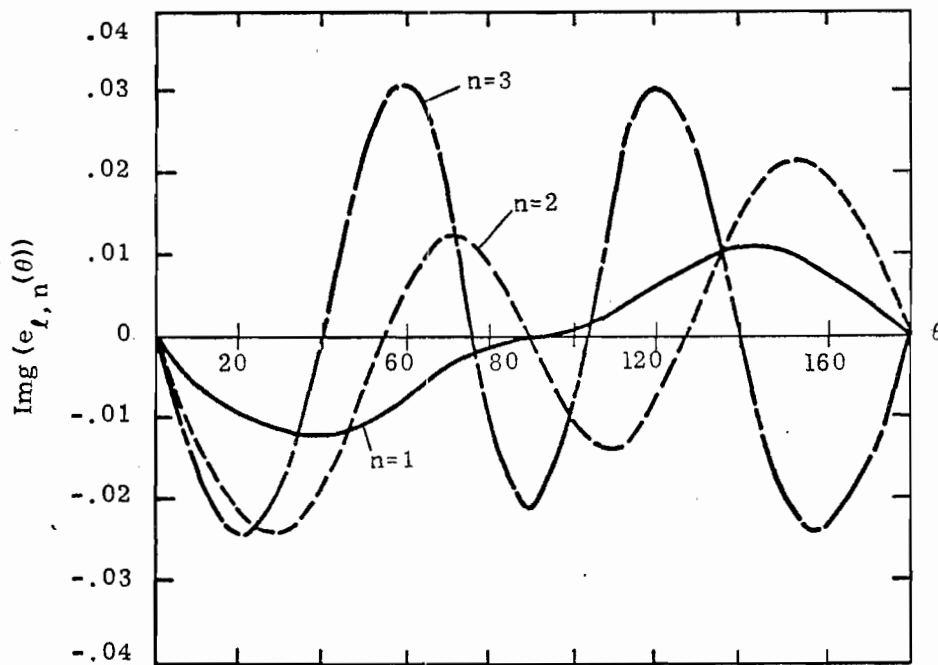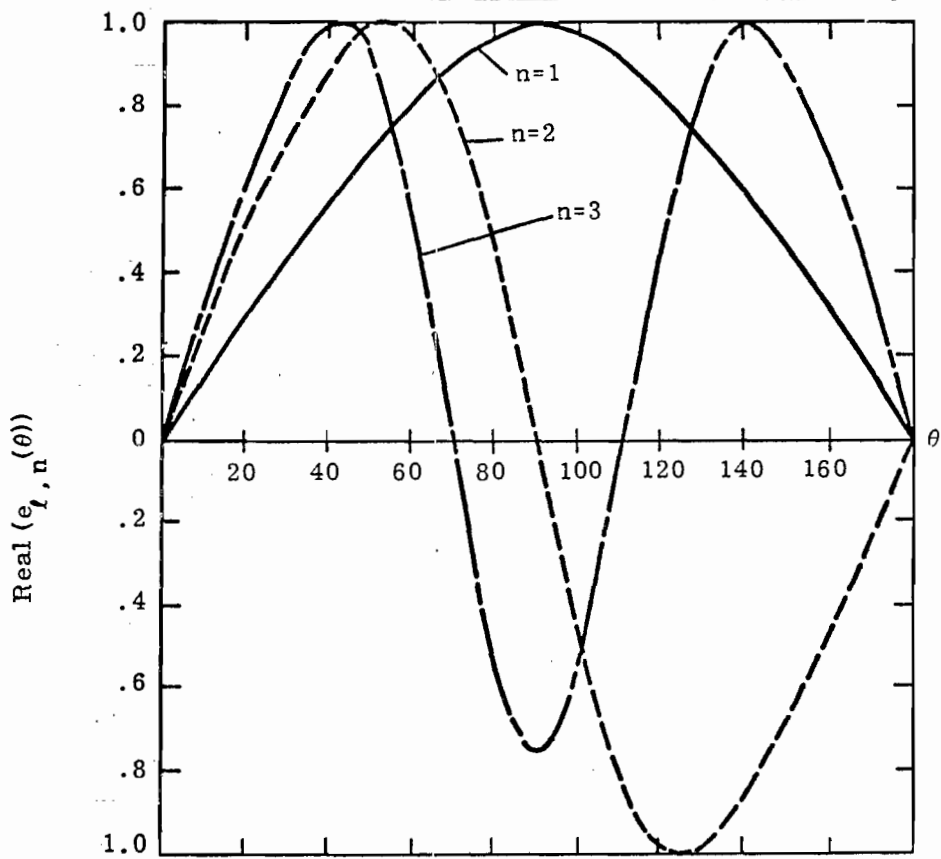
Figure 14 Real and imaginary parts of the normalized far field
mode for the $\ell = 1$ layer poles of an unloaded antenna of
$a/h = .01$.

31
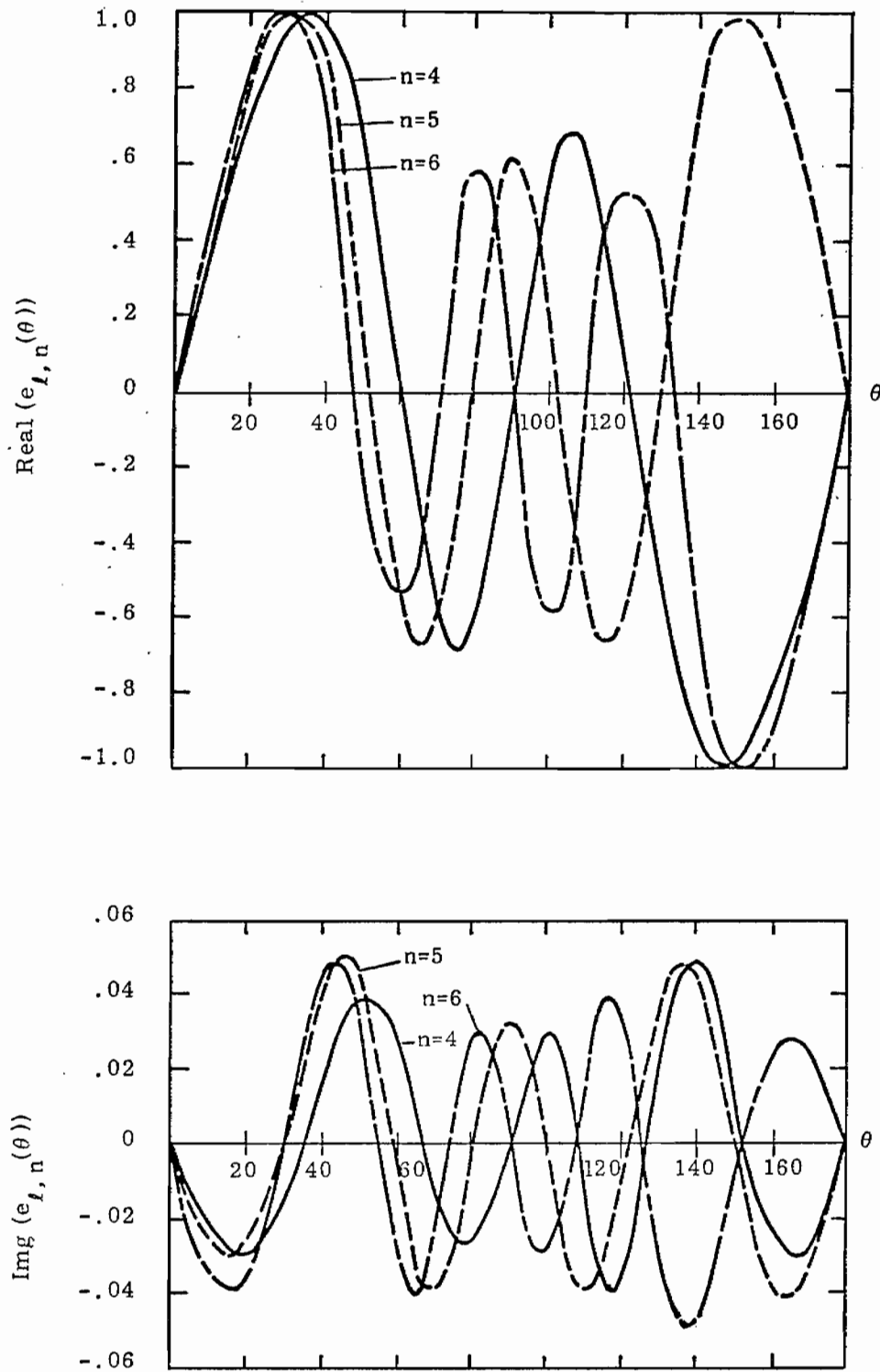
Figure 15 Real and imaginary parts of the normalized far field
mode for the $\ell = 1$ layer poles of an unloaded antenna of
a/h = .01.
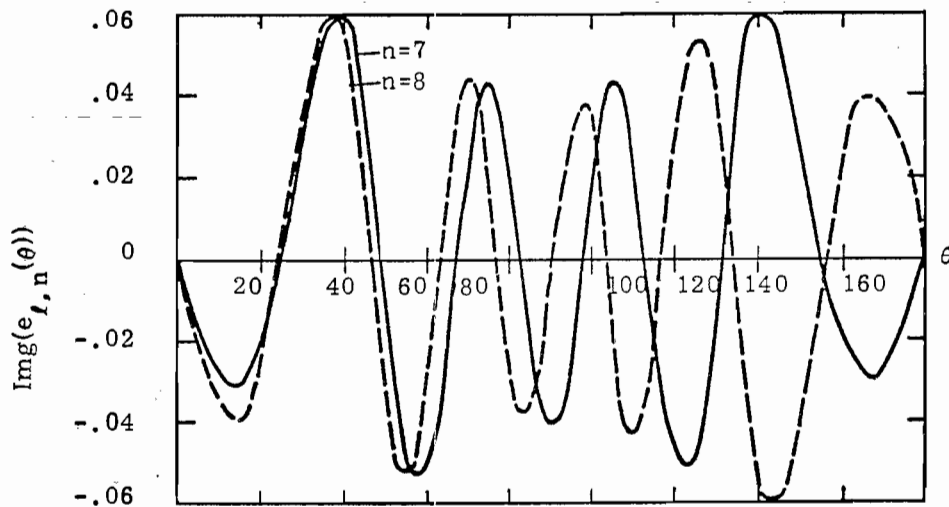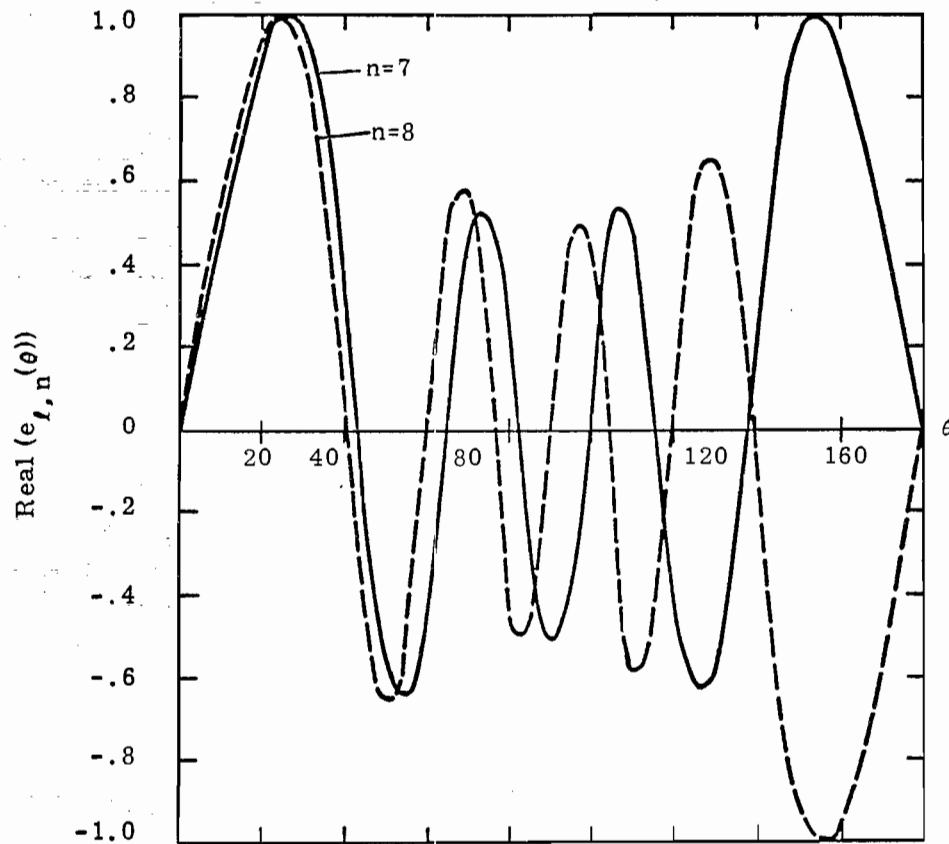
Figure 16 Real and imaginary parts of the normalized far field
mode for the l=1 layer poles of an unloaded antenna of
a/h = .01.
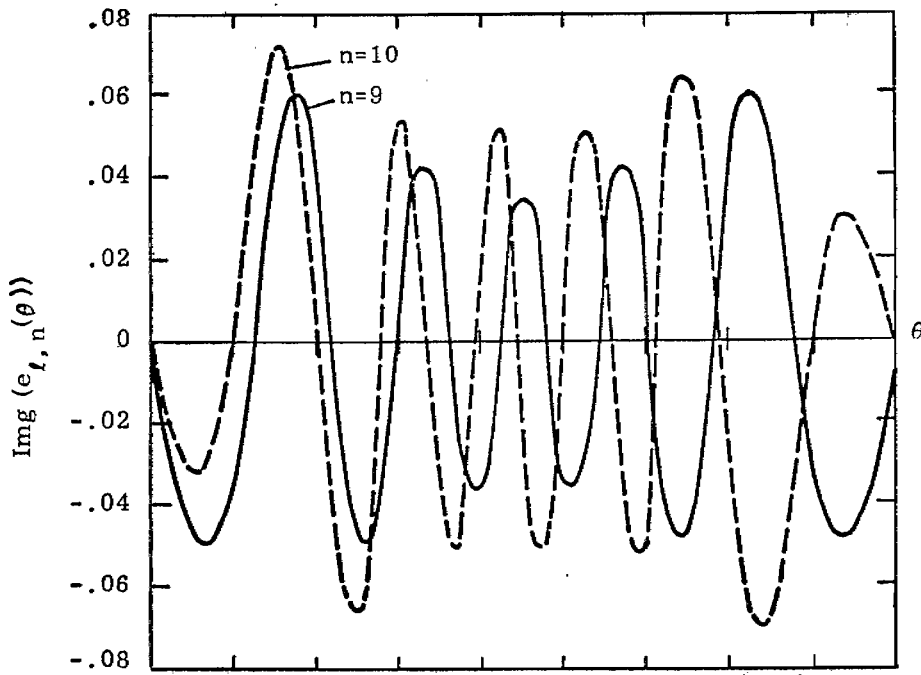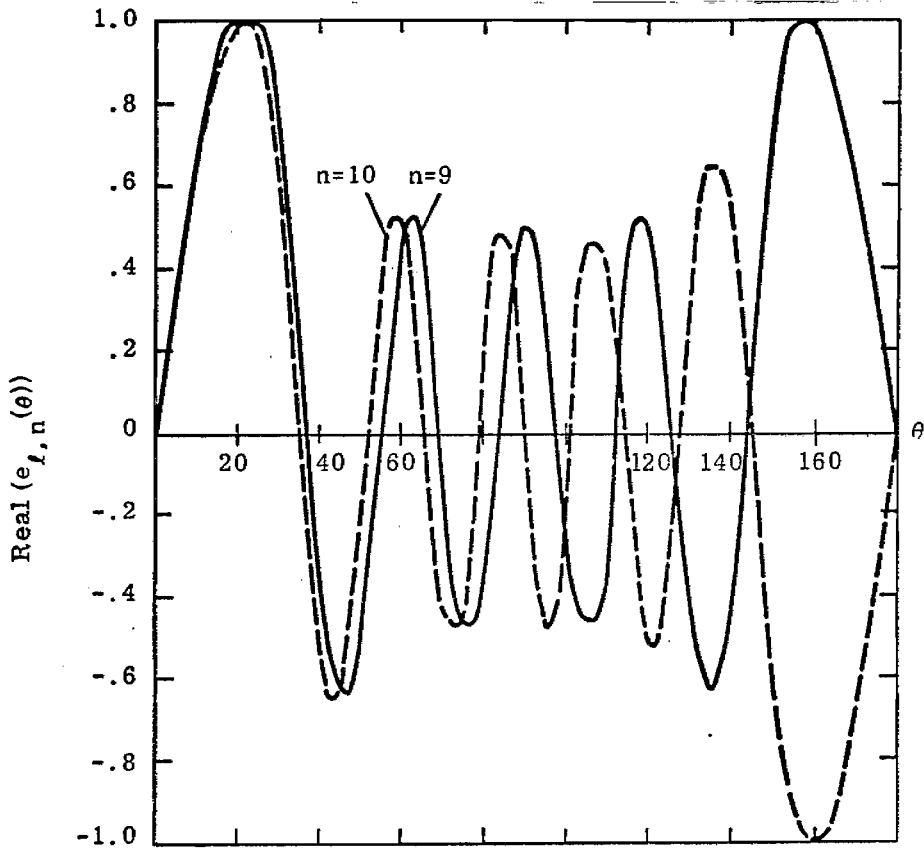
Figure 17 Real and imaginary parts of the normalized far field
mode for the $\ell = 1$ layer poles of an unloaded antenna of
a/h = .01.
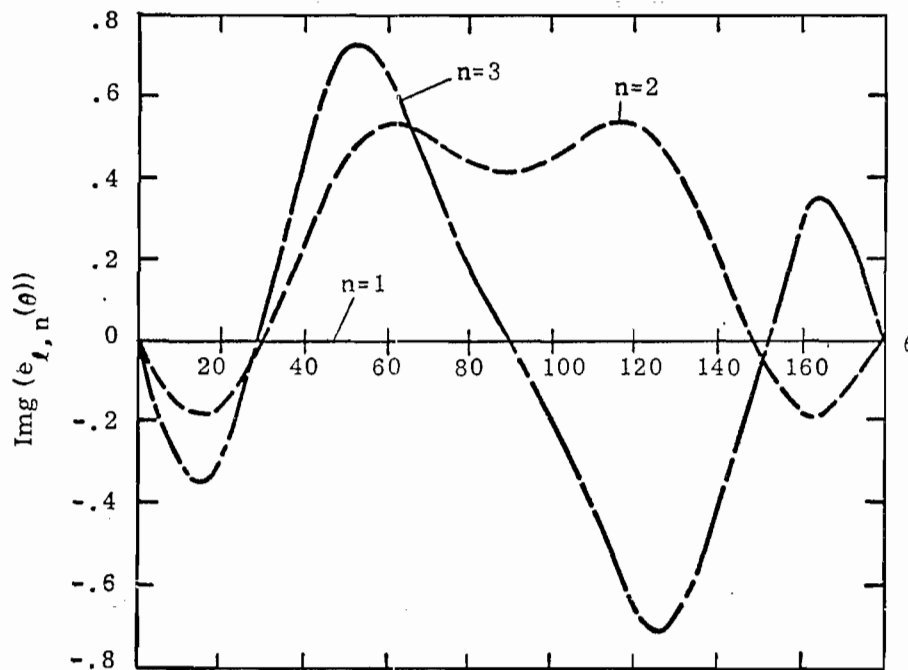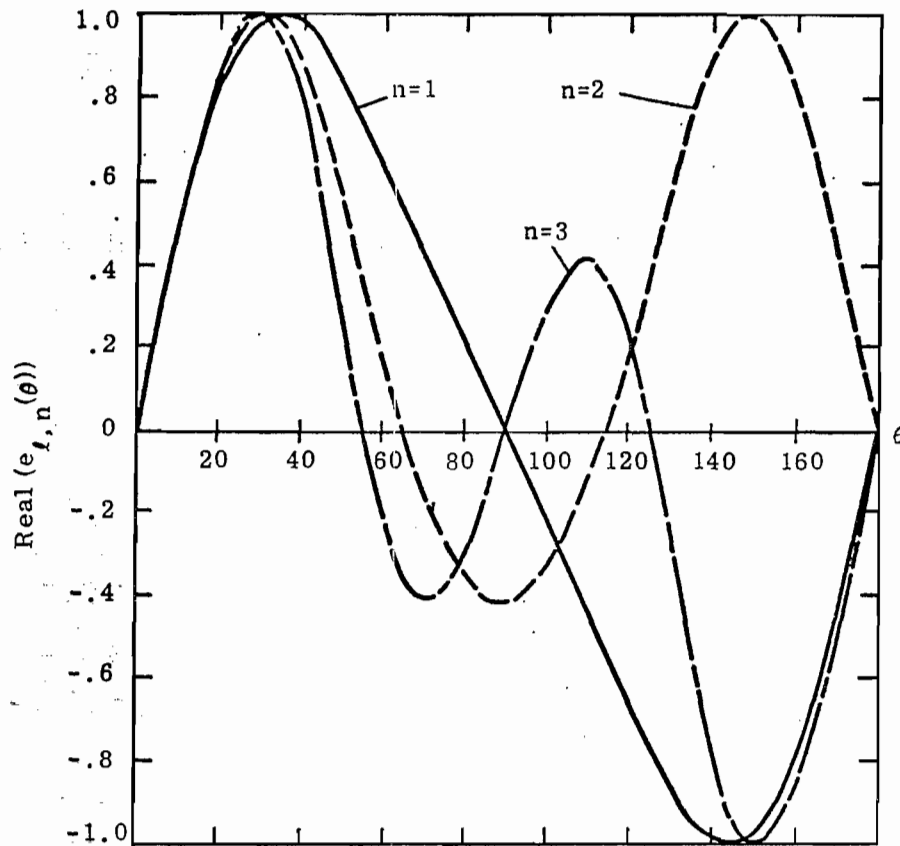
Figure 18 Real and imaginary parts of the normalized far field mode for the $\ell = 2$ layer poles of an unloaded antenna of a/h = .01.

TABLE I

Data for Unloaded Wire of a/h = .01 (Ω=10.59)

Pole α l	n	Natural Frequency $s_\alpha L/c\pi$* $\sigma L/c\pi$	$j\omega L/c\pi$	Current Normalization (x10³) $Re(\beta_\alpha)$	$Im(\beta_\alpha)$	Field Normalization $Re(\beta_\alpha^{(F)})$	$Im(\beta_\alpha^{(F)})$	Coupling Coeff. (x10¹) Step Excitation** $Re(\eta)$	$Im(\eta)$	Decay Time $c\tau_\alpha/h$
1	1	-.082	.926	3.583	1.000	19.631	- .144	-.302	-3.41	7.760
1	2	- .120	1.897	4.062	1.115	.295	-11.433	0.0	0.0	5.306
1	3	- .147	2.874	4.426	-1.307	-8.748	- .228	.077	1.04	4.330
1	4	- .169	3.854	4.724	1.499	- .216	7.319	0.0	0.0	3.765
1	5	- .188	4.835	5.113	1.453	6.298	.314	-.034	-.558	3.386
1	6	- .205	5.817	5.425	1.607	.360	- 5.565	0.0	0.0	3.104
1	7	- .220	6.800	5.716	1.775	-5.040	- .255	.024	.346	2.894
1	8	- .234	7.783	5.976	1.849	- .264	4.600	0.0	0.0	2.720
1	9	- .247	8.767	6.286	2.144	4.166	.284	-.019	- .224	2.578
1	10	- .260	9.752	6.538	2.360	.155	- 3.927	0.0	0.0	2.448
1	11	- .270	10.733	6.664	2.657	-3.700	- .117	.016	.146	2.358
1	12	- .279	11.709	6.875	2.258	- .255	3.462	0.0	0.0	2.282
2	1	-2.174	0.0	- .898	0.0	31.396	0.0	0.0	0.0	.292
2	2	-2.506	1.347	-1.023	-.167	7.599	-26.298	.912	- .494	.254
2	3	-2.725	2.477	-1.248	-.794	-20.607	-6.335	0.0	0.0	.234
2	4	-2.890	3.544	2.538	-.375	0.249	-12.782	.072	.350	.220
2	5	-3.025	4.581	3.627	1.413	10.478	- 7.028	0.0	0.0	.210
2	6	-3.139	5.603	5.026	2.220	1.800	-10.512	-.062	-.150	.202

*L = 2h = Total Antenna Length

**Coupling Coefficient is for a Center Driven Antenna with Gap Δ =.16.

36
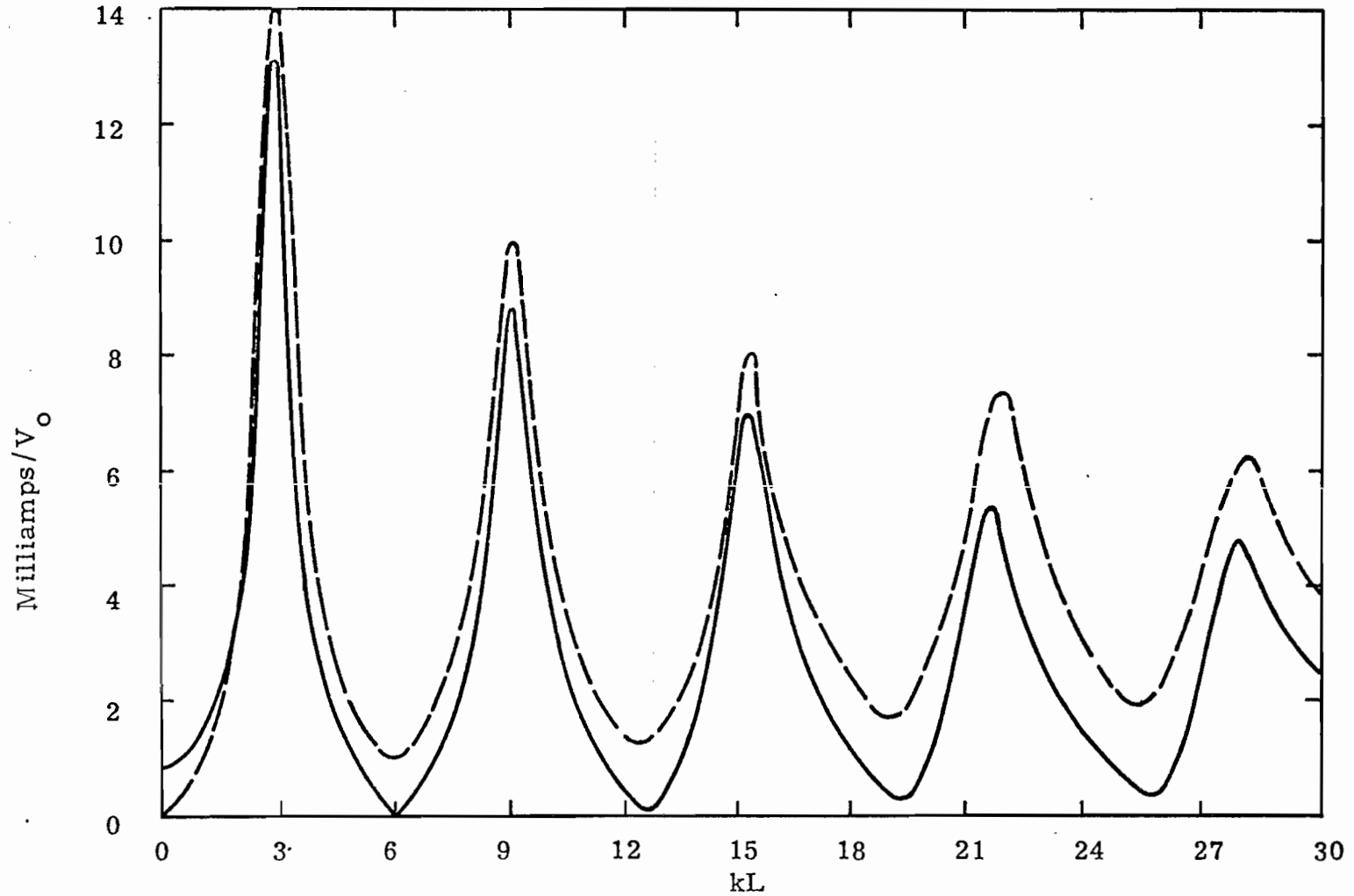
Figure 19.   Plot of the magnitude of the input current at the unloaded antenna as a function of kL.   The solid line represents SEM results, and the dashed represents conventional integral equation results.

One possible reason for the discrepancy between the two curves may be due to the fact that the entire function $[\overline{F_e(s)}]$ in Eq. (22) was not included in the evaluation of the frequency domain response. Another possibility for this discrepancy between the two results may be that not enough poles have been taken in the first layer to adequately represent the driving voltage which is non zero only over the small region Δ.

The time domain responses of the antenna current at the input (z = 0) and at z = $\pm$h/2 are presented in Figure 20a, and the behavior of the linear charge density at z = h is shown in Figure 20b. These are for a step function excitation of the antenna. For the charge at z = -h, the behavior is the negative of that shown here, due to the symmetry of the problem. For comparison purposes, Figure 21 shows the same data as computed by the conventional frequency domain integral equation method and converted to the time domain by the Fast Fourier Transform. In addition, an independent check with results supplied by Miller[17] shows excellent agreement.

Figures 22 and 23 present the radiated field $r_o E_\theta / V_o$ in the time domain for a number of different observation angles as computed by Eq. (33). Again, the antenna is step function excited. These results compare favorably with those determined by Miller and with those reported earlier by Liu.[8] It should be noted in passing that the results obtained by SEM are not extremely accurate for early time unless a large number of poles are taken in the summations. For an accurate early time description of the radiated fields, valid for (ct/h)(1 - cosθ) < 1 the reader is referred to Ref. (20), where the properties of an infinite cylindrical antenna are discussed.
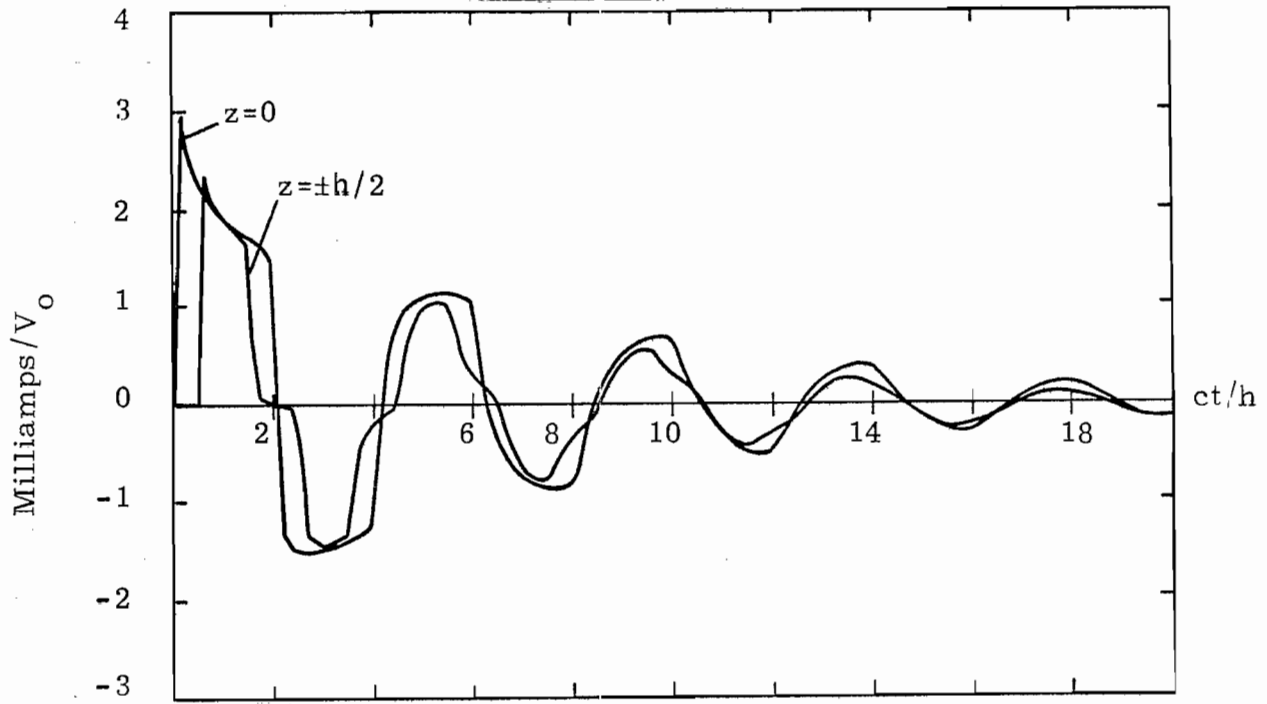
(a)
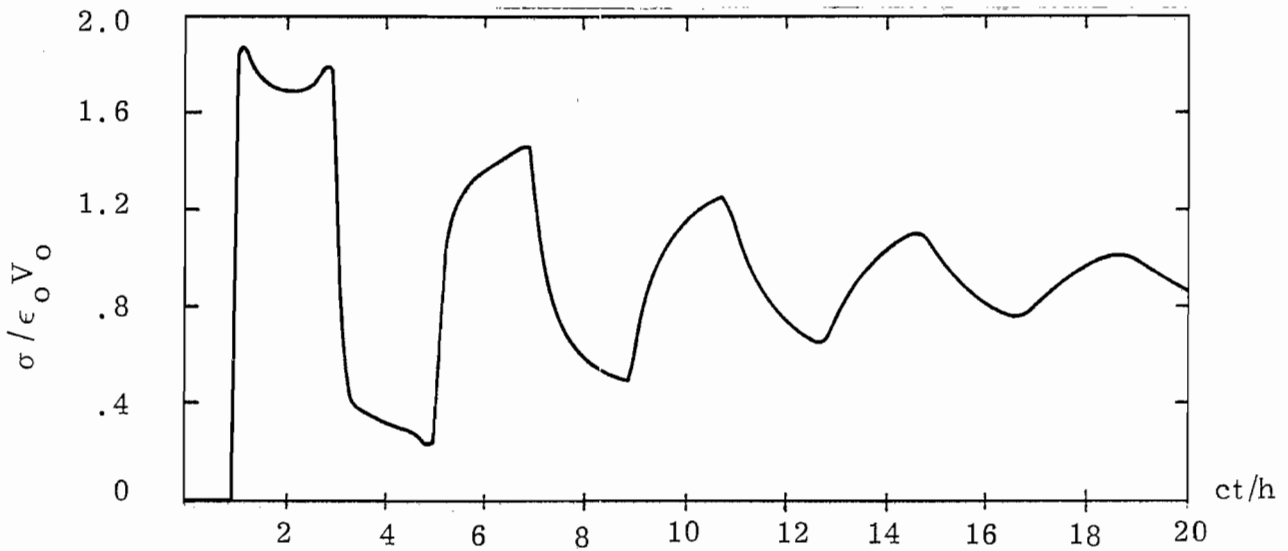
(b)

Figure 20.   Time history plots of (a), the current at the input of
the antenna and at $z = \pm h/z$ and (b), the linear charge
density at $z = h$, for the unloaded antenna of $a/h = .01$,
as computed by SEM with the poles of Table I.
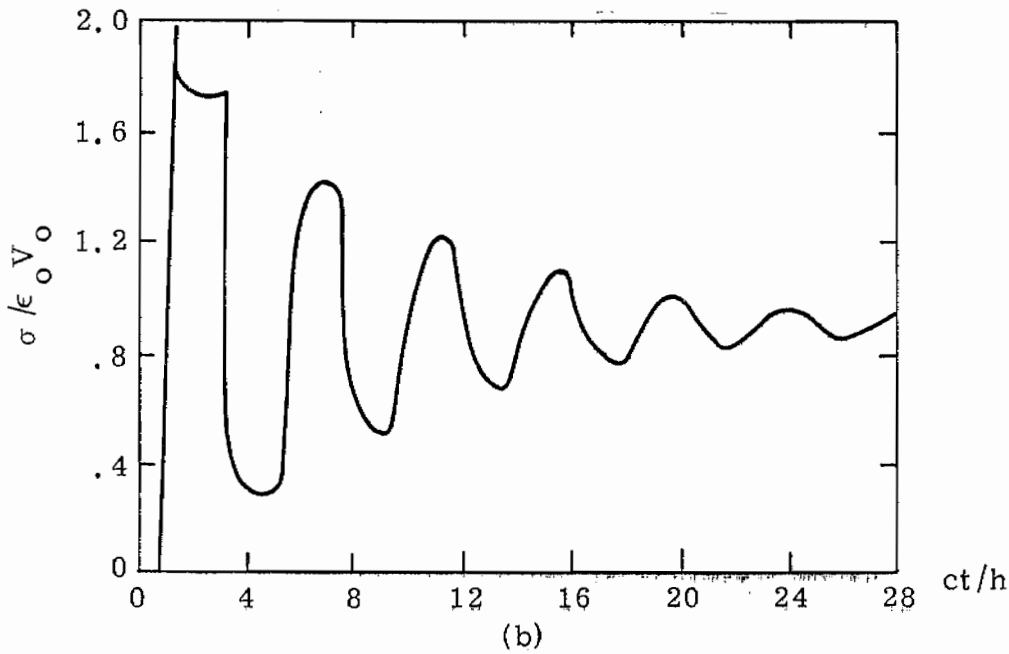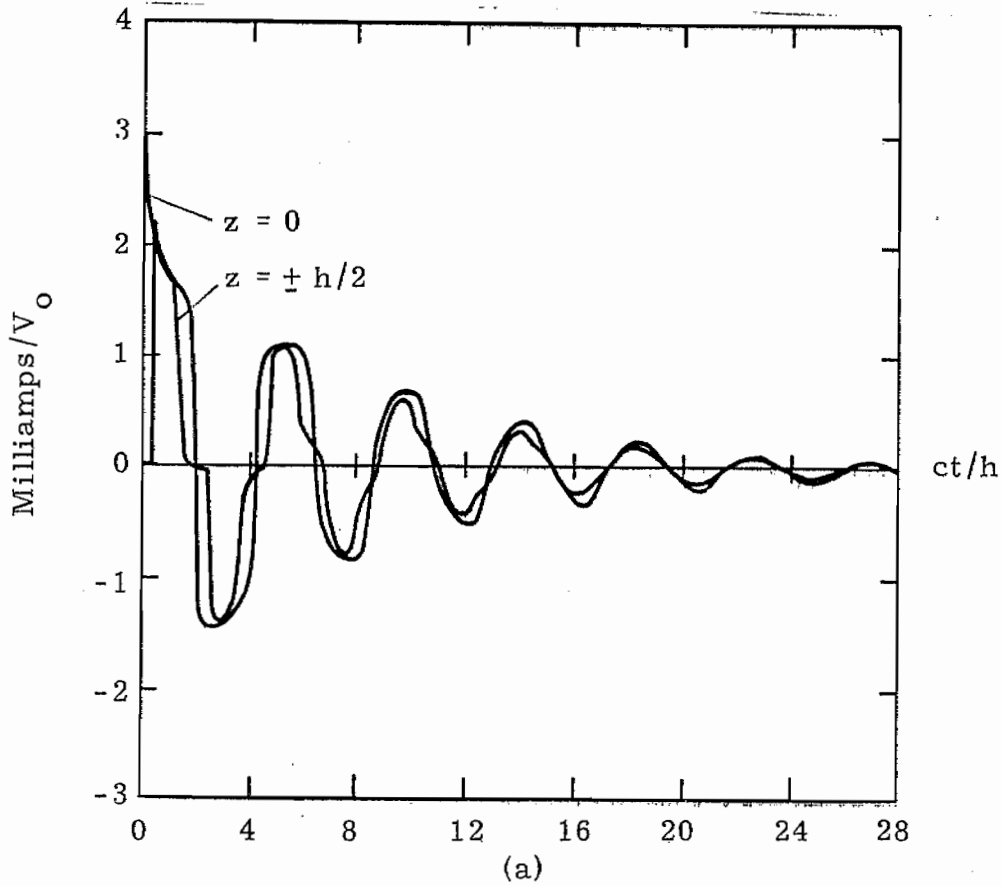
Figure 21. Time history plots of (a), the current at the
input of the antenna and at $z = \pm h/z$ and (b)
the linear charge density at $z = h$, for the
unloaded antenna, as computed by the conven-
tional integral equation technique.

40
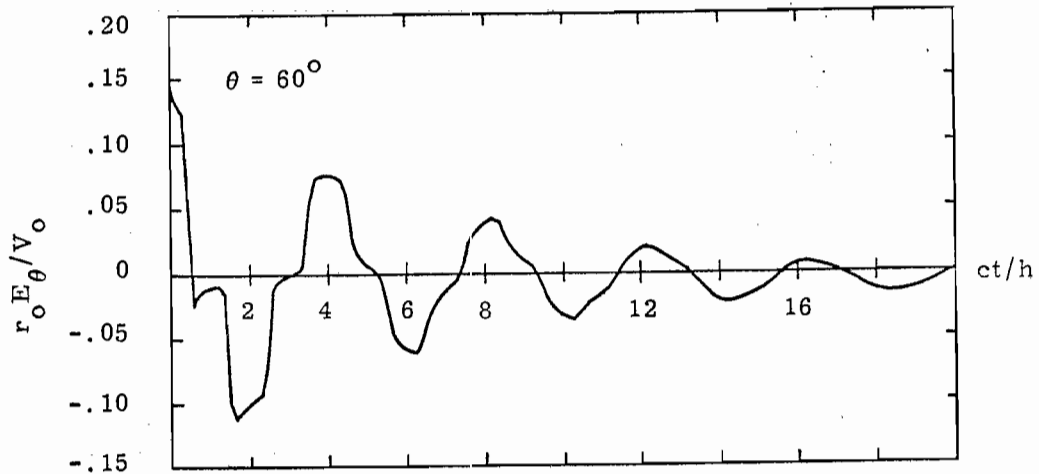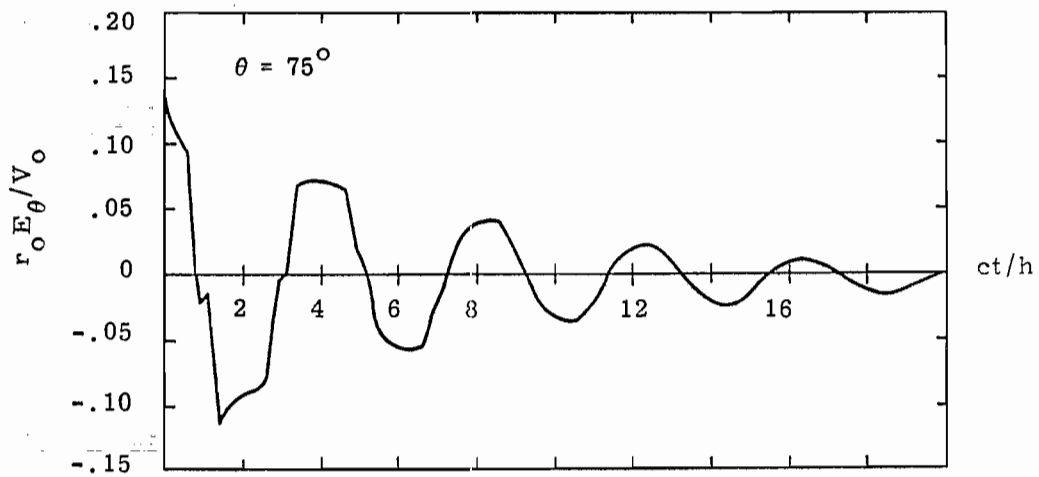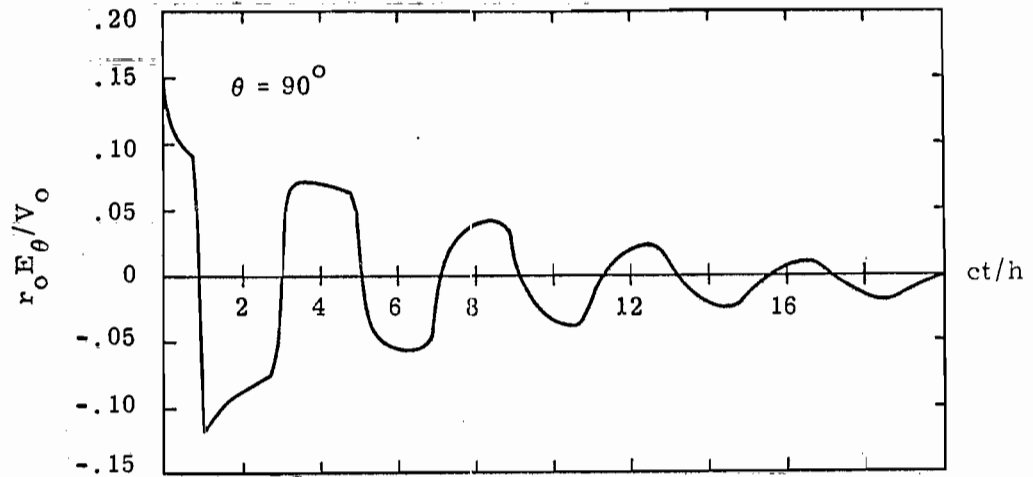
Figure 22. Radiation patterns in the time domain for step excited antenna, a/h = .01, using the poles of Table I.
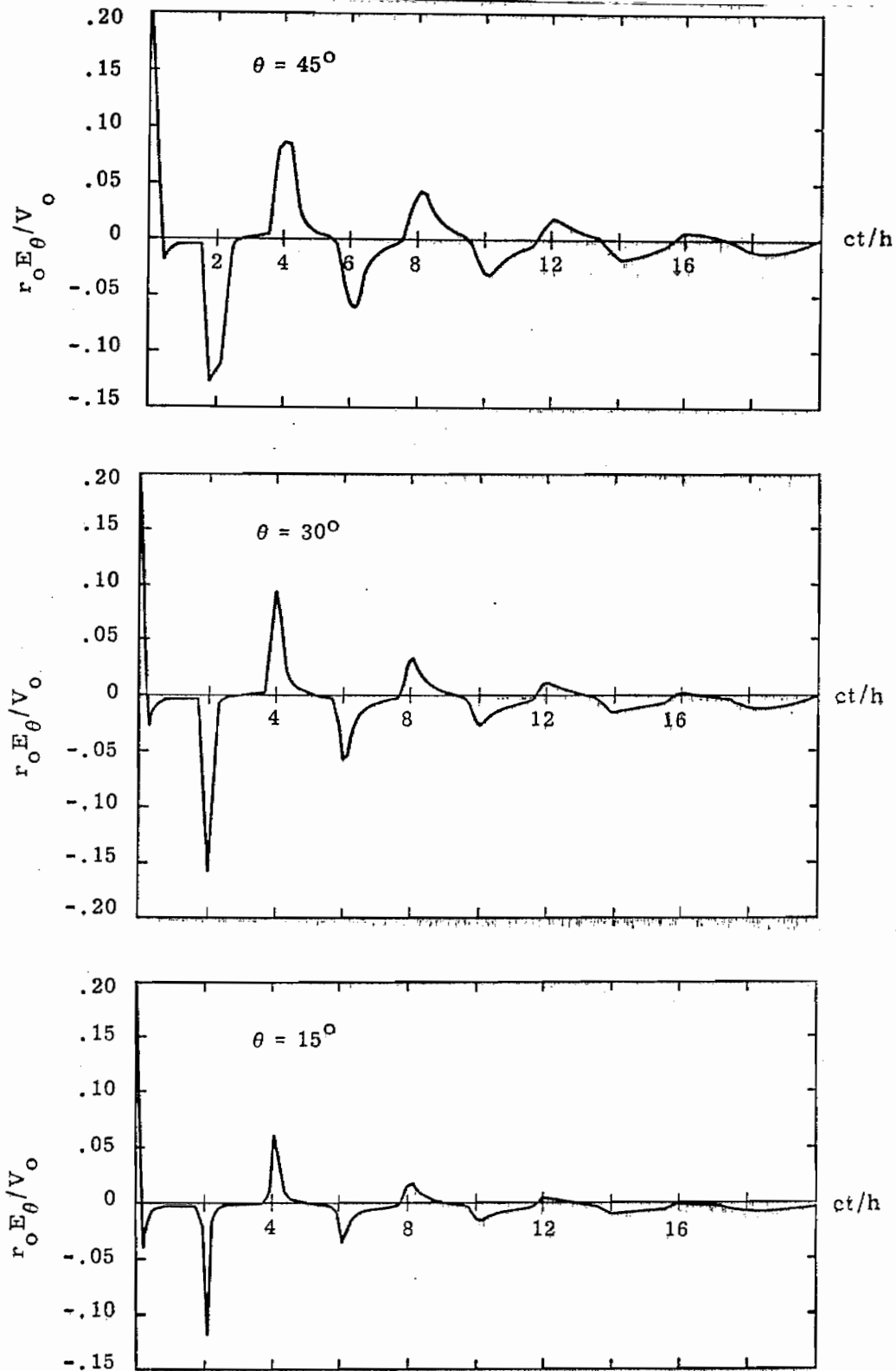
Figure 23. Radiation patterns in the time domain for step
excited antenna, a/h = .01, using the poles of
Table I.

V. <u>Numerical Results: The Uniformly Loaded Antenna</u>

The radiated fields of the unloaded antenna as presented in the last section do not look much like those encountered in a nuclear EMP, due to the marked oscillations in time. One way to modify the radiated fields is to add resistive loading along the structure, so as to reduce the end effects which cause the oscillations. In this section, a resistive load of the form $\Lambda(z) = C_1/L$ ohms/meter is studied. Other forms of the loading, which are slightly more effective for reducing the end effects, will be studied in succeeding sections.

With the constant load $\Lambda(z)$, it is expected that the pole locations, s_α, as well as the natural modes will be a function of the constant C_1. Figure 24 shows the pole trajectories for the uniformly loaded antenna of $a/h = .01$. As the value of C_1 increases, the poles in the first-layer move generally in the $-\sigma$ direction, indicating that their contributions in time attenuate more rapidly. The behavior of the $\ell = 2$ poles is not as simple and has not been thoroughly investigated, but it is known that these are not extremely important in determining the late time behavior of the antenna.

The behavior of the $\ell = 1$, $n = 1$ pole deserves special attention. As the loading is increased, this pole moves on a curved arc down to the $-\sigma$ axis, at which point a double pole is formed with its conjugate pole. As the loading is further increased, this double pole splits, one pole moving to $-\infty$ and the other to 0 along the σ axis. This behavior is completely analogous to that encountered in a resonant R-L-C circuit. At the point where the double pole first is formed, the circuit is referred to as being critically damped. The other two cases are overdamped and underdamped.

The same terminology can be applied to the antenna problem. From Figure 24, it is noted that for $C_1 = 1683\Omega$, the antenna may be defined as being critically damped. The large dots indicate the positions of the other poles for this value of loading.

This value of critical loading should be a function of the wire radius. As shown in Figure 25, the critical value of C_1 is a linear function of $\Omega = 2 \ln (2h/a)$.

The natural modes (and coupling vectors) are presented in Figures 26 and 27 for the $l = 1$ poles only, and are seen to be quite similar to those of the unloaded antenna.

Figures 28 and 29 show the magnitudes of the far field natural modes for $l = 1$ and $n = 1 \cdots 6$ in polar form. Figures 30 and 31 show the real and imaginary parts of the same far field modes.

The data presented in Table II is sufficient to determine the time domain behavior of the antenna current and the radiated fields, which are shown in Figures 32 through 35. Note that the current does not oscillate in time, but shows an exponential like decay. The radiated field, which is proportional to the time derivative of the current, has one zero crossing, but never oscillates in time. It is apparent that the end effects are observable in both the input current and the radiated fields. A loading which is heavier on the ends will suppress some of these effects.
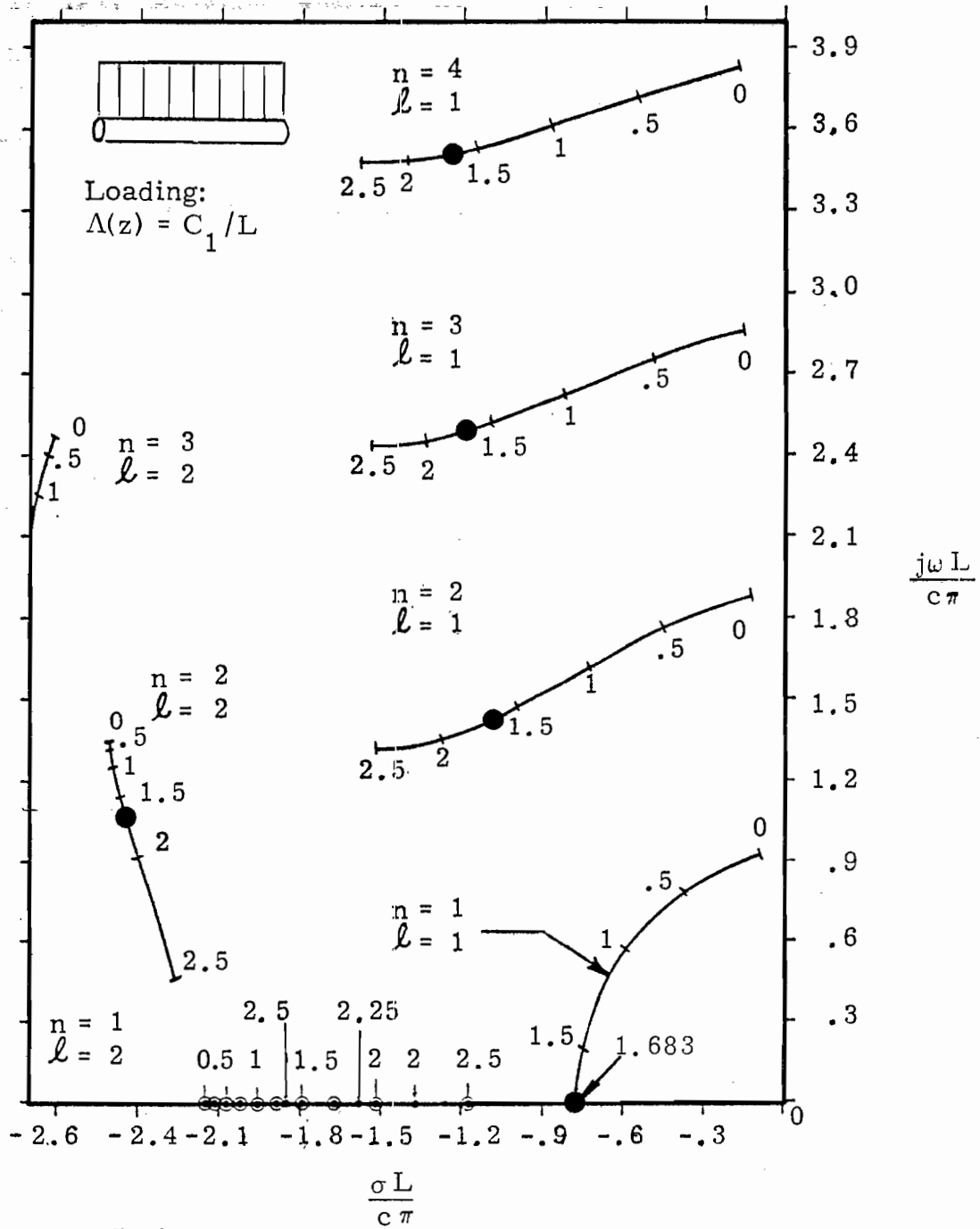
Figure 24. Pole trajectories for wire of a/h = .01 as a function of the constant C_1 (in kilohms)
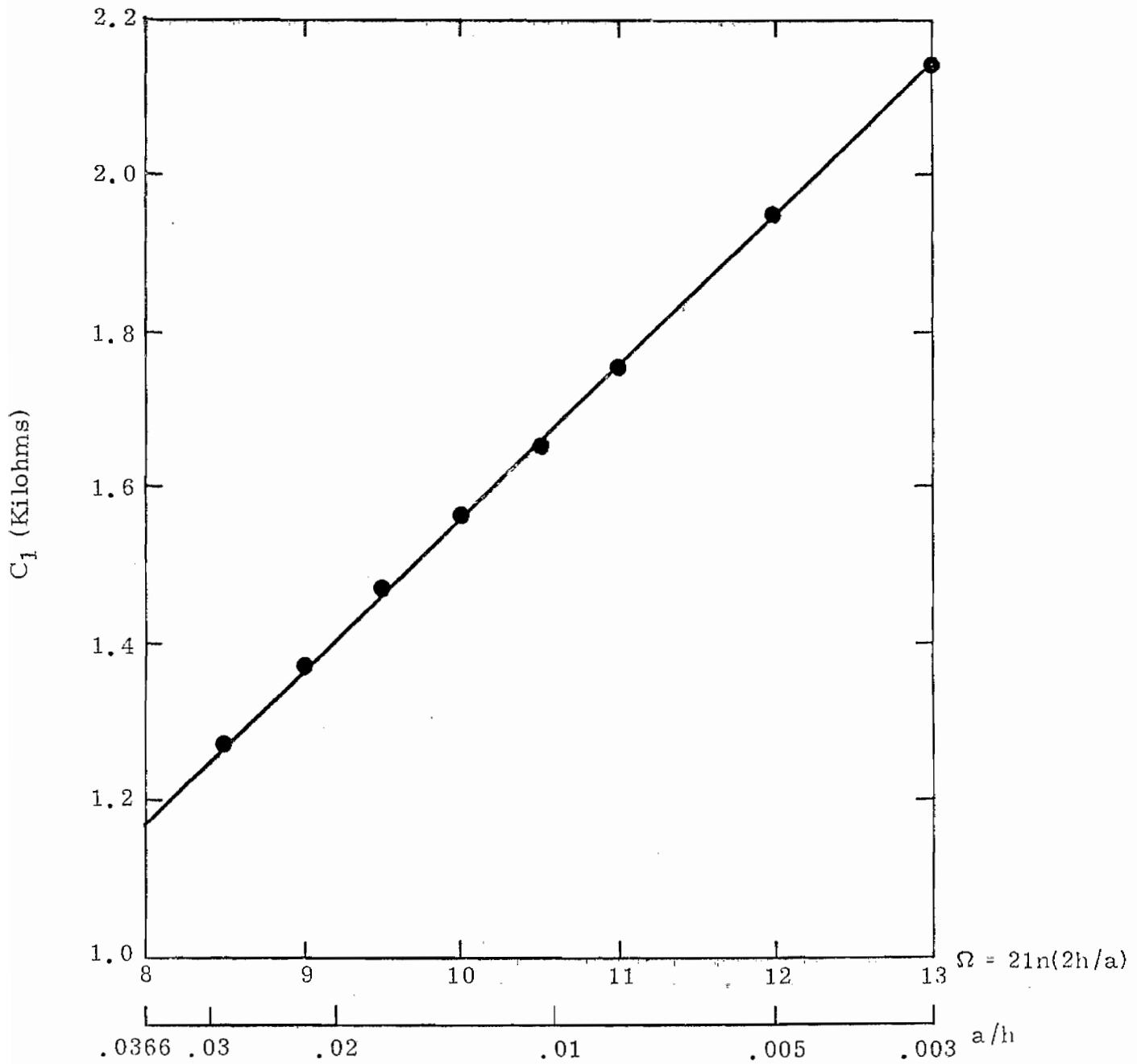
Figure 25. Plot of the constant C_1 for critical loading of the form $\Lambda(z) = C_1/2h$.
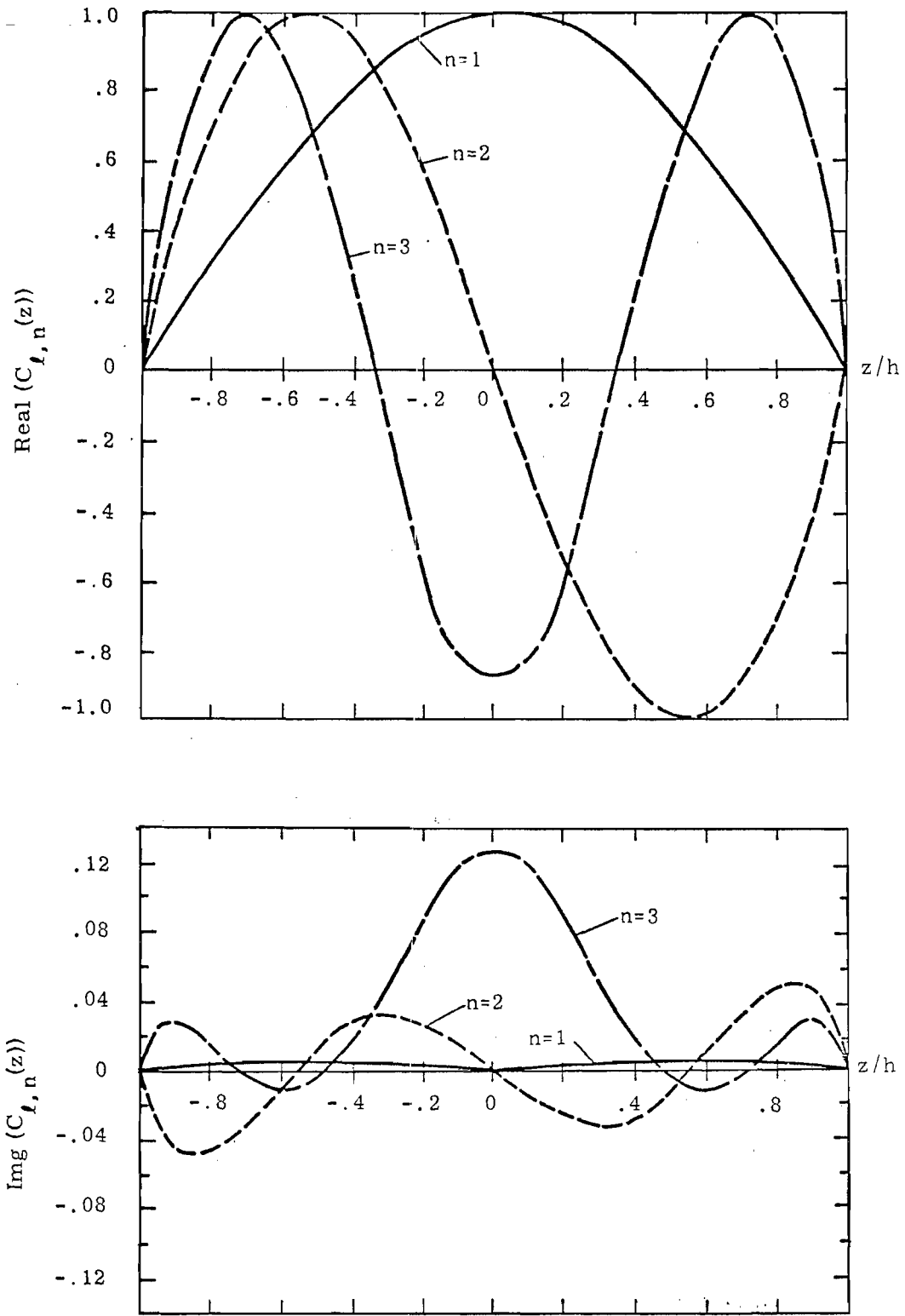
Figure 26. Real and imaginary parts of the natural current
mode (and the coupling vector) for the $\ell = 1$
layer poles of the critically damped antenna
(constant load), $C_1 = 1683\Omega$, $a/h = .01$.
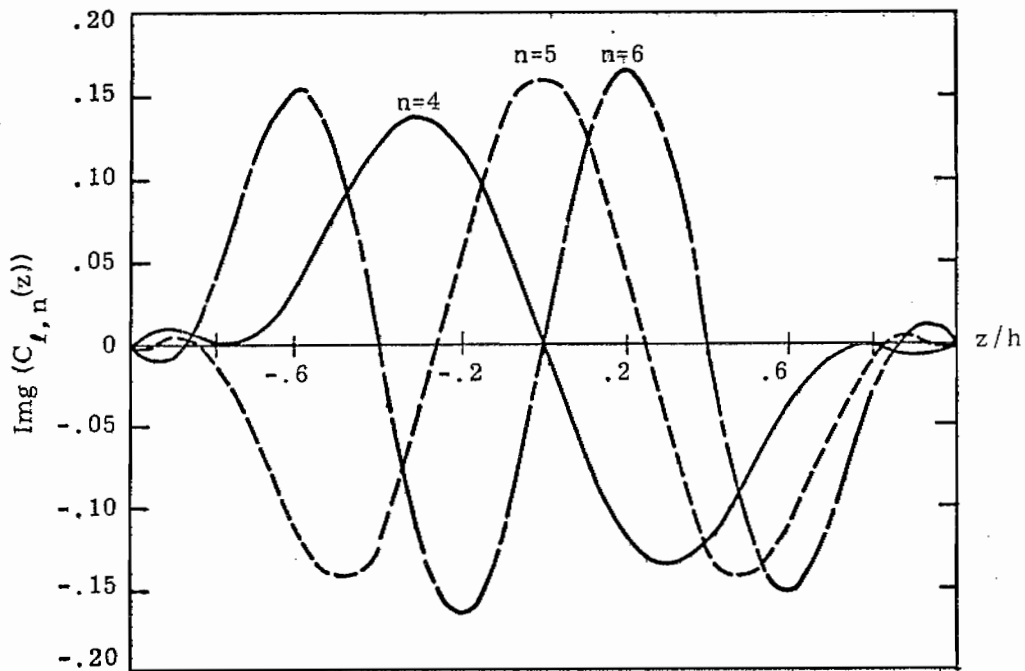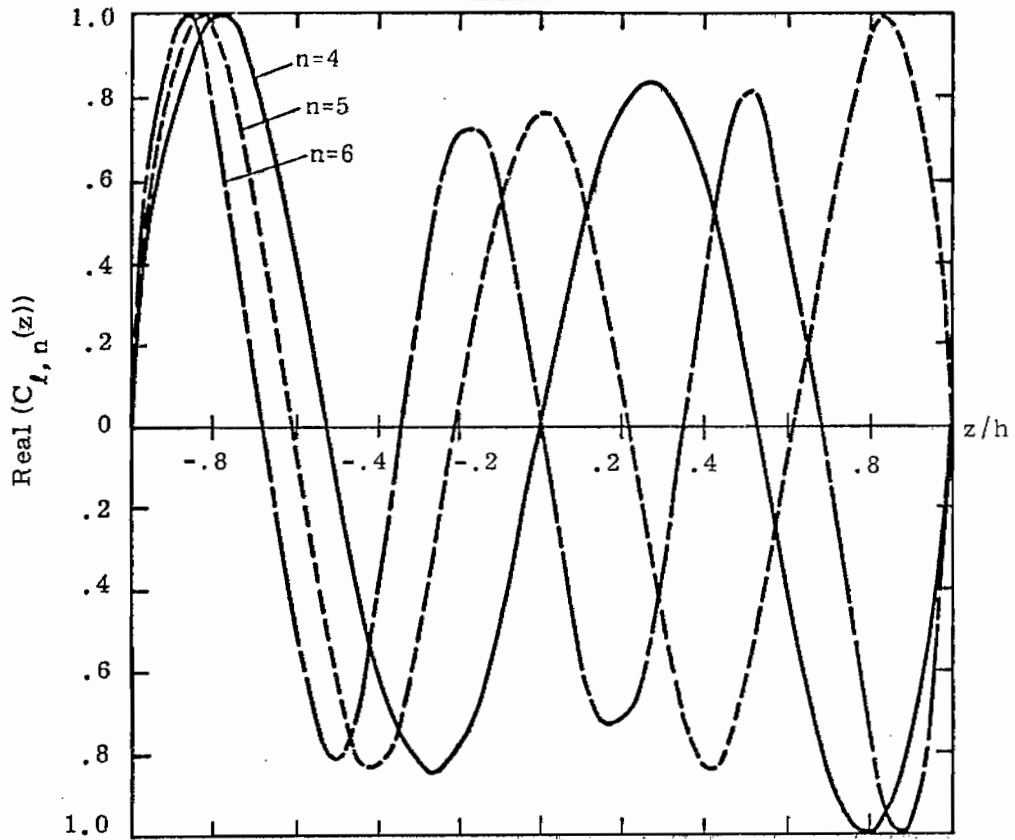
Figure 27. Real and imaginary parts of the natural current
mode (and the coupling vector) for the $\ell = 1$
layer poles of the critically damped antenna
(constant load), $C_1 = 1683\,\Omega$, $a/h = .01$.

48
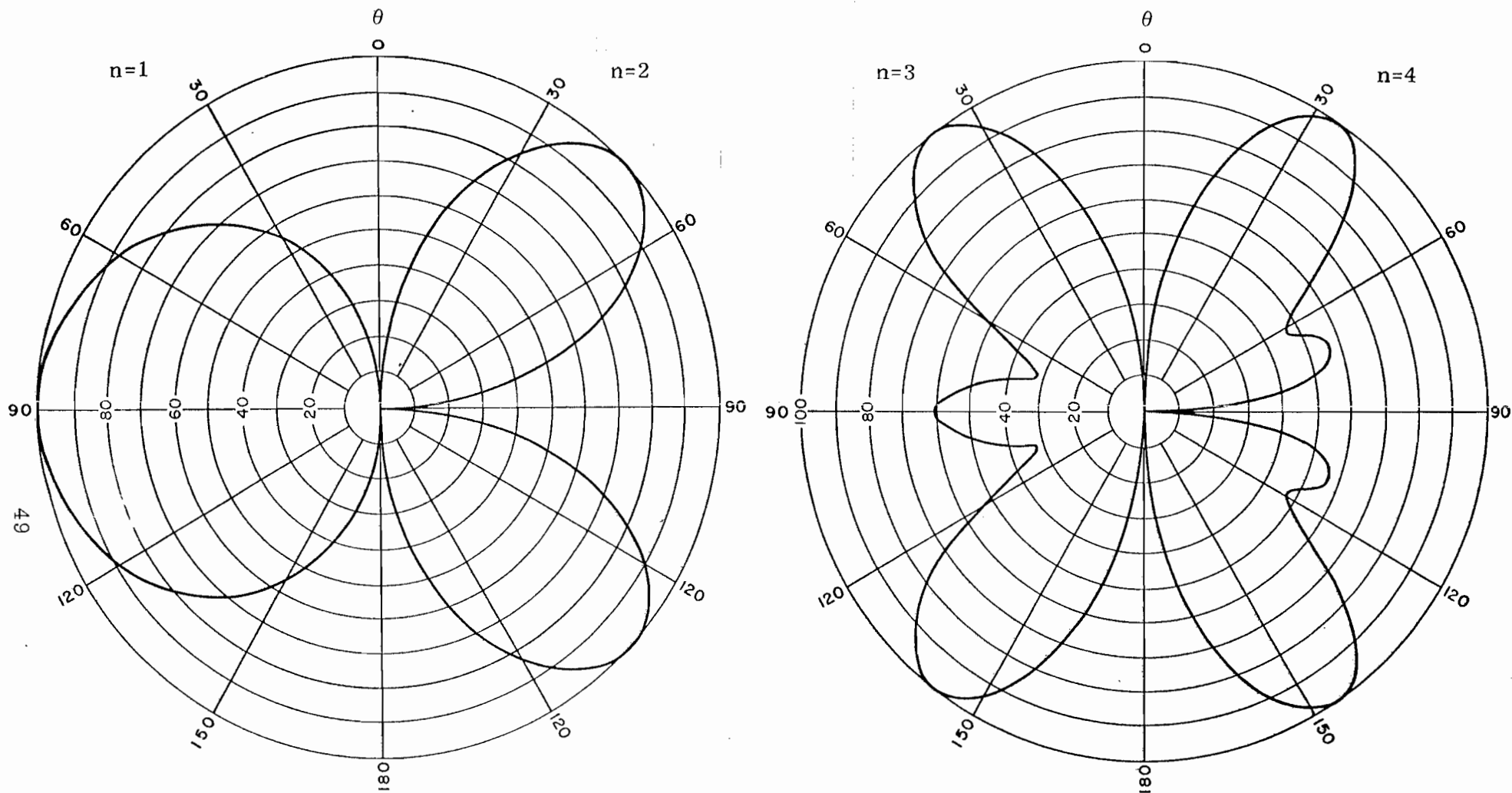
Figure 28. Polar plots of the magnitude of the normalized far field modes $e_{\ell,n}(\theta)$ for the $\ell=1$ poles of a uniform resistively loaded antenna.
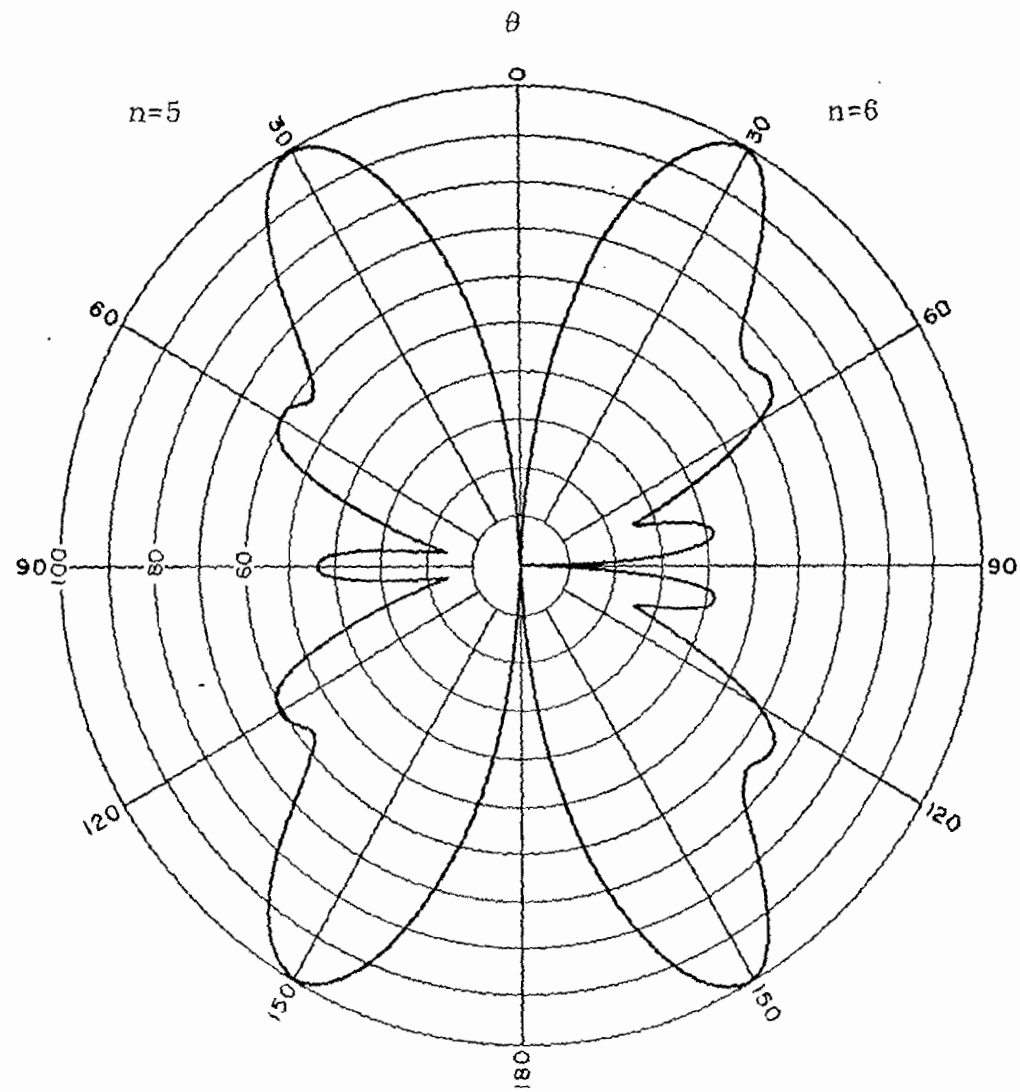
Figure 29. Polar plots of the magnitude of the normalized far field modes $e_{\ell n}(\theta)$ for the $\ell = 1$ poles of a uniform resistively loaded antenna.
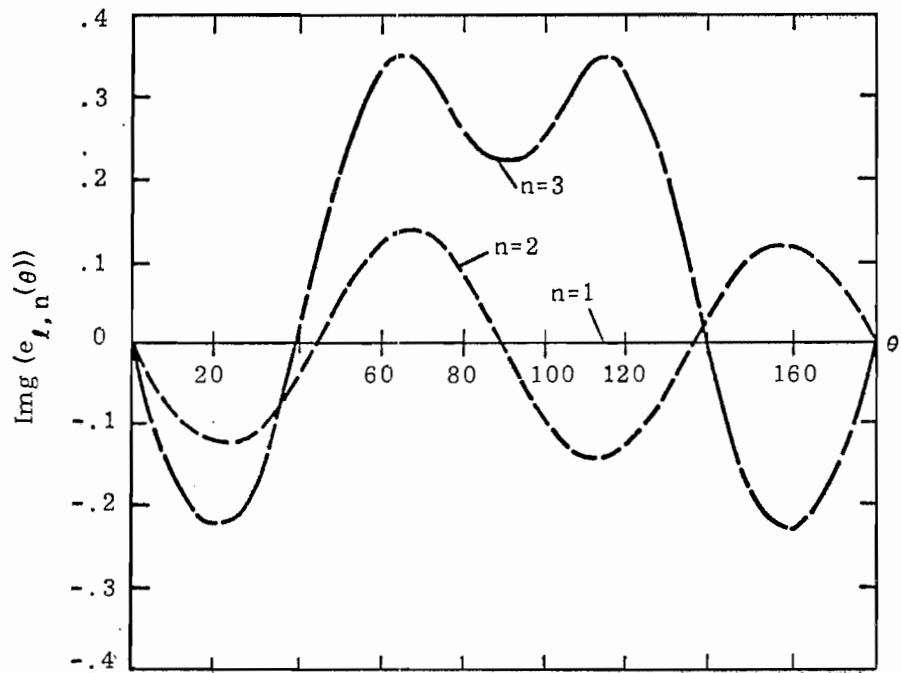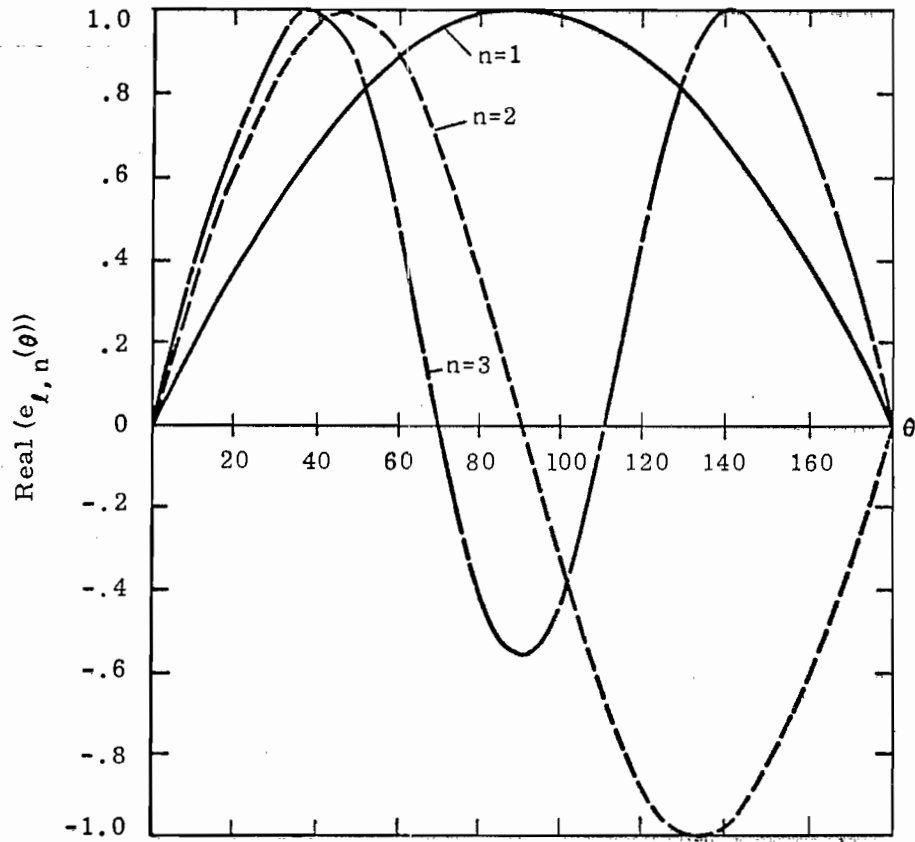
Figure 30. Real and imaginary parts of the normalized far field mode for the $\ell = 1$ layer poles of the critically loaded antenna (constant loading), $a/h = .01$.

51
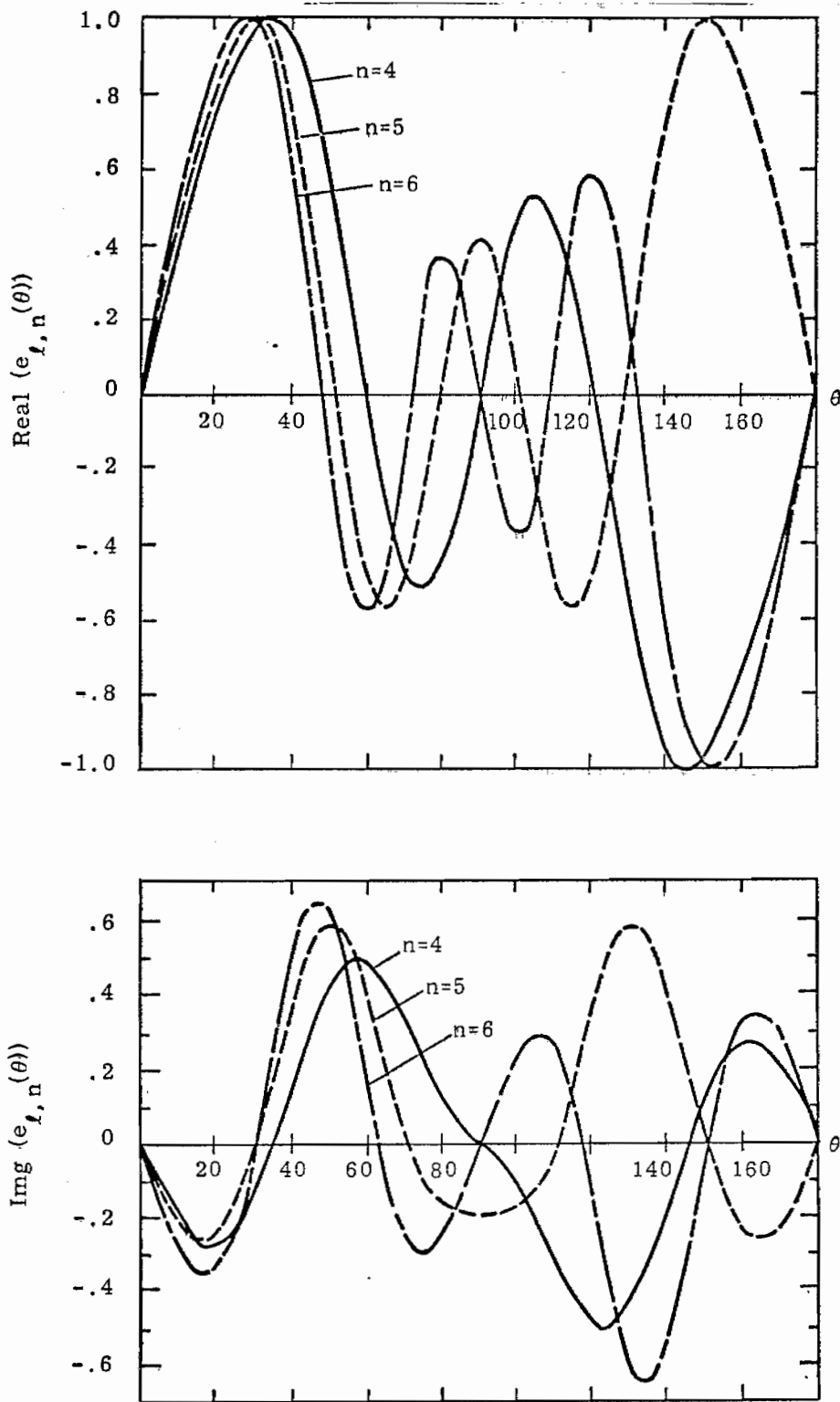
Figure 31. Real and imaginary parts of the normalized
far field mode for the $\ell = 1$ layer poles of
the critically loaded antenna (constant loading),
a/h = .01.

TABLE II

Data for Critically Damped Uniformly Loaded Antenna
of $a/h = .01$ ($\Omega = 10.59$)

Loading Function is $\Omega(z) = C_1/L$; $C_1 = 1683\Omega$

| Pole α | | Natural Frequency $s_\alpha L/c\pi$* | | Current Normalization (x 10^3) | | Field Normalization | | Coupling Coeff. (x10^1) Step Excitation ** | | Decay Time |
l	n	$\sigma L/c\pi$	$j\omega L/c\pi$	$Re(\beta_\alpha)$	$Im(\beta_\alpha)$	$Re(\beta_\alpha^{(F)})$	$Im(\beta_\alpha^{(F)})$	$Re(\eta)$	$Im(\eta)$	$c\tau_\alpha/h$
1	1	- .772	.023	1.784	7.159	19.106	.004	- .412	-.125	.825
1	2	-1.032	1.465	3.009	1.635	4.749	-12.193	0	0	.617
1	3	-1.127	2.523	3.159	1.319	-9.547	- 5.754	.533	.849	.565
1	4	-1.191	3.543	3.427	1.282	-5.750	7.986	0	0	.534
1	5	-1.241	4.549	3.846	1.509	7.218	5.170	- .221	-.429	.513
1	6	-1.282	5.548	3.977	1.375	5.643	- 5.815	0	0	.496
1	7	-1.318	6.544	4.240	1.454	-5.935	- 4.552	.122	.251	.483
1	8	-1.349	7.538	4.216	1.514	-4.846	5.085	0	0	.472
1	9	-1.377	8.530	4.721	1.646	4.227	5.056	- .075	-.156	.462
1	10	-1.403	9.522	4.951	1.746	5.183	- 3.368	0	0	.454
1	11	-1.425	10.510	5.167	1.541	-4.310	- 3.947	.047	.098	.447
1	12	-1.445	11.494	5.495	1.742	-4.000	3.752	0	0	.441
2	1	-1.796	0.0	-2.416	0.0	20.278	0.0	0.0	0	.354
2	2	-2.476	1.136	- .683	3.452	-9.802	9.325	-1.051	-.473	.257

*$L = 2h = $ Total Antenna Length

**Coupling Coefficient is for a Center Driven Antenna with Gap $\Delta = .1L$
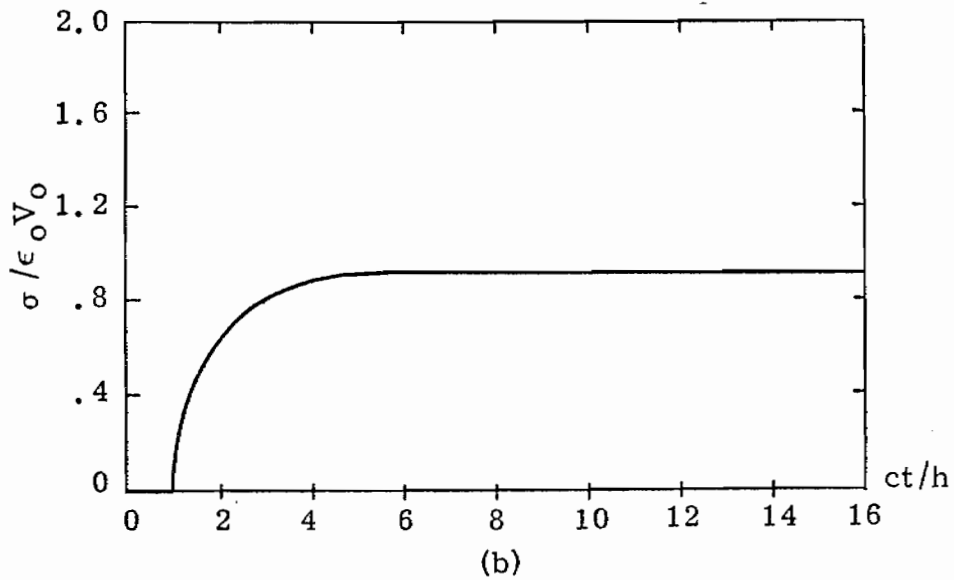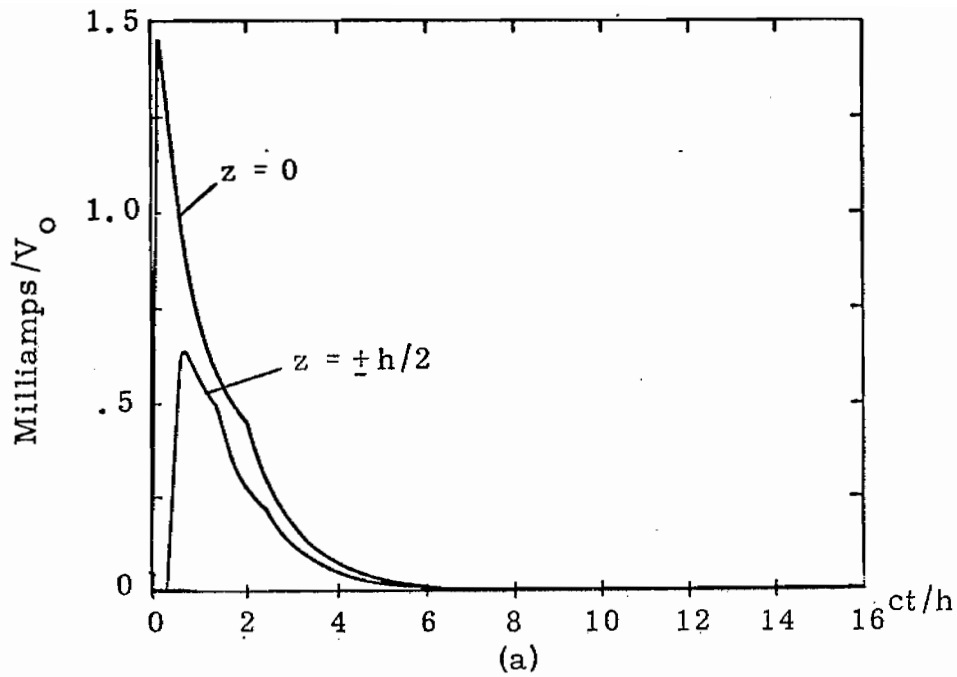
Figure 32. Time history plots of (a) the current at the input of the antenna and at $z = \pm h/2$ and (b), the linear charge density at $z = h$ for the uniform resistively loaded antenna, with $C_1 = 1683\Omega$, $a/h = .01$, and using the poles of Table II.
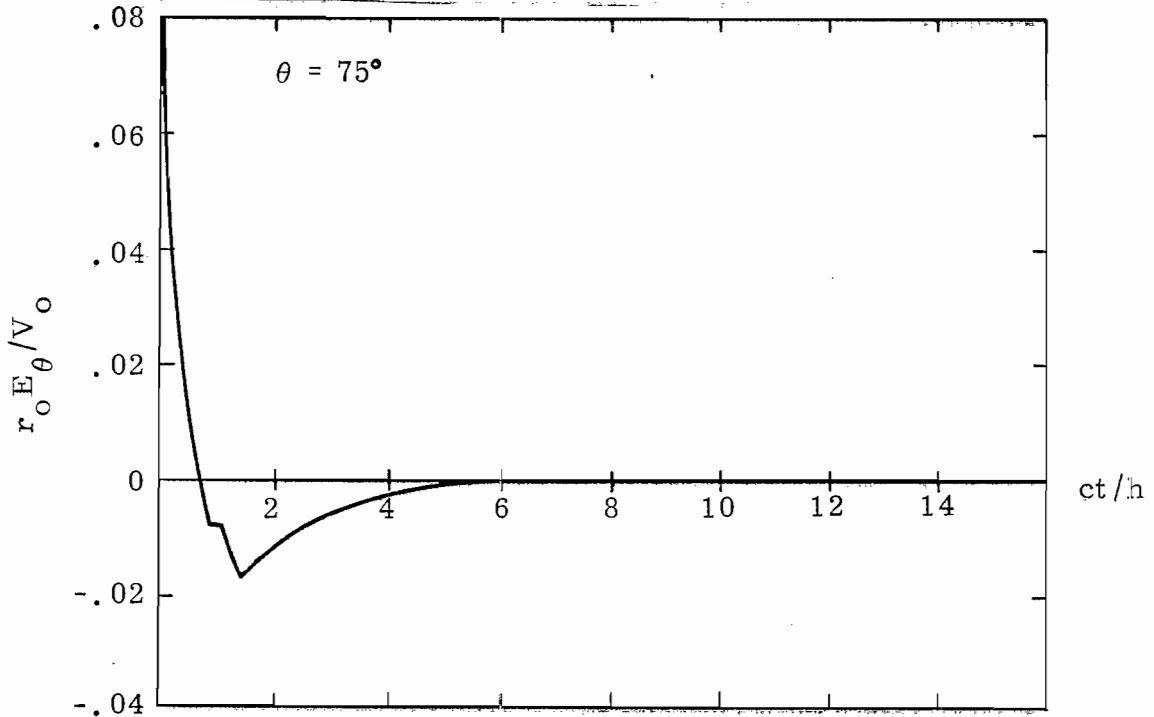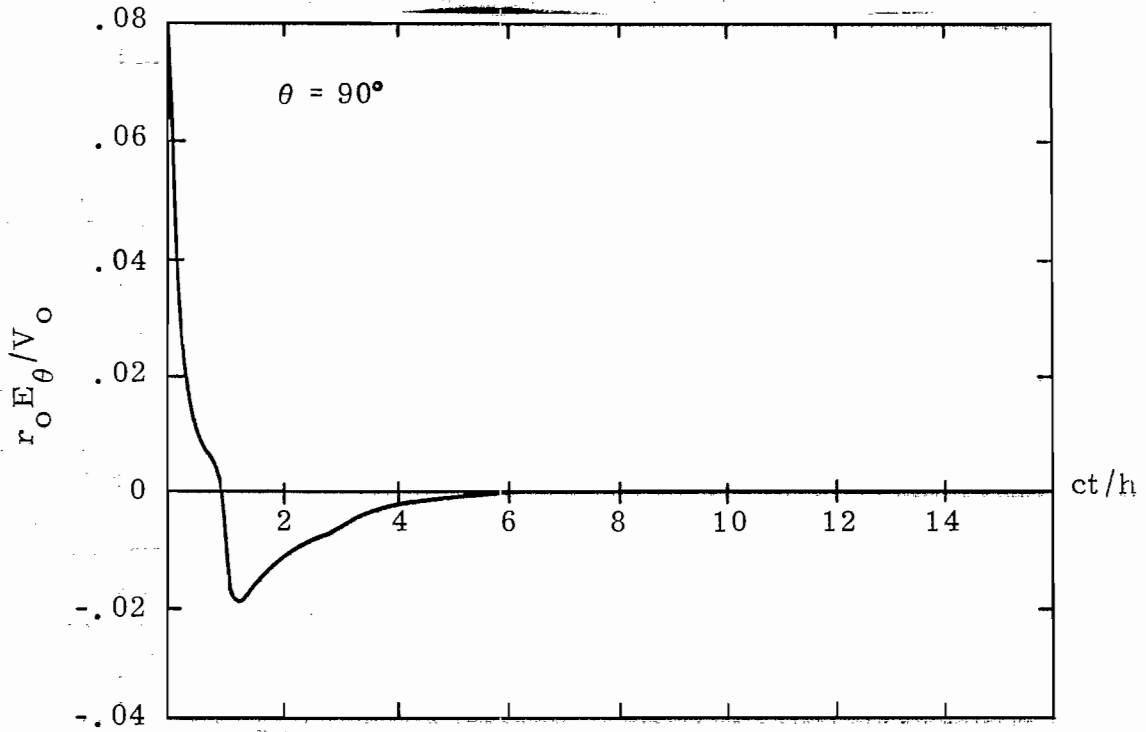
Figure 33. Time history plots of the radiated electric field
from a uniform resistively loaded antenna,
with $C_1 = 1683\Omega$, $a/h = .01$ and using the poles
of Table II.
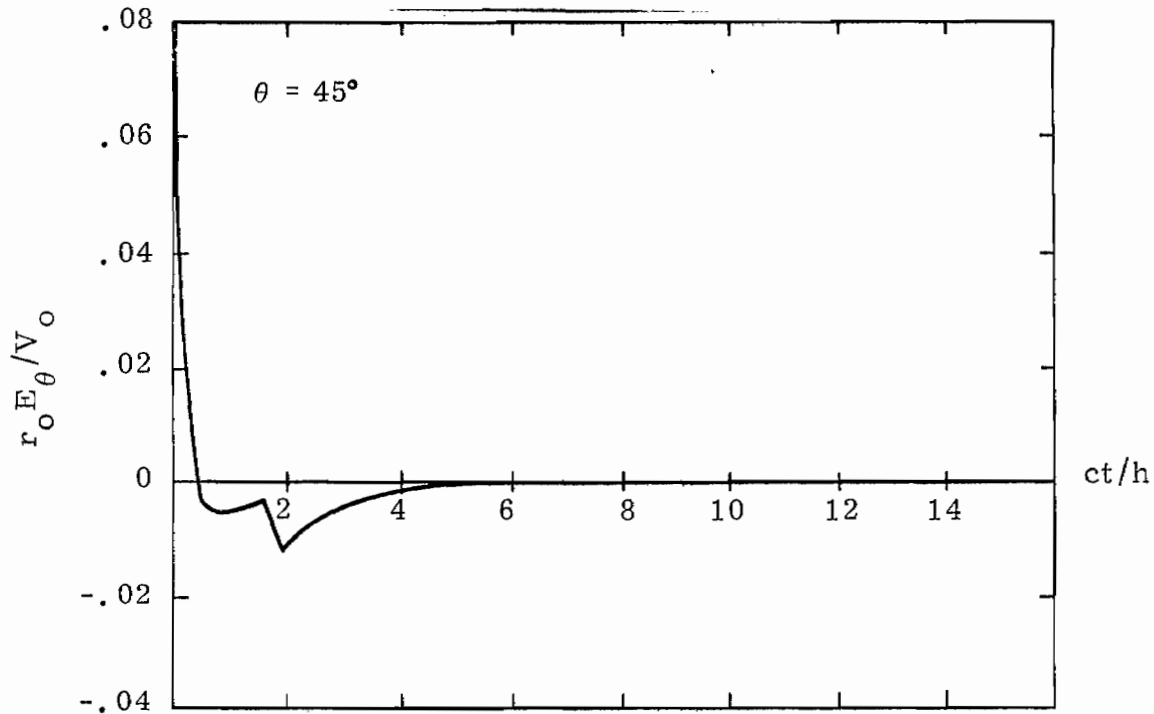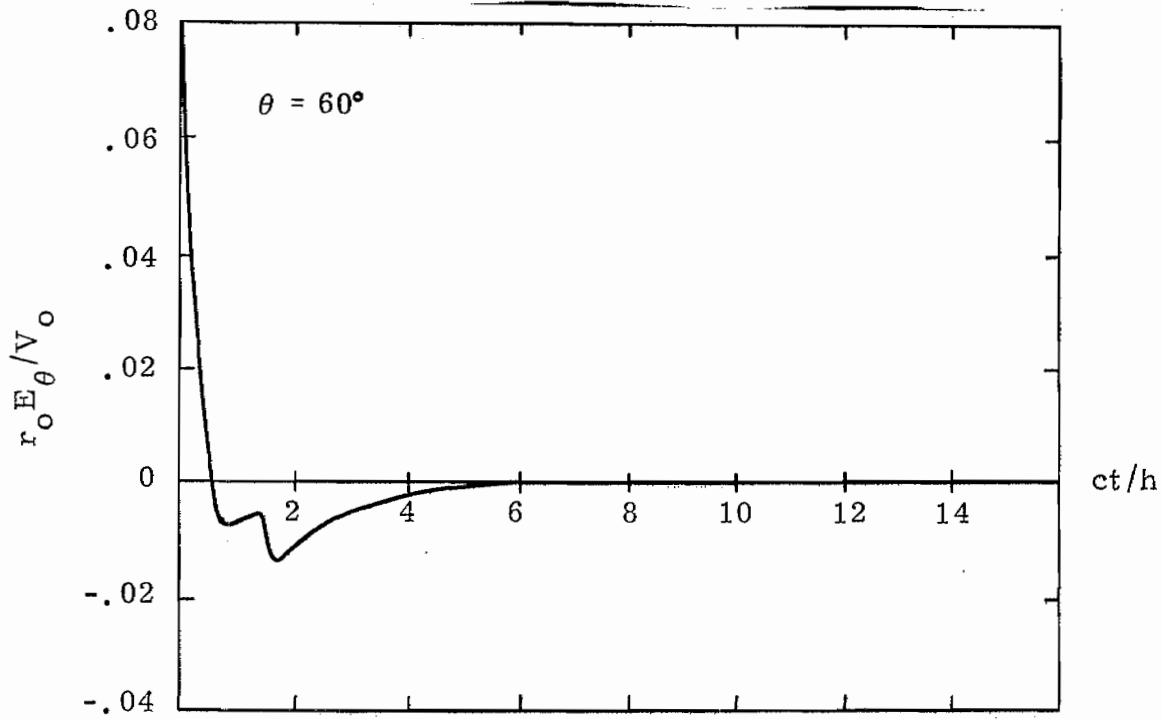
Figure 34. Time history plots of the radiated electric field from a uniform resistively loaded antenna, with $C_1 = 1683\Omega$, $a/h = .01$ and using the poles of Table II.
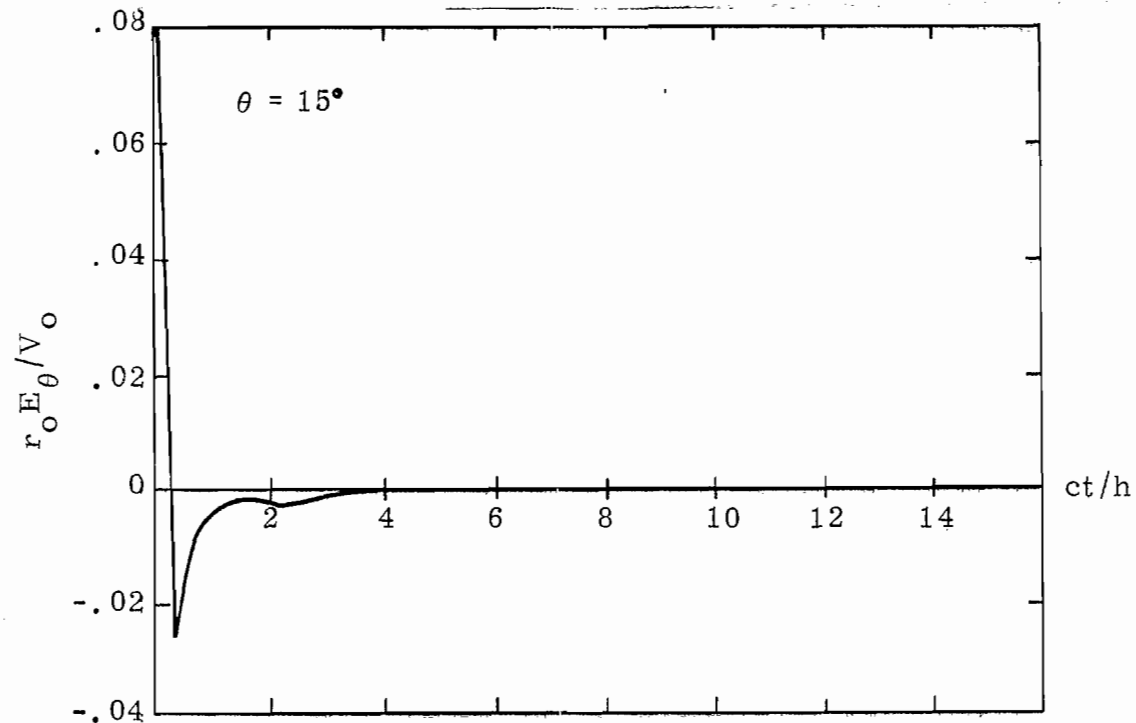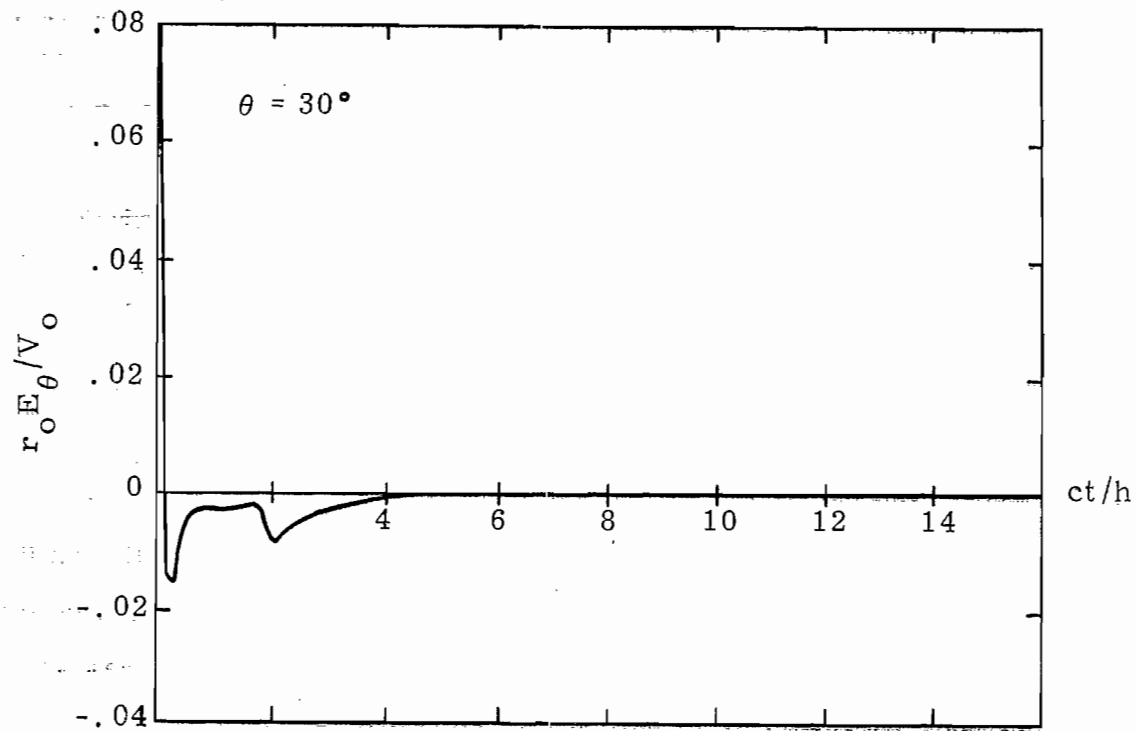
Figure 35. Time history plots of the radiated electric
field from the uniform resistively loaded antenna,
with $C_1 = 1683\Omega$, $a/h = .01$ and using the poles
of Table II.

VI. Numerical Results: The Linearly Loaded Antenna

Another class of loading distributions that may be useful in EMP simulation is the linear loading, described by the function $\Lambda(z) = C_2 |z|/L^2$. This loading is investigated in this section. As before, $a/h = .01$.

The data presented here is in the same form as in the previous two sections. Figure 36 shows the pole trajectories as a function of the constant C_2 and Figure 37 shows C_2 as a function of Ω for critical damping. The natural current modes are shown in Figures 38 and 39, while the radiated field modes are presented in Figures 40 through 43. The time domain responses of the currents, charge and far fields are shown in Figures 44 through 47, and Table II gives the normalizing constants.

Referring to Figure 44a, it is seen that the end effects in the current which occur at $ct/h \approx 2$ are much less than in the previous uniformly loaded case. This is due to the fact that the loading is much heavier near the ends in the present case, and this tends to alleviate the traveling waves reflected at the antenna ends.
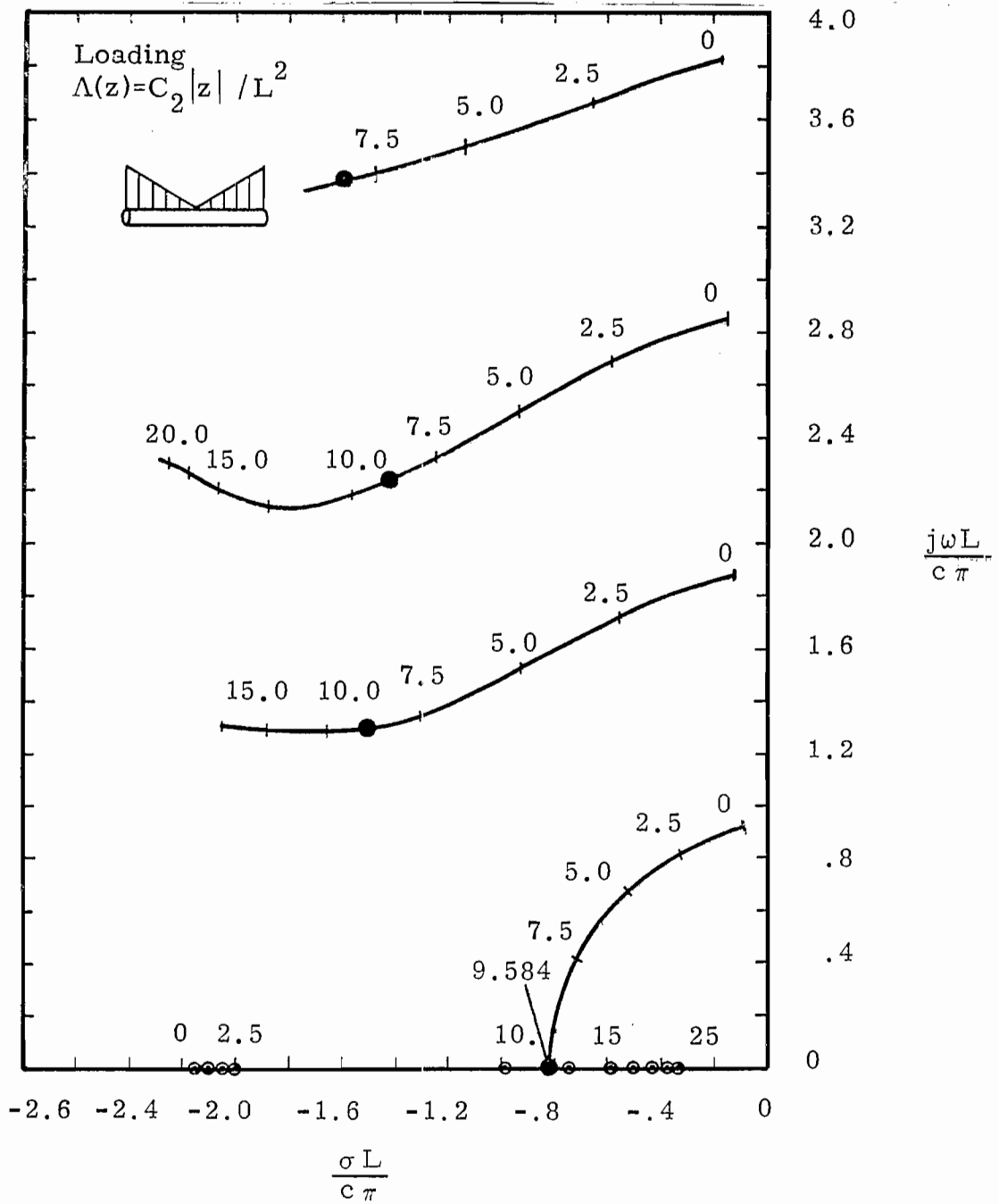
Figure 36. Pole trajectories for wire of a/h = .01 as a function of the constant C_2 (in Kilohms).
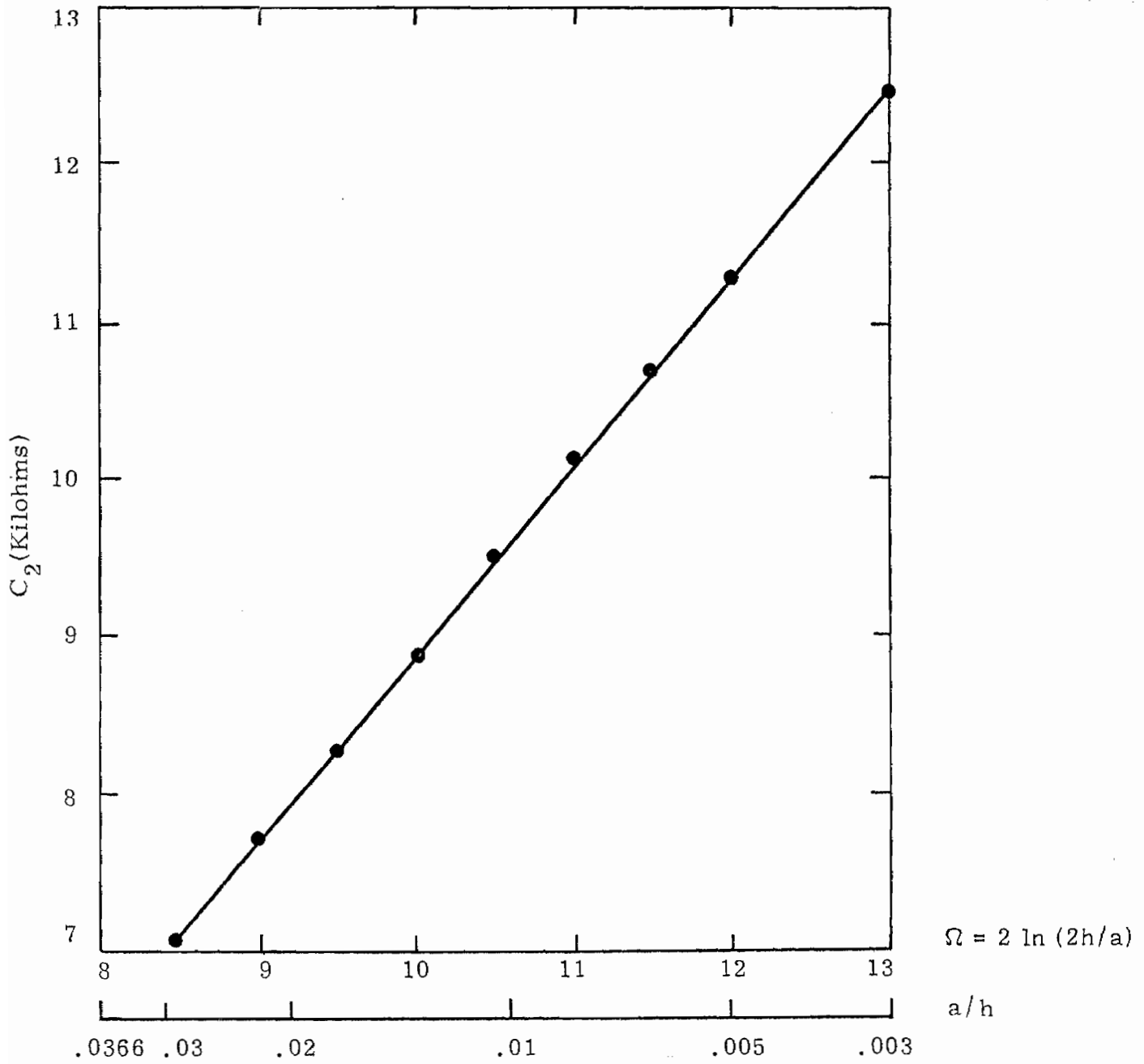
Figure 37. Plot of the constant C_2 for critical loading of the form $\Lambda(z) = C_2 |z| /(2h)^2$.
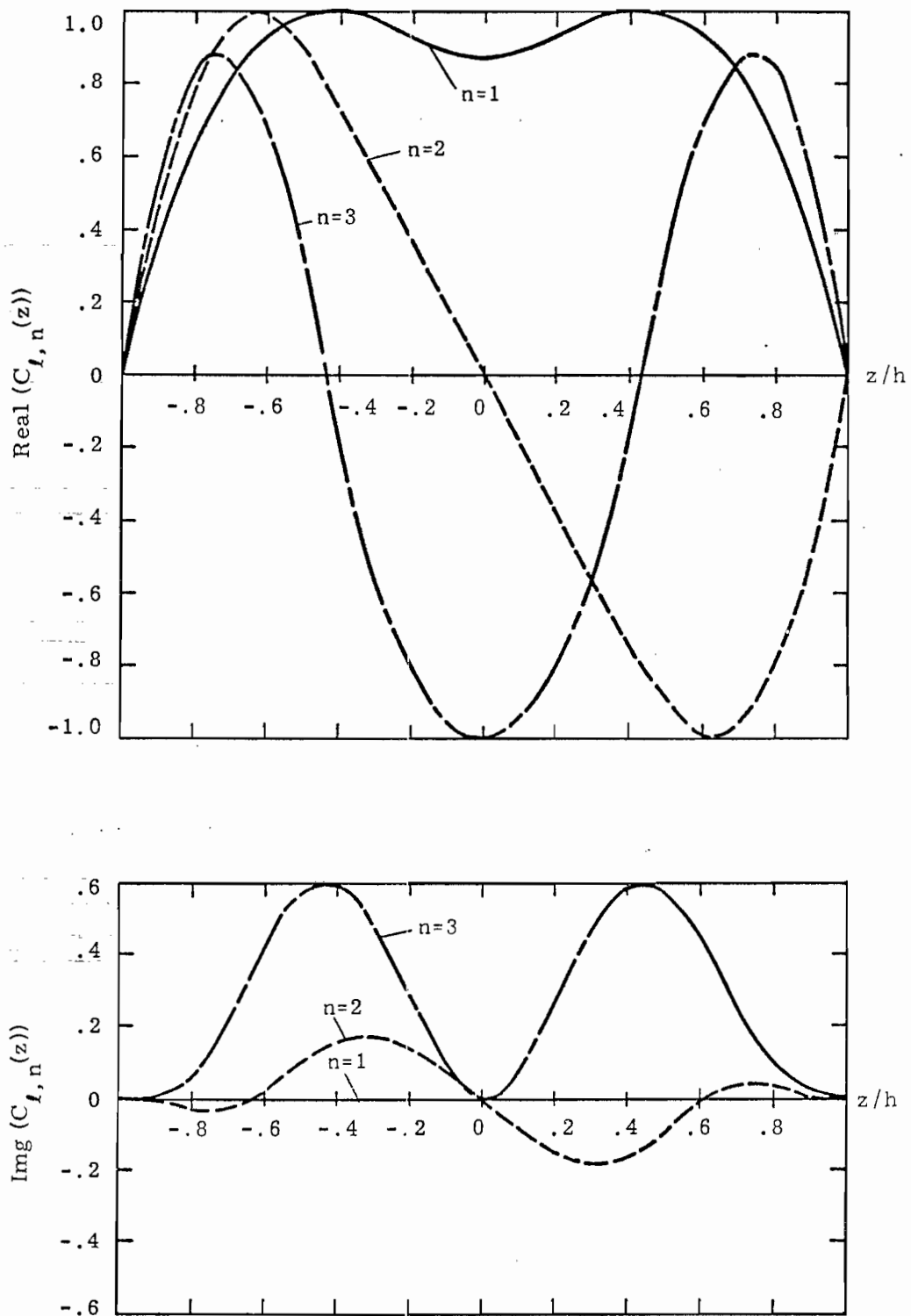
Figure 38. Real and imaginary parts of the natural current mode (and the coupling vector) for the $\ell = 1$ layer poles of the critically damped antenna (linear load), with $C_2 = 9548\Omega$, and a/h = .01.

61

Figure 39. Real and imaginary parts of the natural current mode (and the coupling vector) for the $l = 1$ layer poles of the critically damped antenna (linear load), with $C_2 = 9548\Omega$, and $a/h = .01$.

62
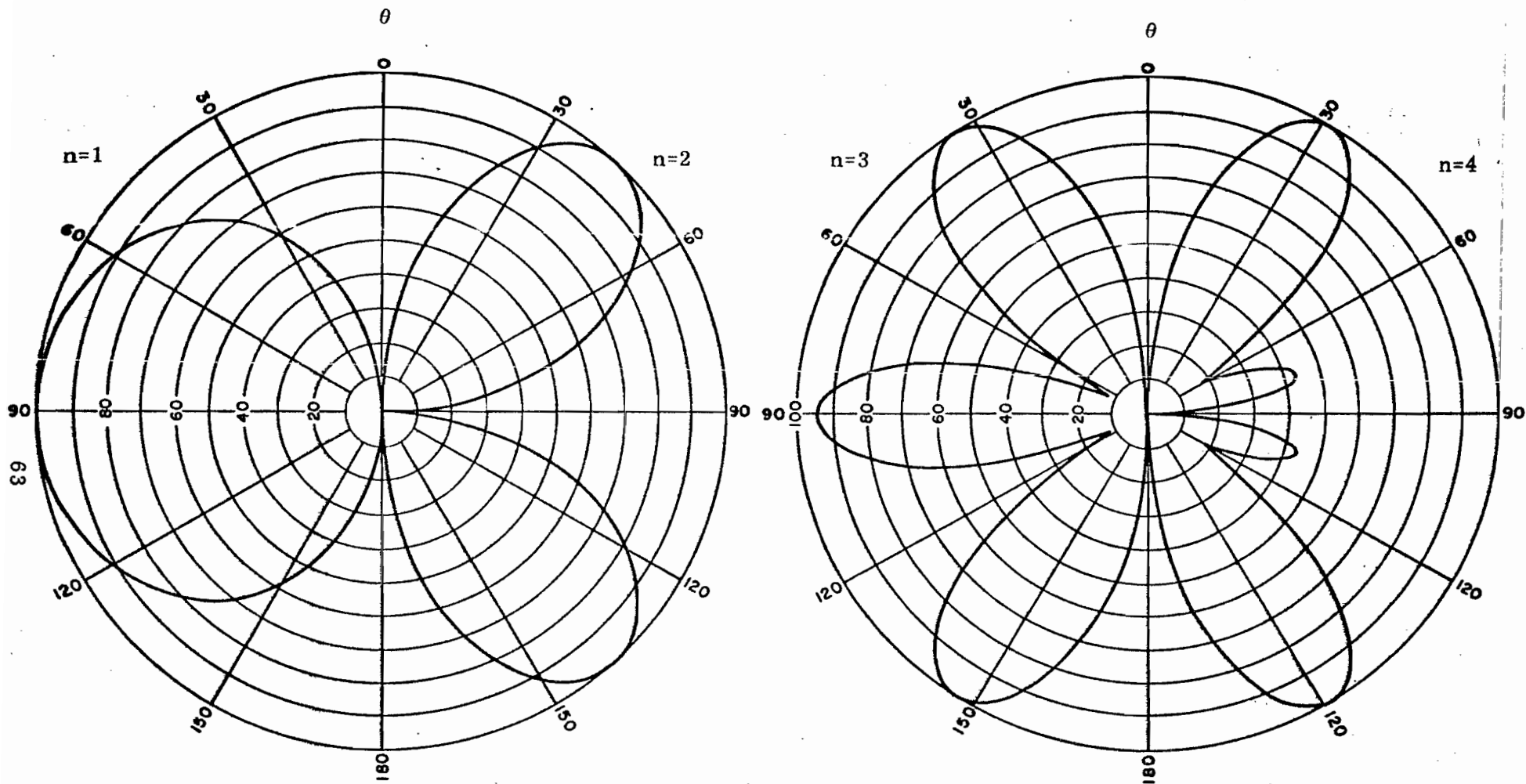
Figure 40. Polar plots of the magnitude of the normalized far field modes $e_{\ell,n}(\theta)$ for $\ell=1$ poles of a constant slope resistively loaded antenna.
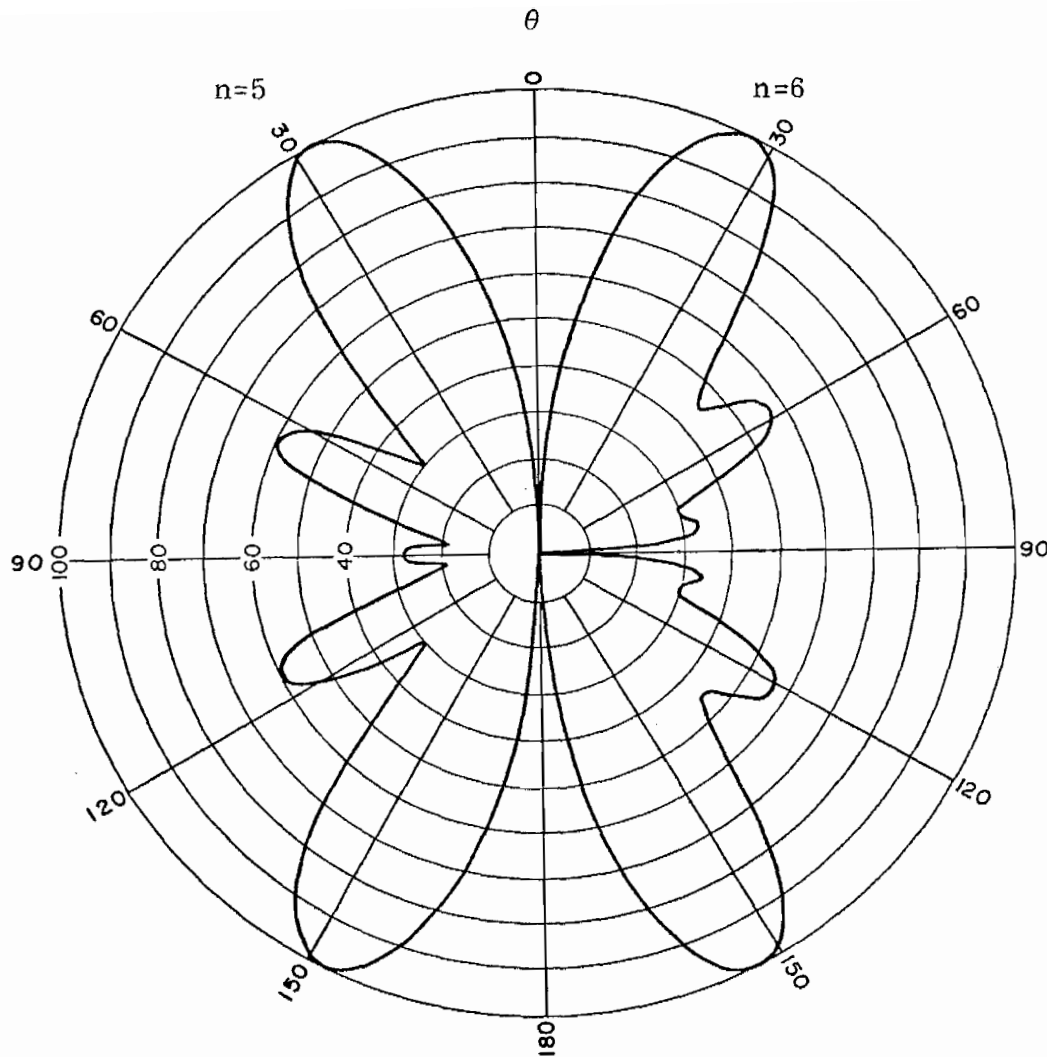
Figure 41. Polar plots of the magnitude of the normalized far field modes $e_{\ell,n}(\theta)$ for $\ell=1$ poles of a constant slope resistively loaded antenna.
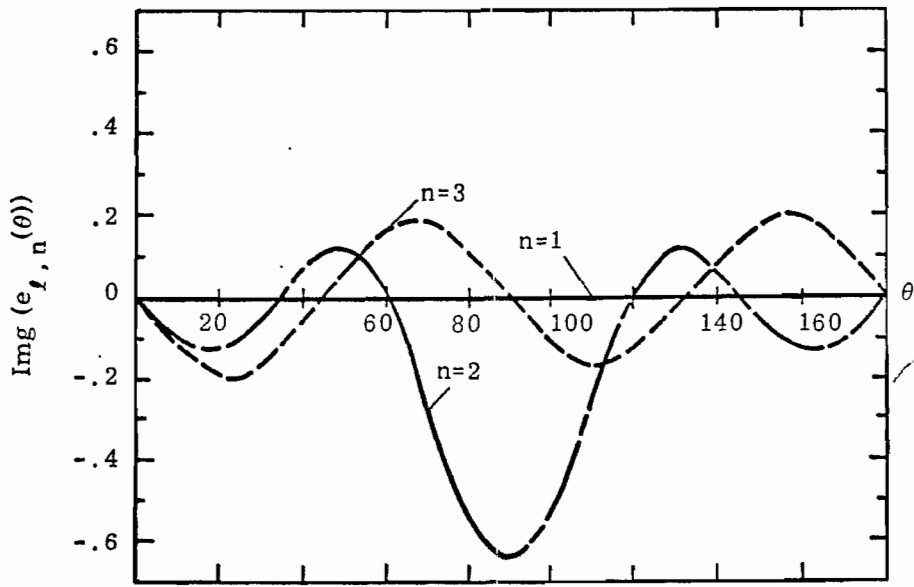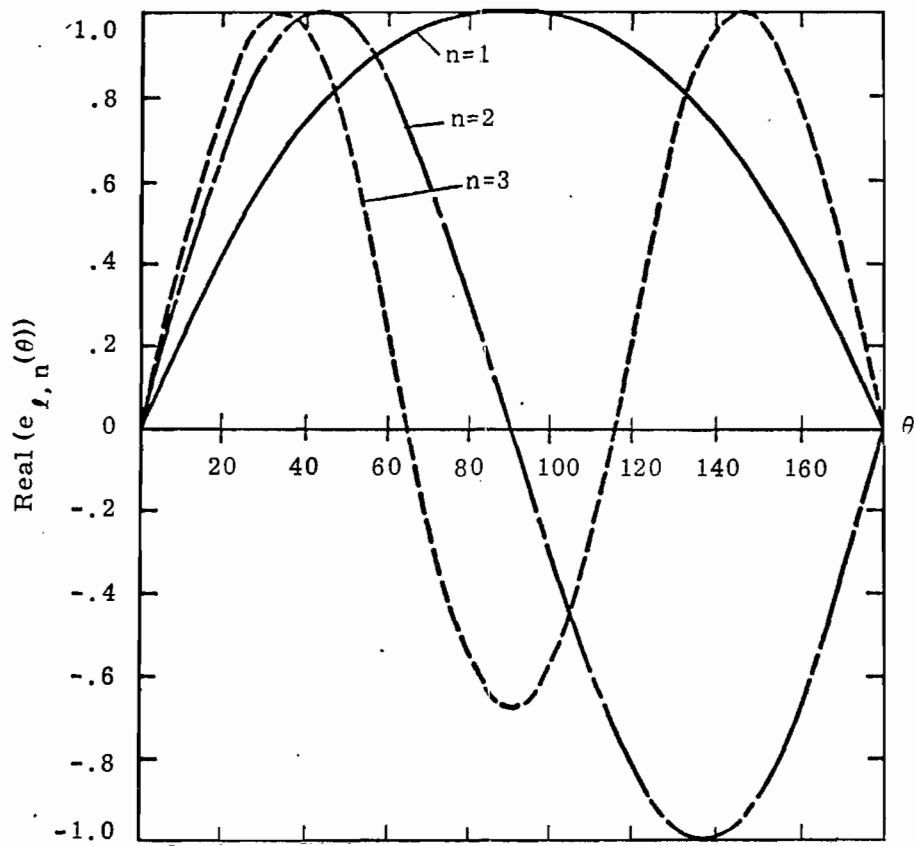
Figure 42. Real and imaginary parts of the normalized far
field mode for the $l=1$ layer poles of the critically
damped antenna (linear load), with $C_2 = 9548\Omega$,
and a/h = .01.
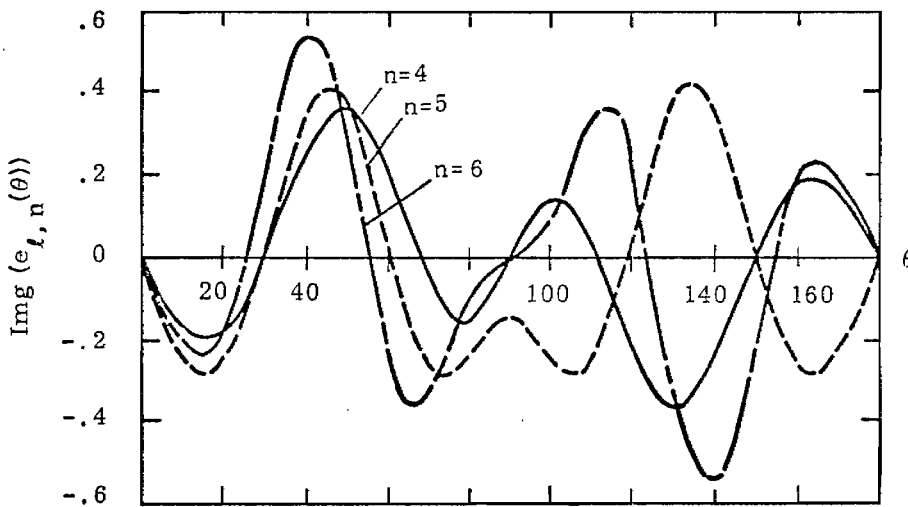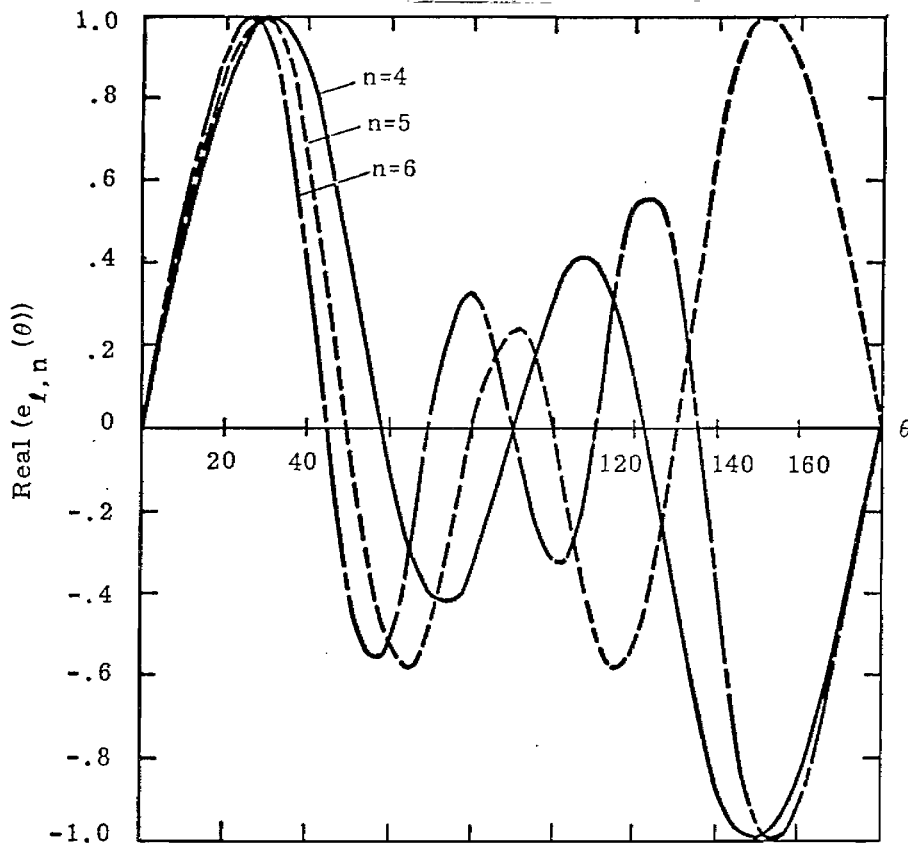
Figure 43. Real and imaginary parts of the normalized far field mode for the $\ell=1$ layer poles of the critically damped antenna (linear load), with $C_2 = 9548\,\Omega$, and $a/h = .01$.

TABLE III

Data for Critically Damped Linearly Loaded Antenna
of $a/h = .01$ ($\Omega = 10.59$)

Loading function is $\Omega(z) = C_2|z|/L^2$; $C_2 = 9584\Omega$

| Pole α | | Natural Frequency $s_\alpha L/c\pi$* | | Current Normalization (x 10^3) | | Field Normalization | | Coupling Coeff. (x10^1) Step Excitation ** | | Decay Time |
l	n	$\sigma L/c\pi$	$j\omega L/c\pi$	$Re(\beta_\alpha)$	$Im(\beta_\alpha)$	$Re(\beta_\alpha^{(F)})$	$Im(\beta_\alpha^{(F)})$	$Re(\eta)$	$Im(\eta)$	$c\tau_\alpha/h$
1	1	-.834	.031	1.485	42.536	23.660	-.019	-3.321	-.173	.763
1	2	-1.529	1.296	3.222	.222	8.85	-14.374	0	0	.416
1	3	-1.416	2.237	5.238	.631	-6.527	-5.542	-.666	-.987	.449
1	4	-1.590	3.383	3.609	-.282	-6.953	7.618	0	0	.400
1	5	-1.634	4.381	4.052	-.718	5.199	6.958	.210	.537	.390
1	6	-1.703	5.414	3.563	-.928	6.868	-5.593	0	0	.374
1	7	-1.739	6.414	3.682	-.985	-4.506	-6.908	.102	.355	.366
1	8	-1.786	7.425	3.578	-1.166	-7.275	3.438	0	0	.356
1	9	-1.814	8.422	3.643	-1.399	2.192	7.142	-.054	-.237	.351
1	10	-1.851	9.425	3.911	.436	5.177	-5.143	0	0	.344

*$L = 2h$ = Total Antenna Length

**Coupling Coefficient is for a Outer Driven Antenna with gap $\Delta = .1L$.
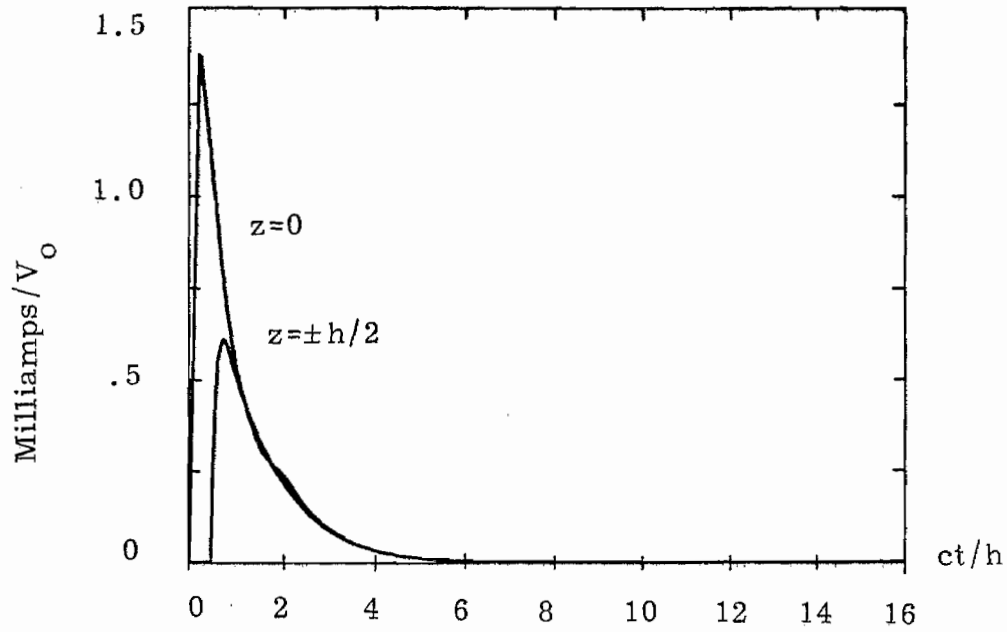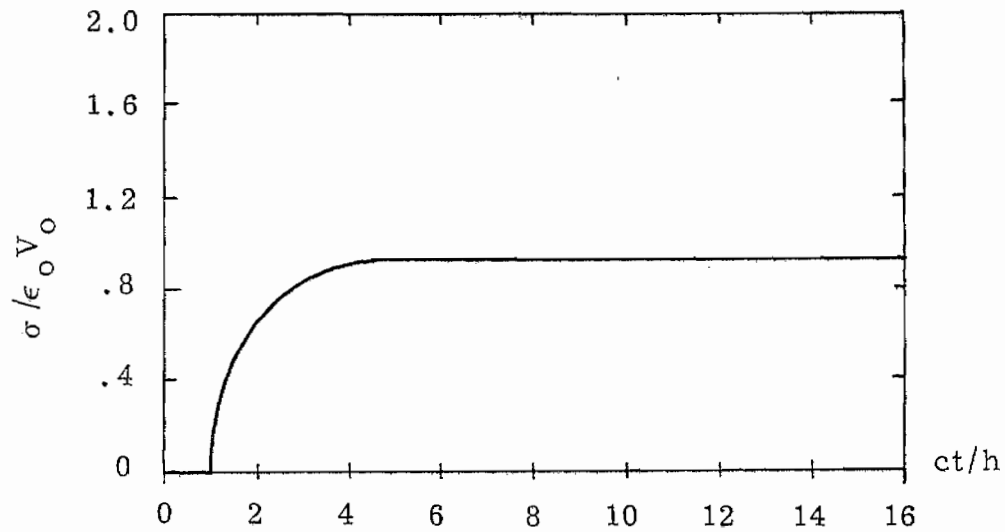
Figure 44. Time history plots of (a) the current at the
input of the antenna and at $z=\pm h/2$ and (b),
the linear charge density at $z=h$, for the
constant slope resistively loaded antenna,
with $C_2 = 9548\Omega$, $a/h = .01$ and using the
poles of Table III.
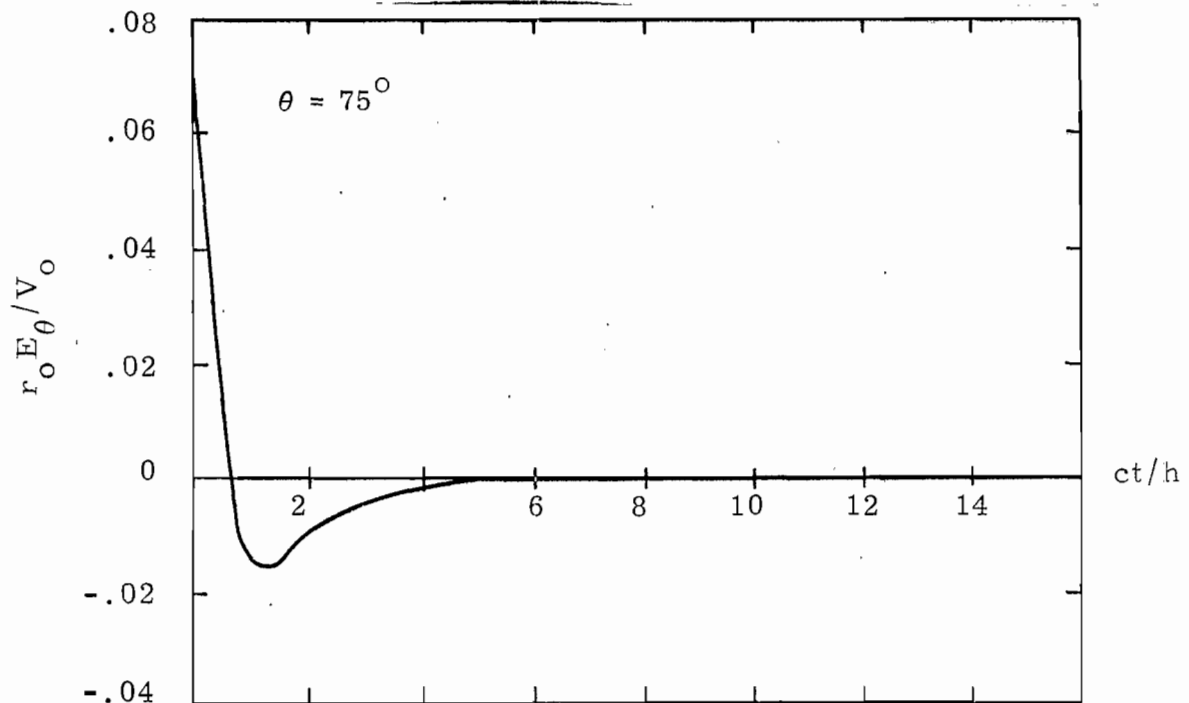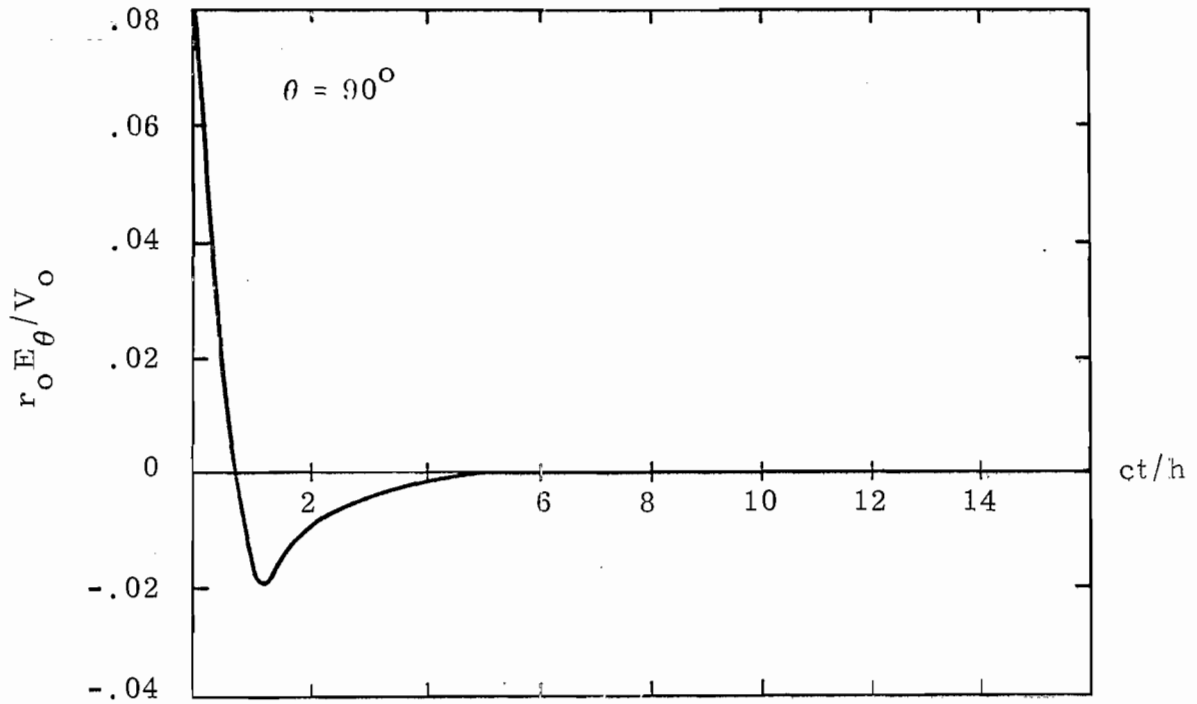
Figure 45. Time history plots of the radiated electric field from the constant slope resistively loaded antenna, with $C_2 = 9548\Omega$, $a/h = .01$ and using the poles of Table III.
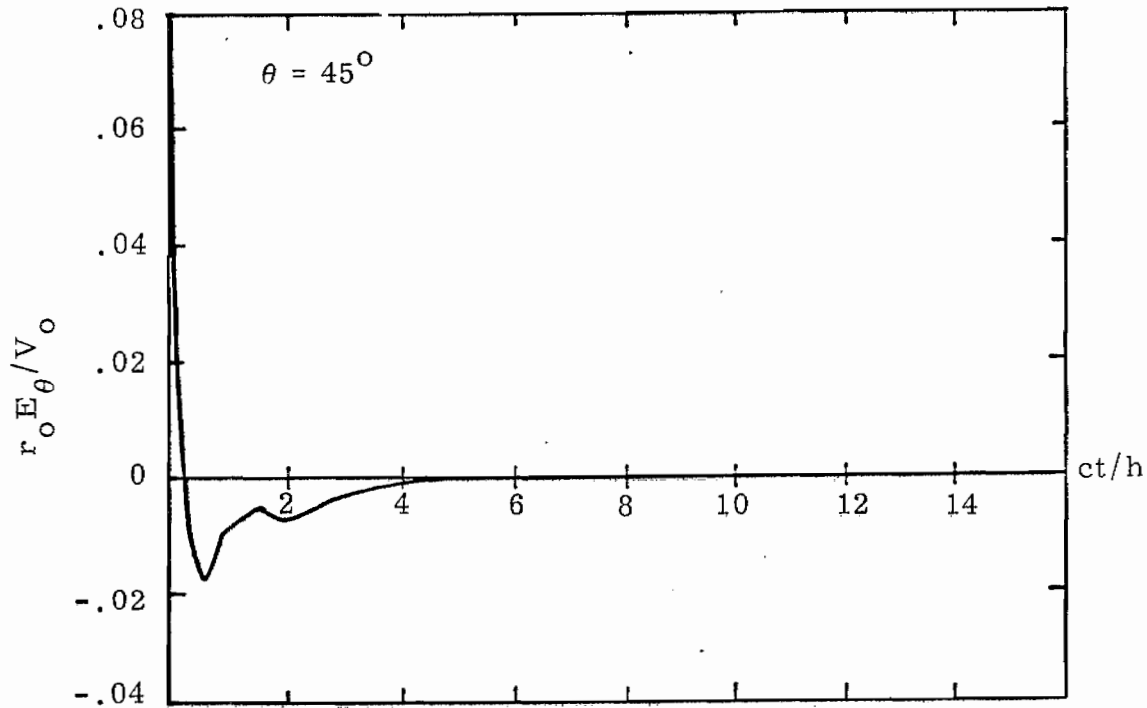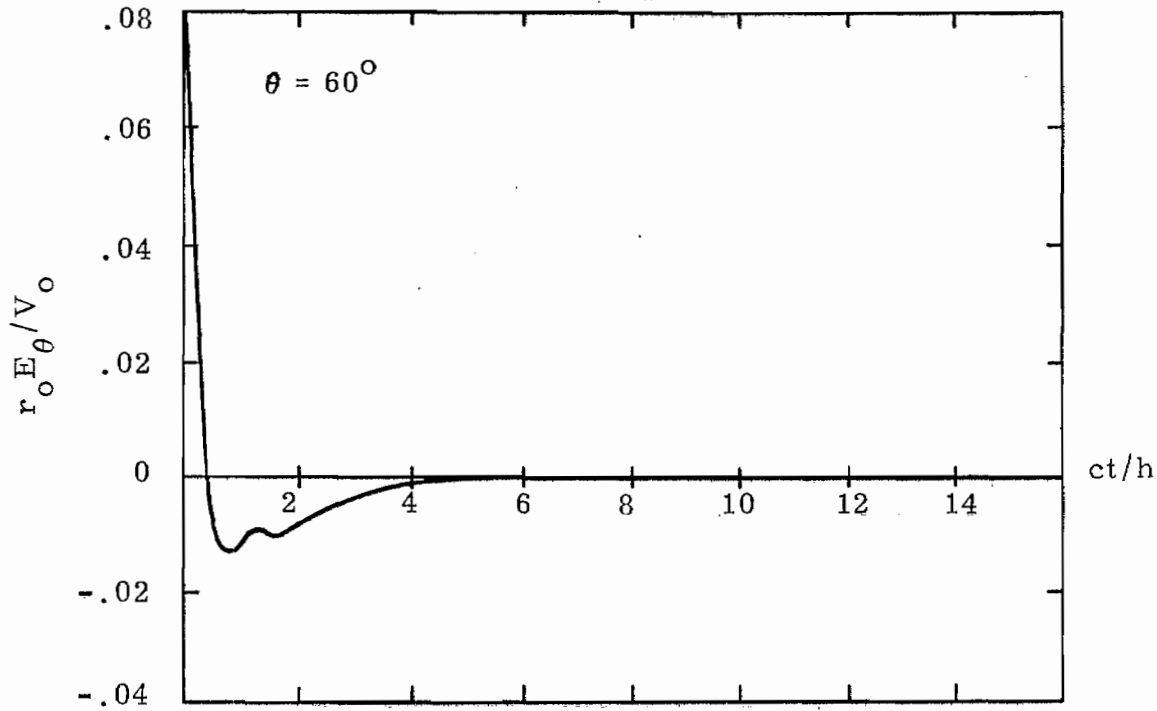
Figure 46. Time history plots of the radiated electric field from the constant slope resistively loaded antenna, with $C_2 = 9548\Omega$, $a/h = .01$ and using the poles of Table III.
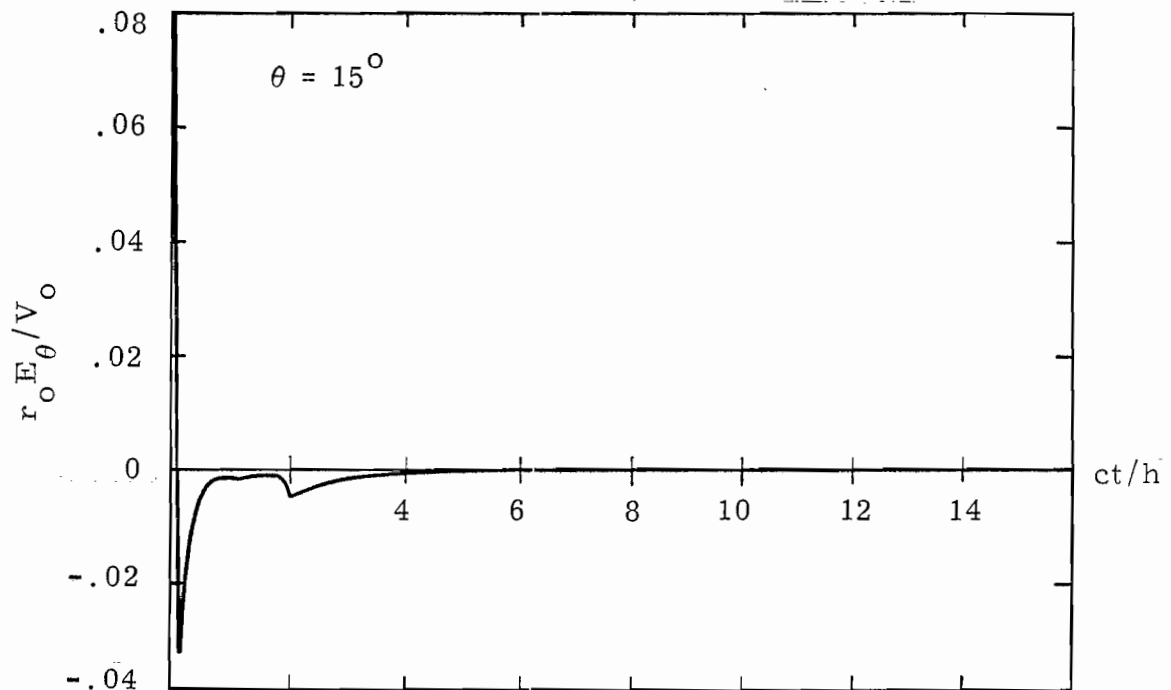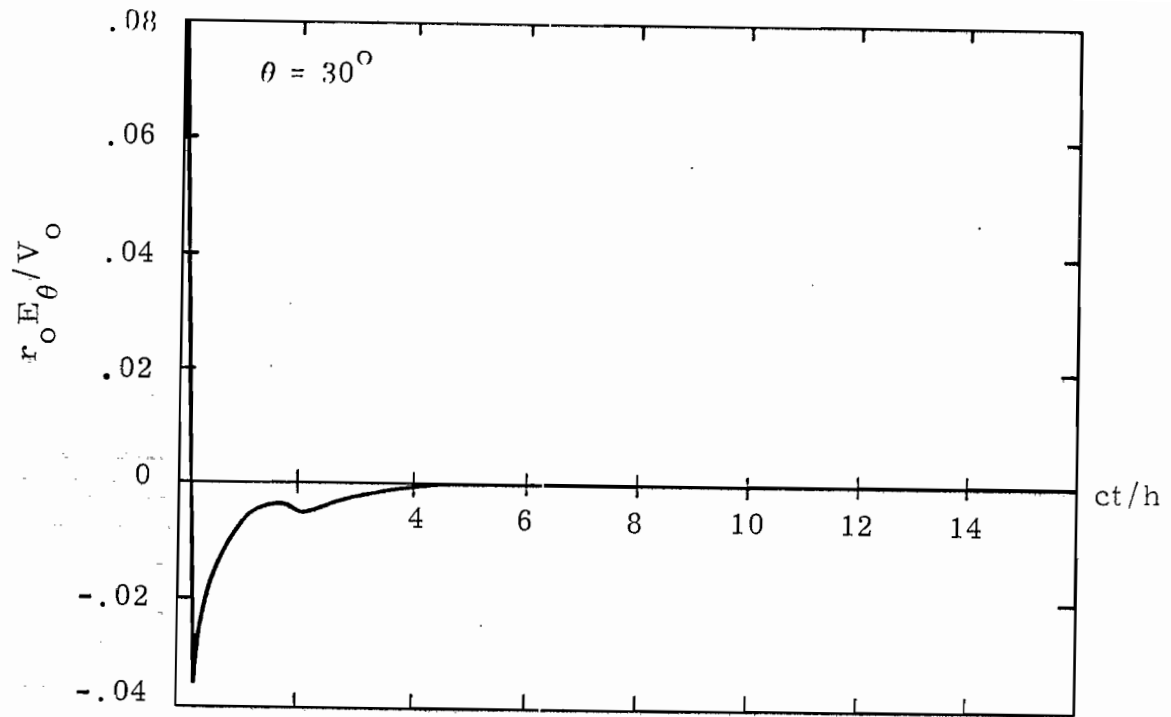
Figure 47. Time history plots of the radiated electric field from the constant slope resistively loaded antenna, with $C_2 = 9548\Omega$, $a/h = .01$ and using the poles of Table III.

VII. Numerical Results: The $(h - |z|)^{-1}$ Loaded Antenna

The final class of resistance loading to be treated in this note is described by the function $\Lambda(z) = C_3/(h - |z|)$. In this manner, the loading is infinite at $z = \pm h$ and has a value $\Lambda(0) = C_3/h$ at $z = 0$. This class of loading has been studied by King, Shen, and Wu.[18, 22] By using an approximate solution to Hallen's integral equation, it was found that the current consisted of only an outward propagating wave for the correct value of loading. Similarly, Liu and Sengupta[9, 10] have studied this problem using a numerical solution to the integral equation for the loaded structure.

As before, the data in this section is in the same form as in the previous sections. The pole trajectories as a function of C_3 are shown in Figure 48 while the plot of C_3 vs Ω for critical loading is in Figure 49. The natural current and field modes are given in Figures 50 through 55 and the time domain results are shown in Figures 56 through 59. Table III gives the other pertinent data for this case.

In comparing the results of Liu and Sengupta for this class of loading functions, it is seen that at $z = 0$, $C_3/h = r_o$ where r_o is their loading function, defined by Eq. (12) in their note. For the antenna of $h/a = 100.$, they considered values of $r_o = 240$, 480, and 720 ohms/meter, and showed the time domain radiated fields at various angles of observation. For the present problem, C_3/h has been chosen to be 445.9 ohms/meter and the results are very similar to those by Liu and Sengupta. The method employed here offers a precise way to define the critical value of loading.

As a final curve, Figure 60 shows the value of $\sigma_o L/C\pi$ for the three classes of loading considered here as a function of the parameter Ω. It is obvious that the $(h - |z|)^{-1}$ loading has the maximum damping for the thicker antennas.
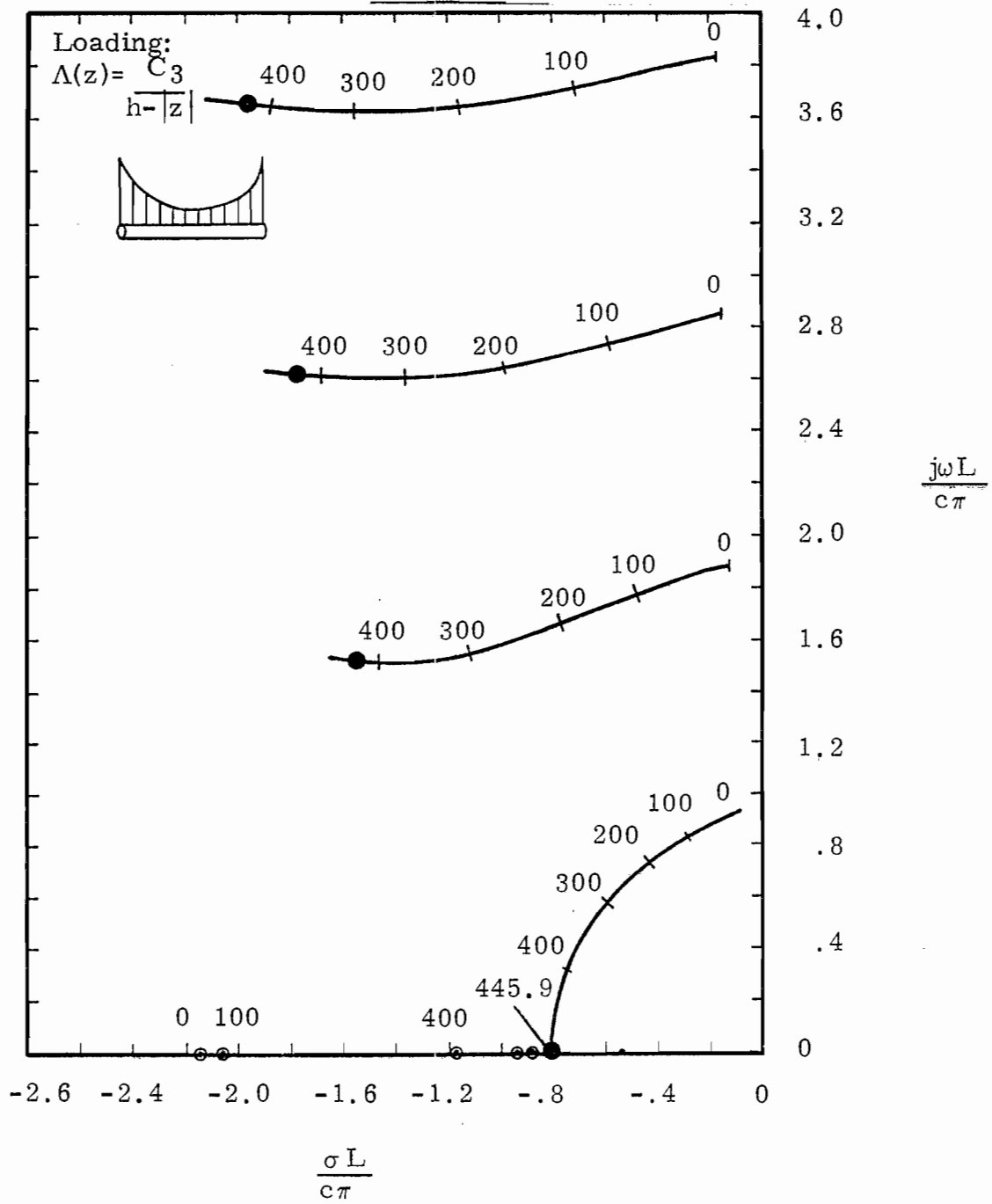
Figure 48. Pole trajectories for wire of a/h = .01 as a function of the constant C_3 (in kilohms).
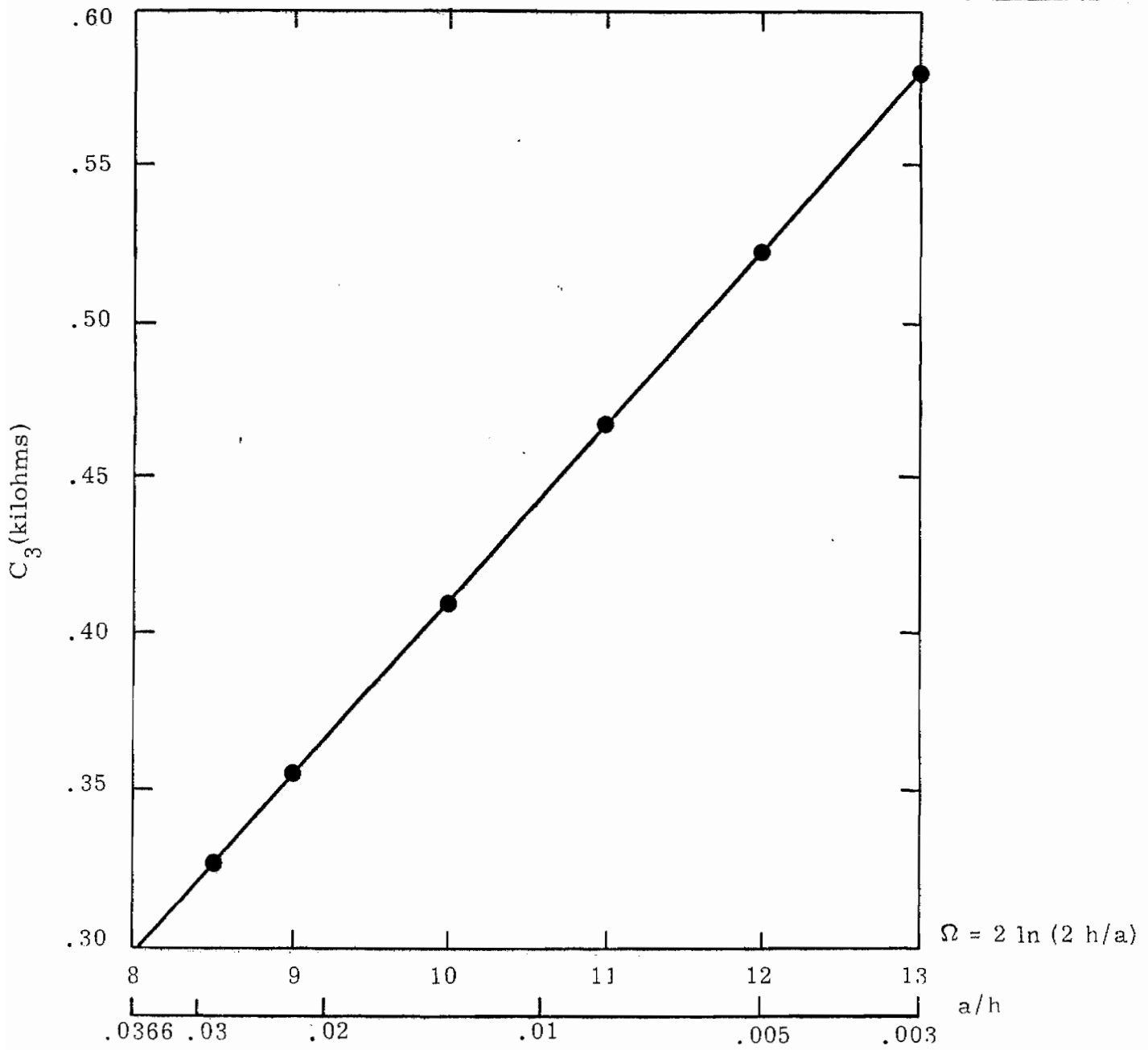
Figure 49. Plot of the constant C_3 for critical loading of the form $\Lambda(z) = C_3/h - |z|$.
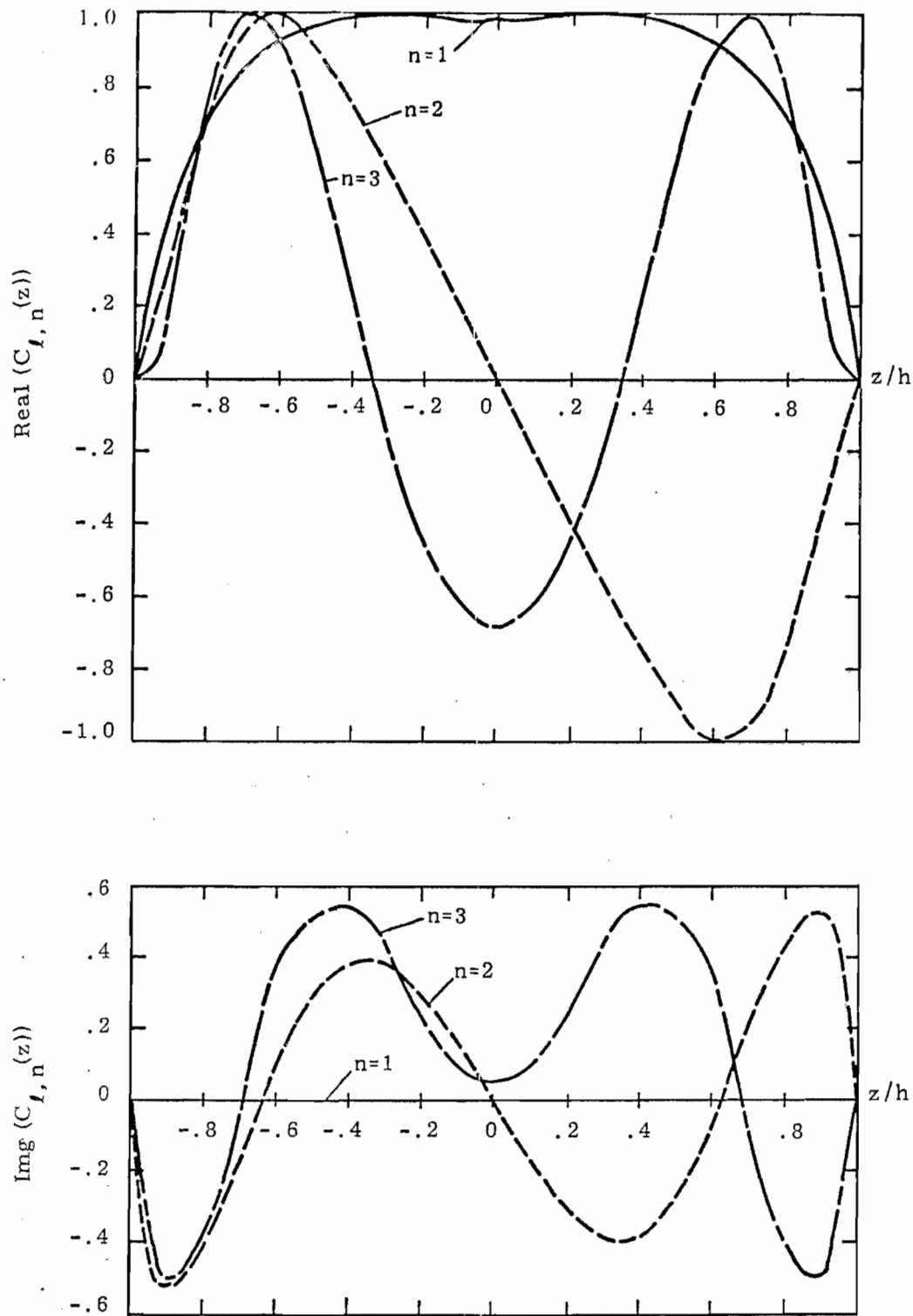
Figure 50. Real and imaginary parts of the natural current mode (and the coupling vector) for the $\ell=1$ layer poles of the critically damped antenna ($(h-|z|)^{-1}$ loading), with $C_3 = 445.9\,\Omega$ and $a/h = .01$.
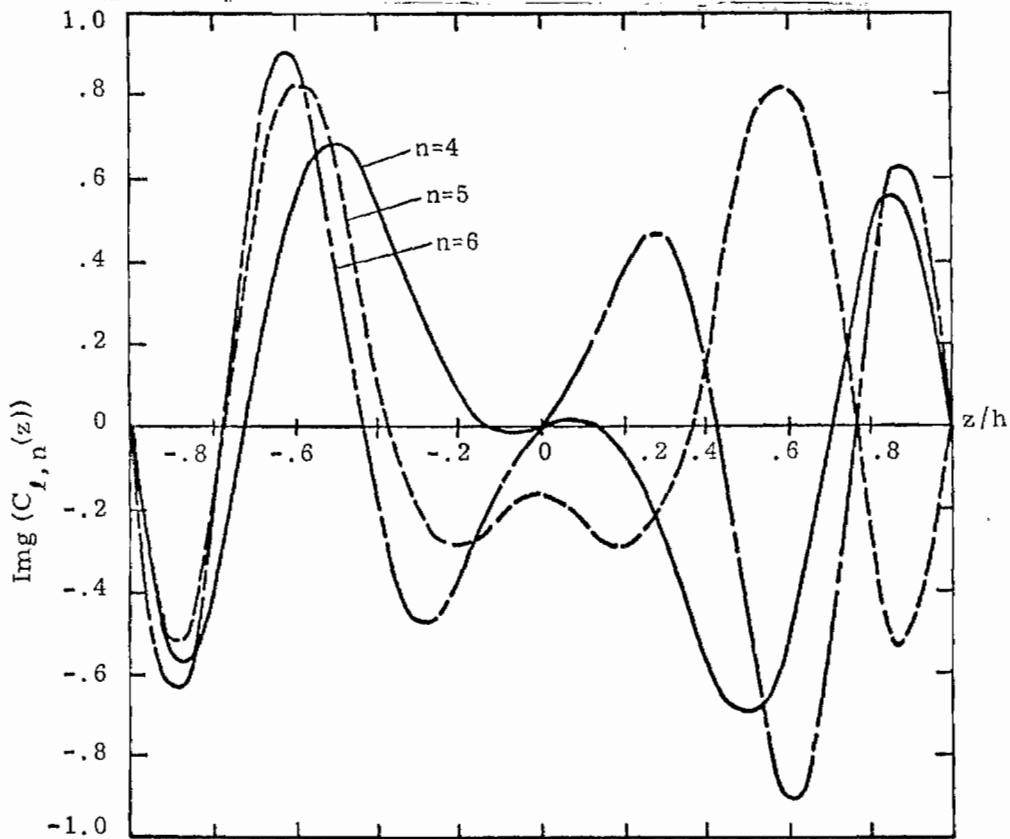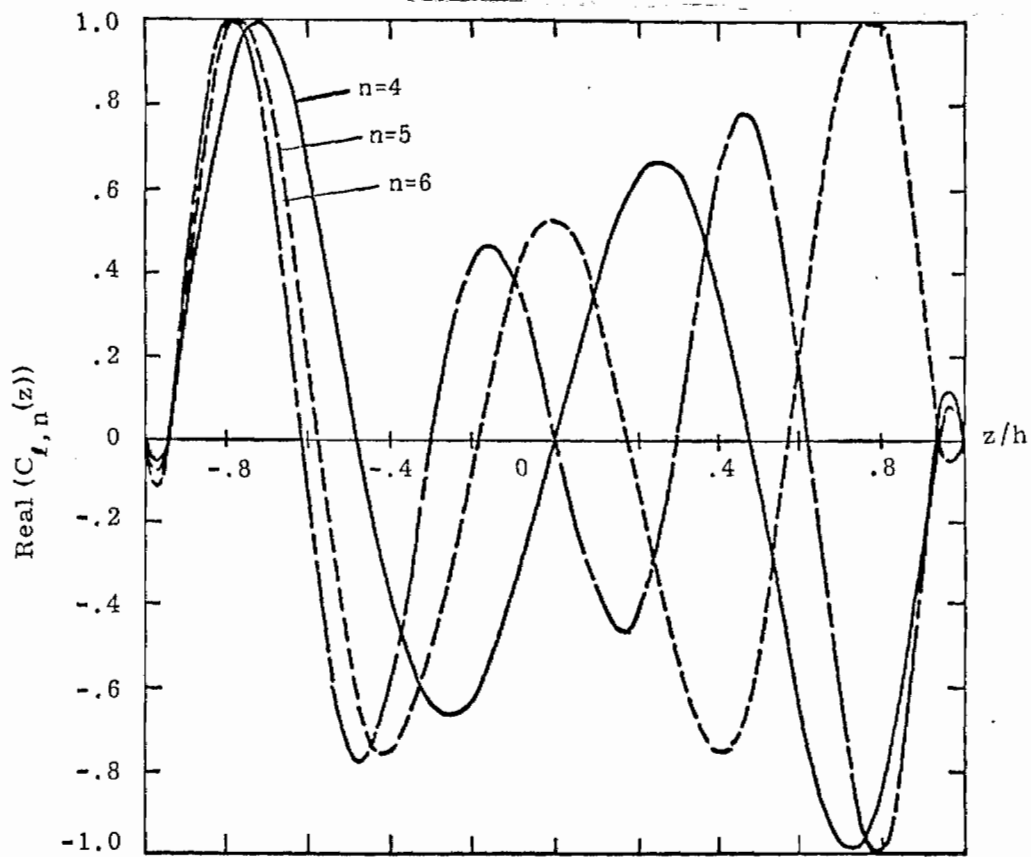
Figure 51. Real and imaginary parts of the natural current mode (and the coupling vector) for the $\ell = 1$ layer poles of the critically damped antenna ($(h-|z|)^{-1}$ loading), with $C_3 = 445.9\Omega$ and $a/h = .01$.
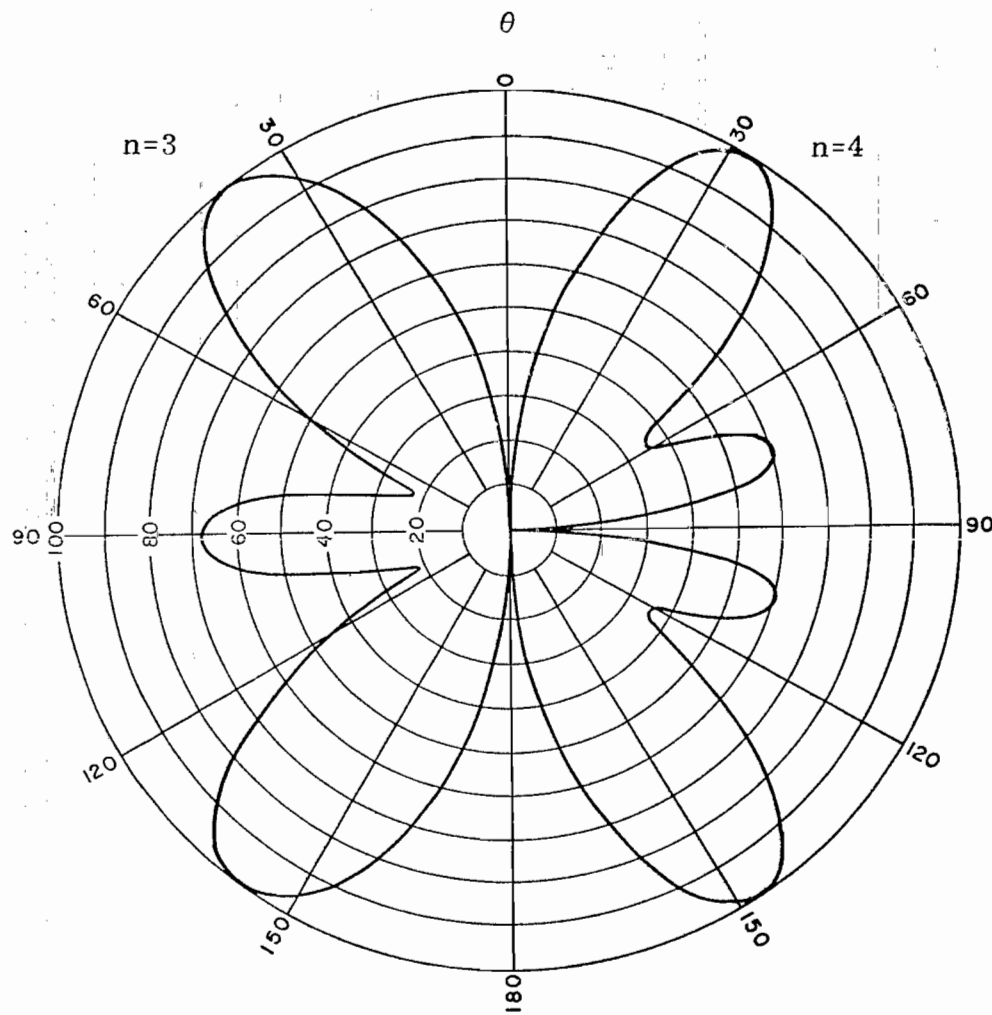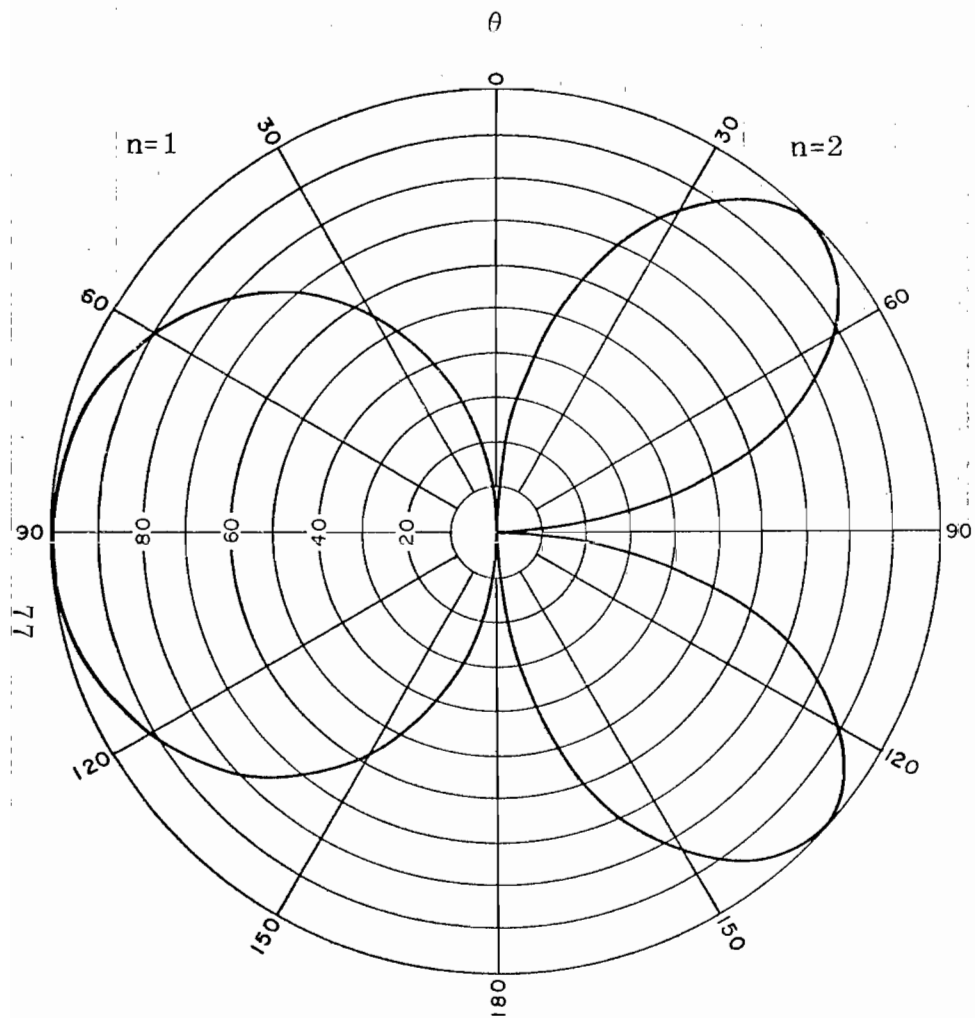
Figure 52. Polar plots of the magnitude of the normalized far field modes $e_{\ell, n}(\theta)$ for $\ell = 1$ poles of a $(h - |z|)^{-1}$ resistively loaded antenna.

θ

n=5   0   n=6
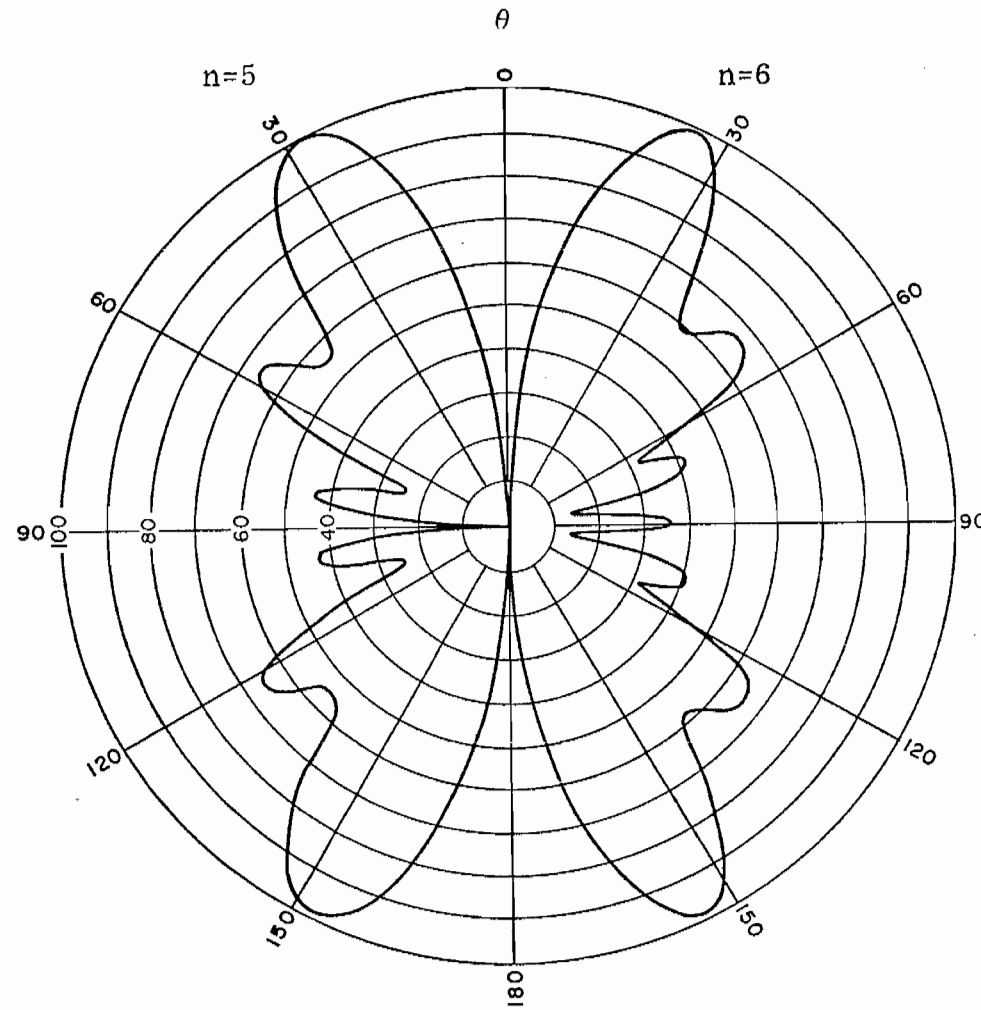
Figure 53.   Polar plots of the magnitude of the normalized far field modes $e_{\ell,n}(\theta)$ for $\ell=1$ poles of a $(h-|z|)^{-1}$ resistively loaded antenna.
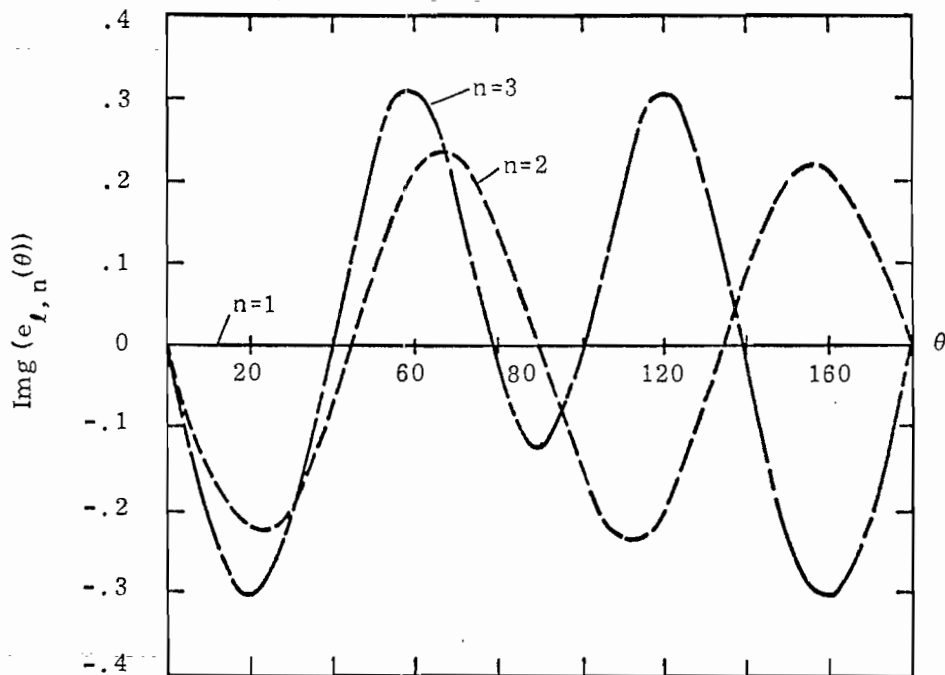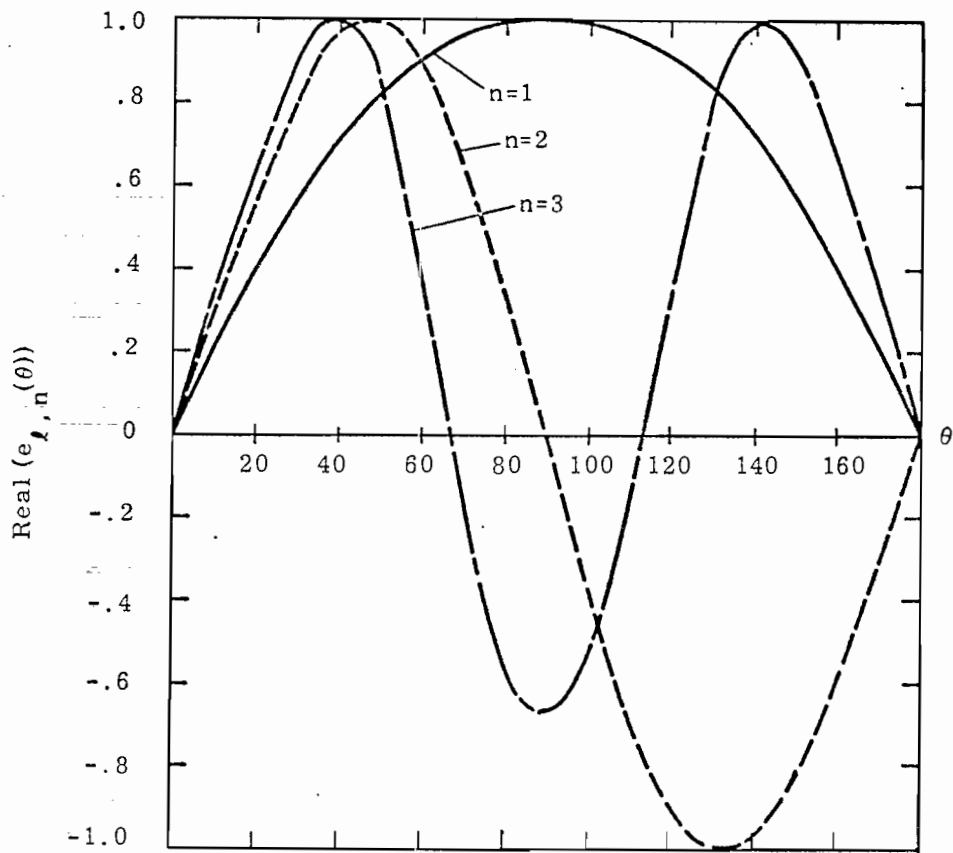
Figure 54. Real and imaginary parts of the normalized far
field mode for the $\ell = 1$ layer poles of a critically
loaded antenna $((h-|z|)^{-1}$ loading), with
$C_3 = 445.9\,\Omega$, and $a/h = .01$.
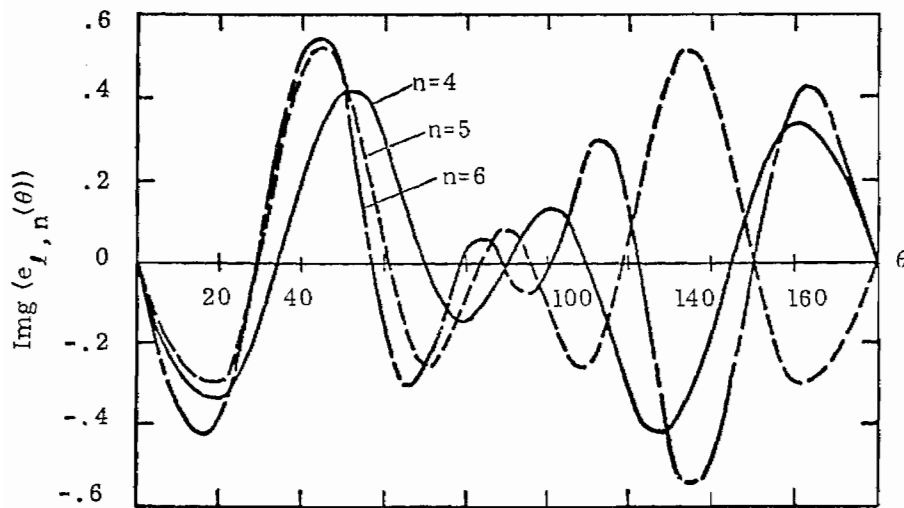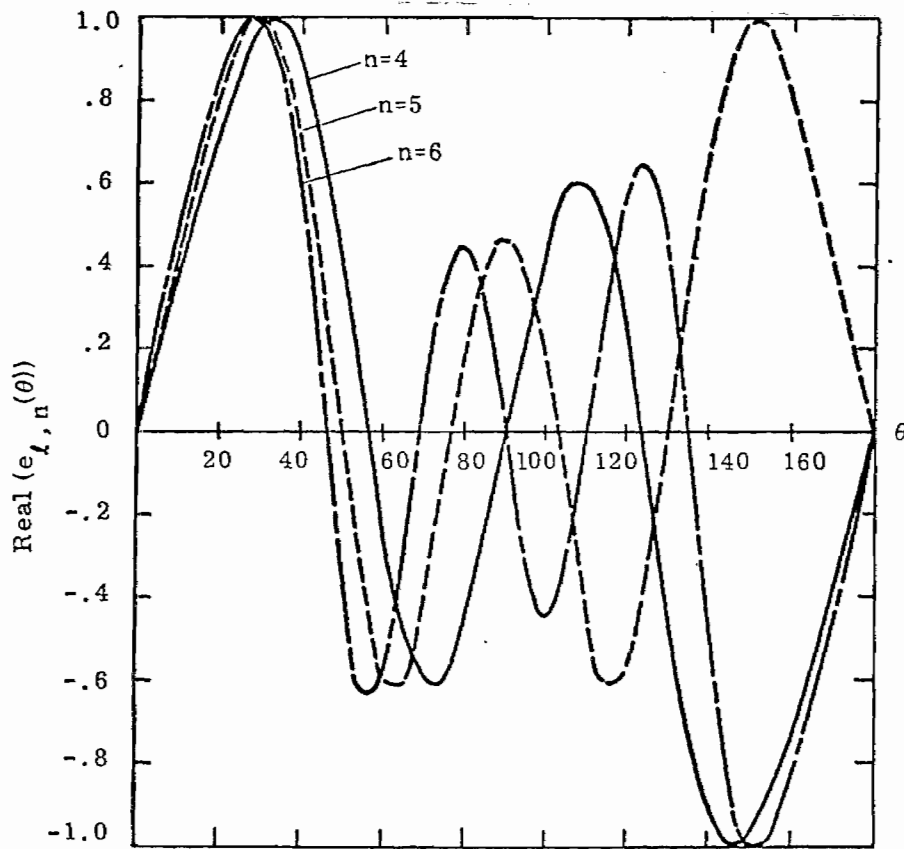
Figure 55. Real and imaginary parts of the normalized far
field mode for the $l=1$ layer poles of a critically
loaded antenna $((h-|z|)^{-1}$ loading), with
$C_3 = 445.9\Omega$, and $a/h = .01$.

TABLE IV

Data for Critically Damped, $(h-|z|)^{-1}$ Loaded Antenna of $a/h = .01$ ($\Omega = 10.59$)

Loading Function is $\Omega(z) = C_3/(h-|z|)$; $C_3 = 445.9\Omega$

Pole α		Natural Frequency $s_\alpha L/c\pi$*		Current Normalization (x 10^3)		Field Normalization		Coupling Coeff. (x10^1) Step Excitation **		Decay Time $c\tau_\alpha/h$
l	n	$\sigma L/c\pi$	$j\omega L/c\pi$	$\mathrm{Re}(\beta_\alpha)$	$\mathrm{Im}(\beta_\alpha)$	$\mathrm{Re}(\beta_\alpha^{(F)})$	$\mathrm{Im}(\beta_\alpha^{(F)})$	$\mathrm{Re}(\eta)$	$\mathrm{Im}(\eta)$	
1	1	- .831	.030	.555	42.392	23.874	-.256	-3.795	-.147	.766
1	2	-1.563	1.533	3.845	1.553	3.247	-14.620	0	0	.407
1	3	-1.777	2.607	4.636	2.954	-9.777	-3.364	.426	.517	.358
1	4	-1.956	3.643	3.846	5.293	-2.127	8.190	0	0	.325
1	5	-2.097	4.662	5.019	5.764	6.859	2.200	- .228	-.223	.311
1	6	-2.219	5.676	11.851	8.547	1.448	-6.088	0	0	.287
1	7	-2.321	6.686	-3.461	.932	-5.534	- .983	.175	.039	.274

*L = 2h = Total Antenna Length

**Coupling Coefficient is for a Center Driven Antenna with Gap $\Delta = .1L$.
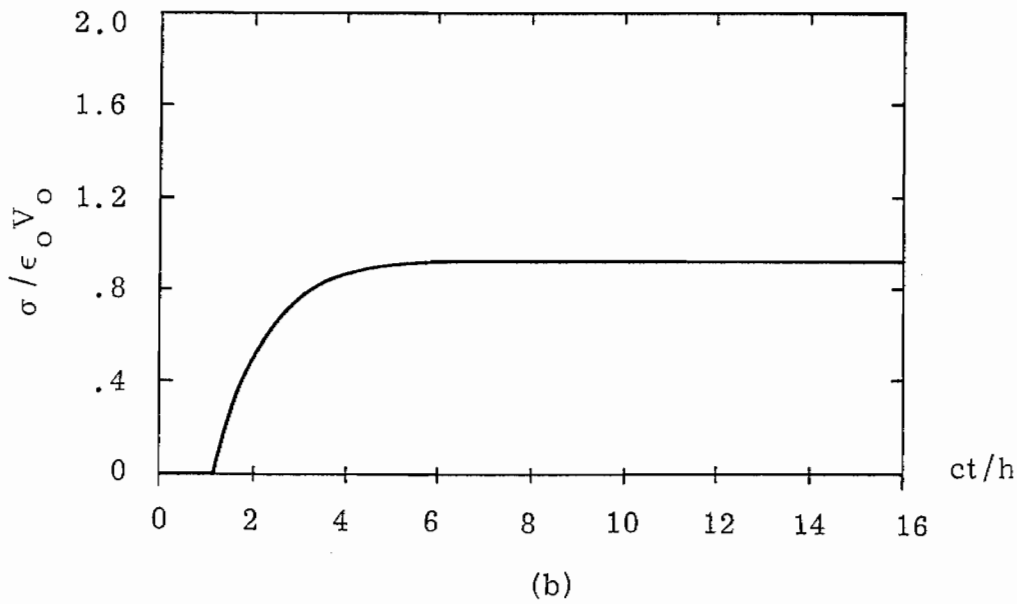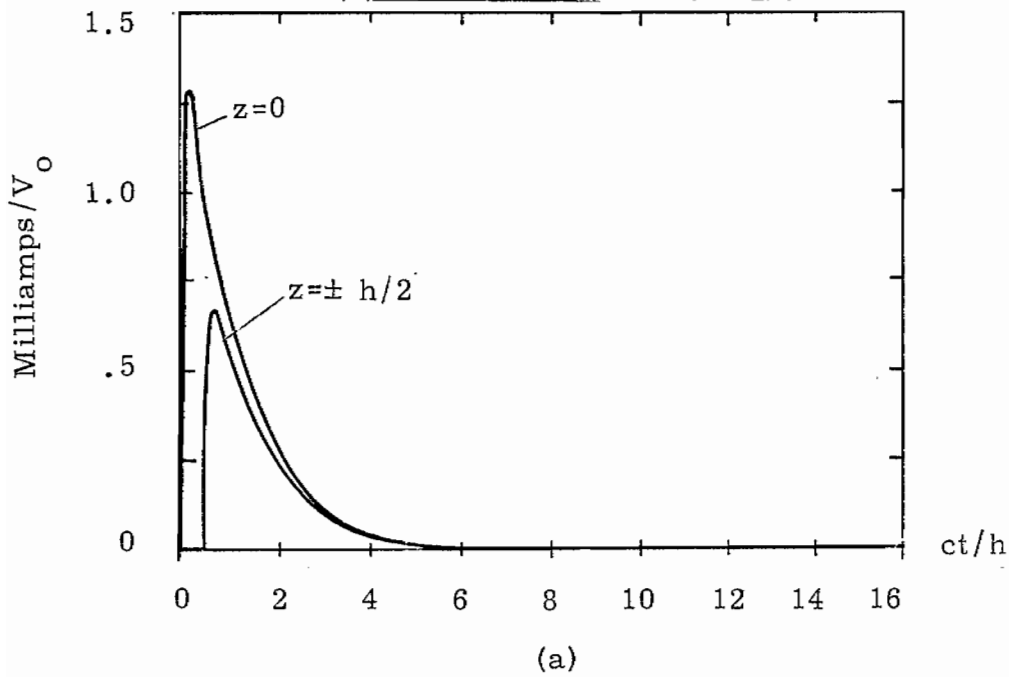
Figure 56. Time history plots of (a) the current at the
input of the antenna and at $z = \pm h/2$ and (b),
the linear charge density at $z=h$ for the $(h-|z|)^{-1}$
resistively loaded antenna, with $C_3 = 445.9\Omega$,
$a/h = .01$ and using the poles in Table IV.
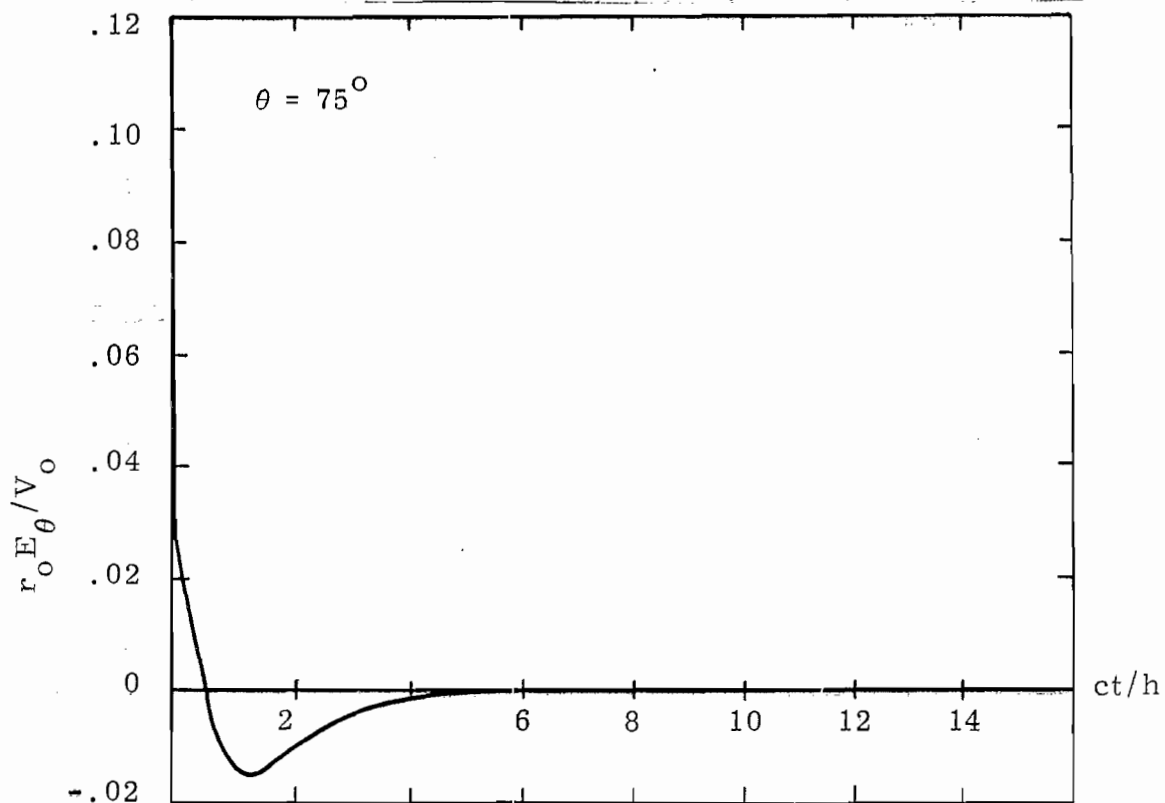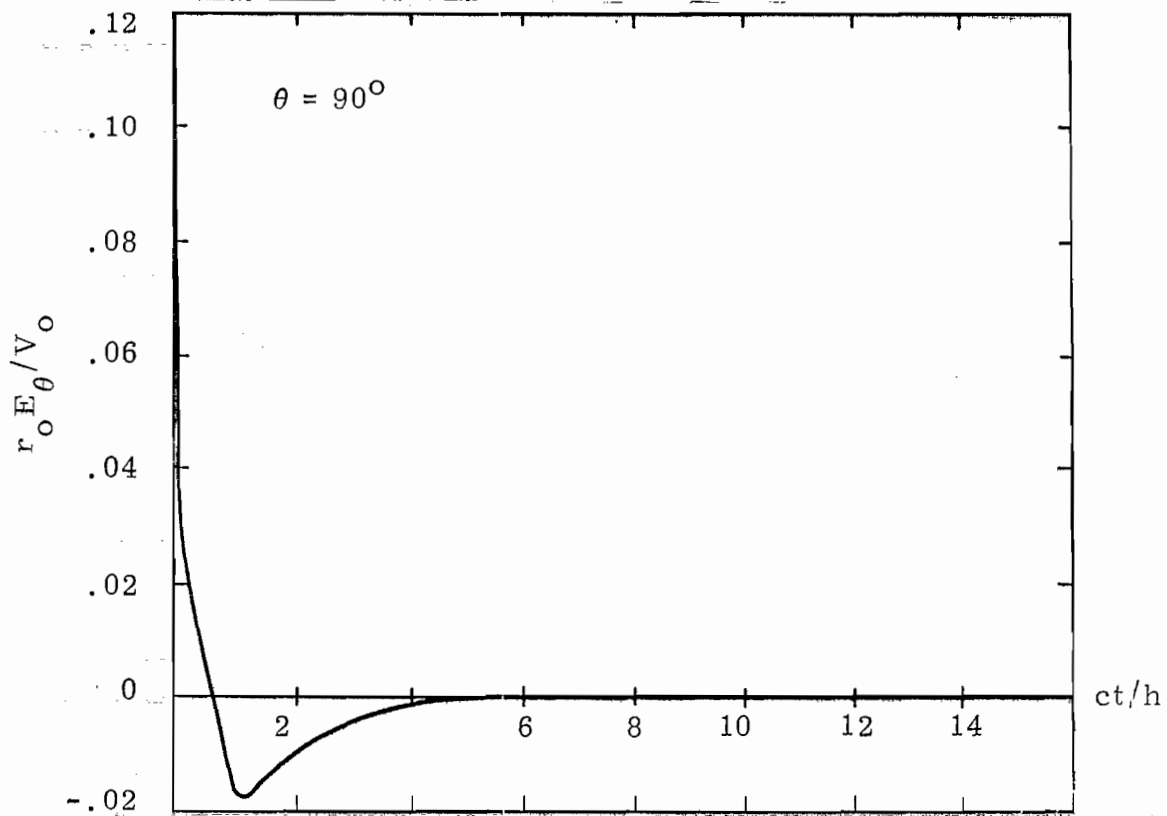
Figure 57. Time history plots of the radiated electric field from the $(h-|z|)^{-1}$ resistively loaded antenna, with $C_3 = 445.9\Omega$, $a/h = .01$ and using the poles of Table IV.
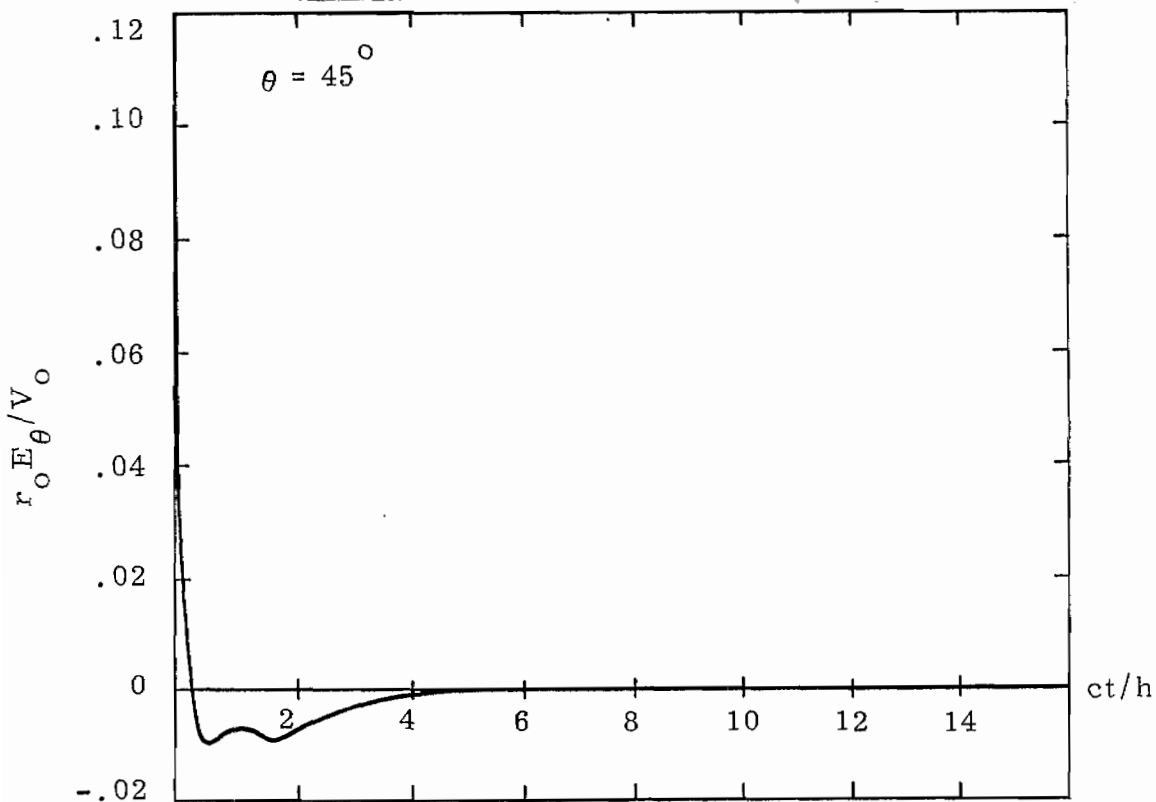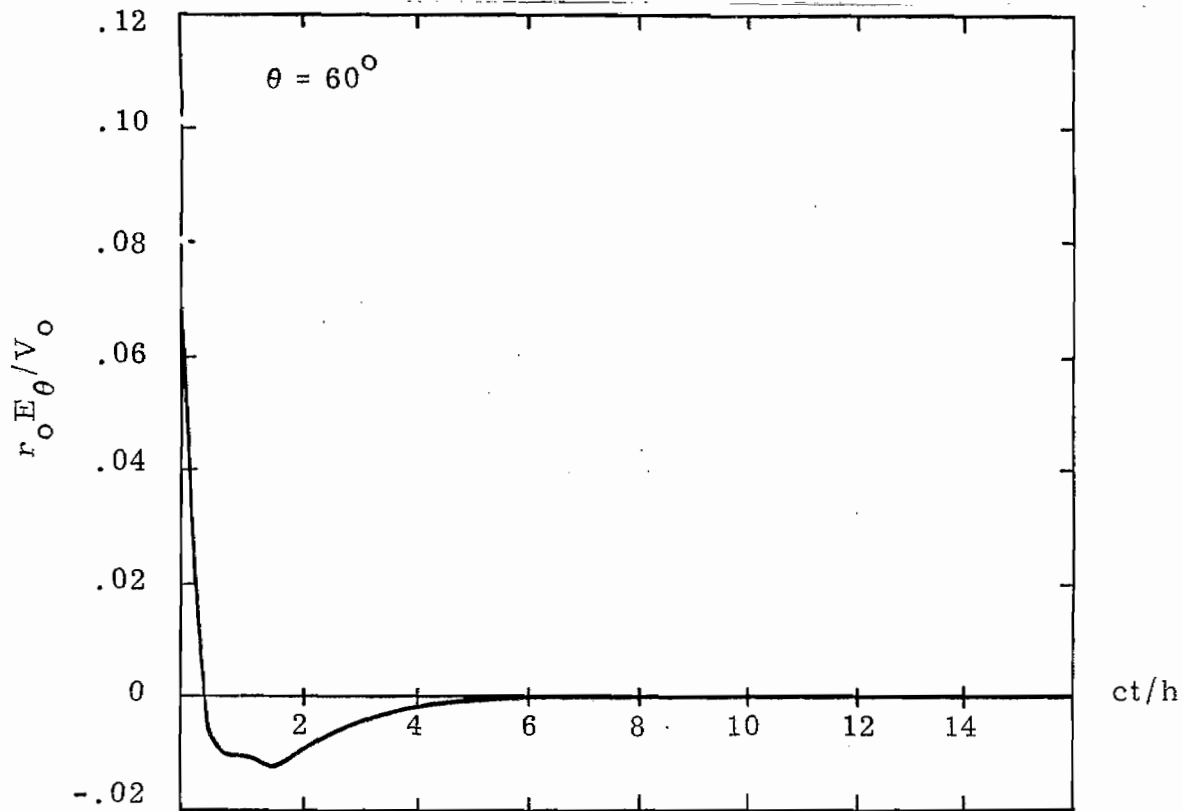
Figure 58. Time history plots of the radiated electric field from the $(h-|z|)^{-1}$ resistively loaded antenna, with $C_3 = 445.9\Omega$, $a/h = .01$ and using the poles of Table IV.

84
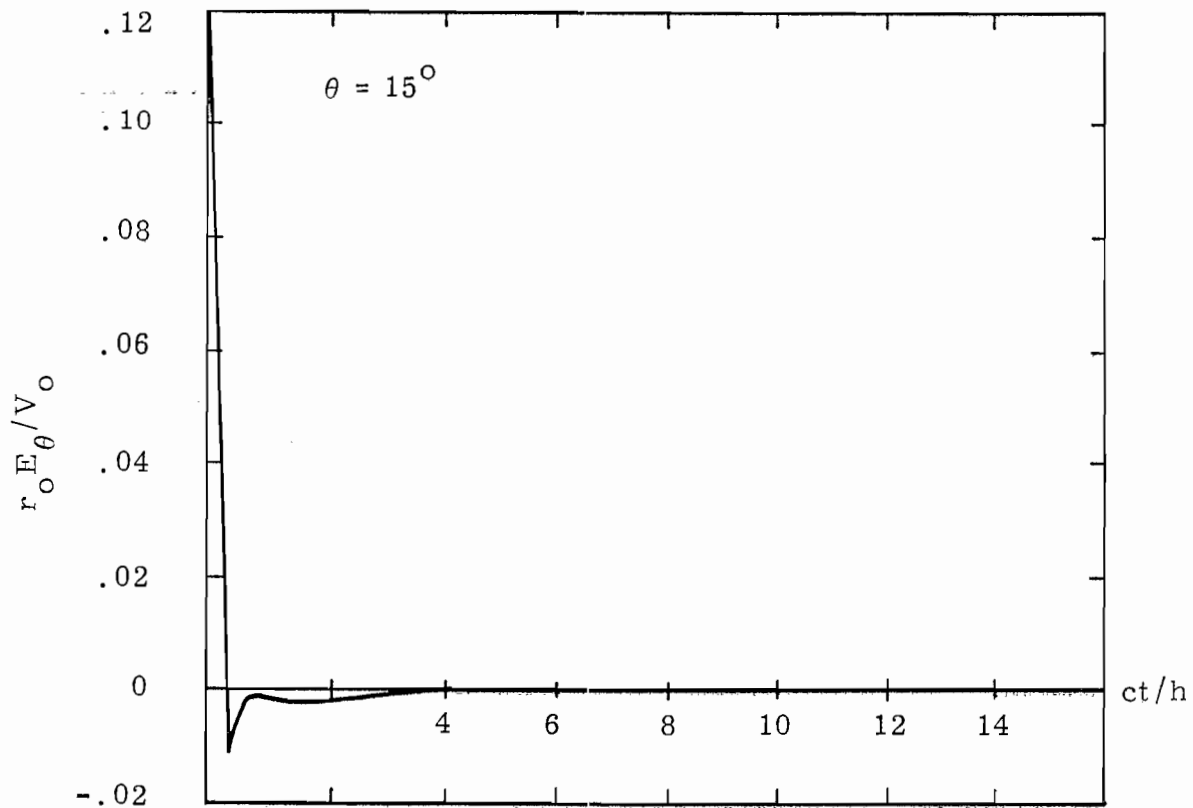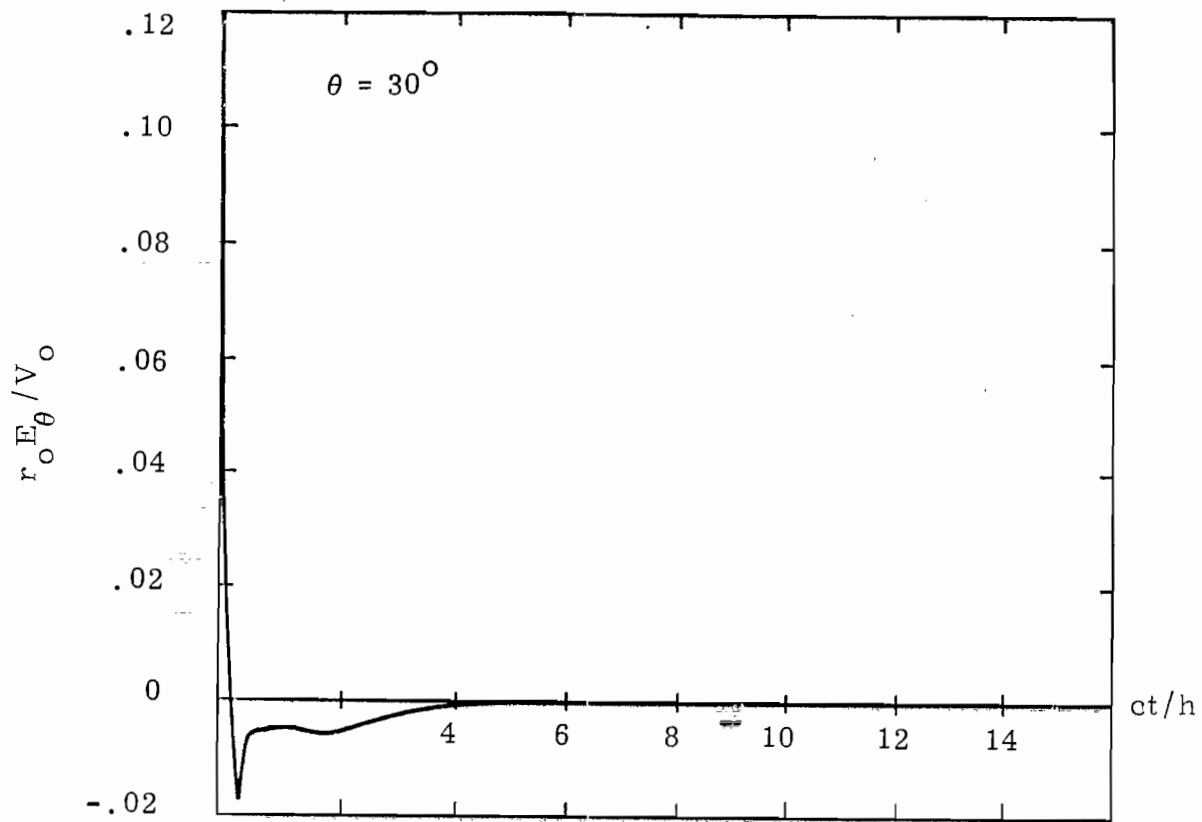
Figure 59. Time history plots of the radiated electric field from the $(h-|z|)^{-1}$ resistively loaded antenna, with $C_3 = 445.9\,\Omega$, $a/h = .01$ and using the poles of Table IV.
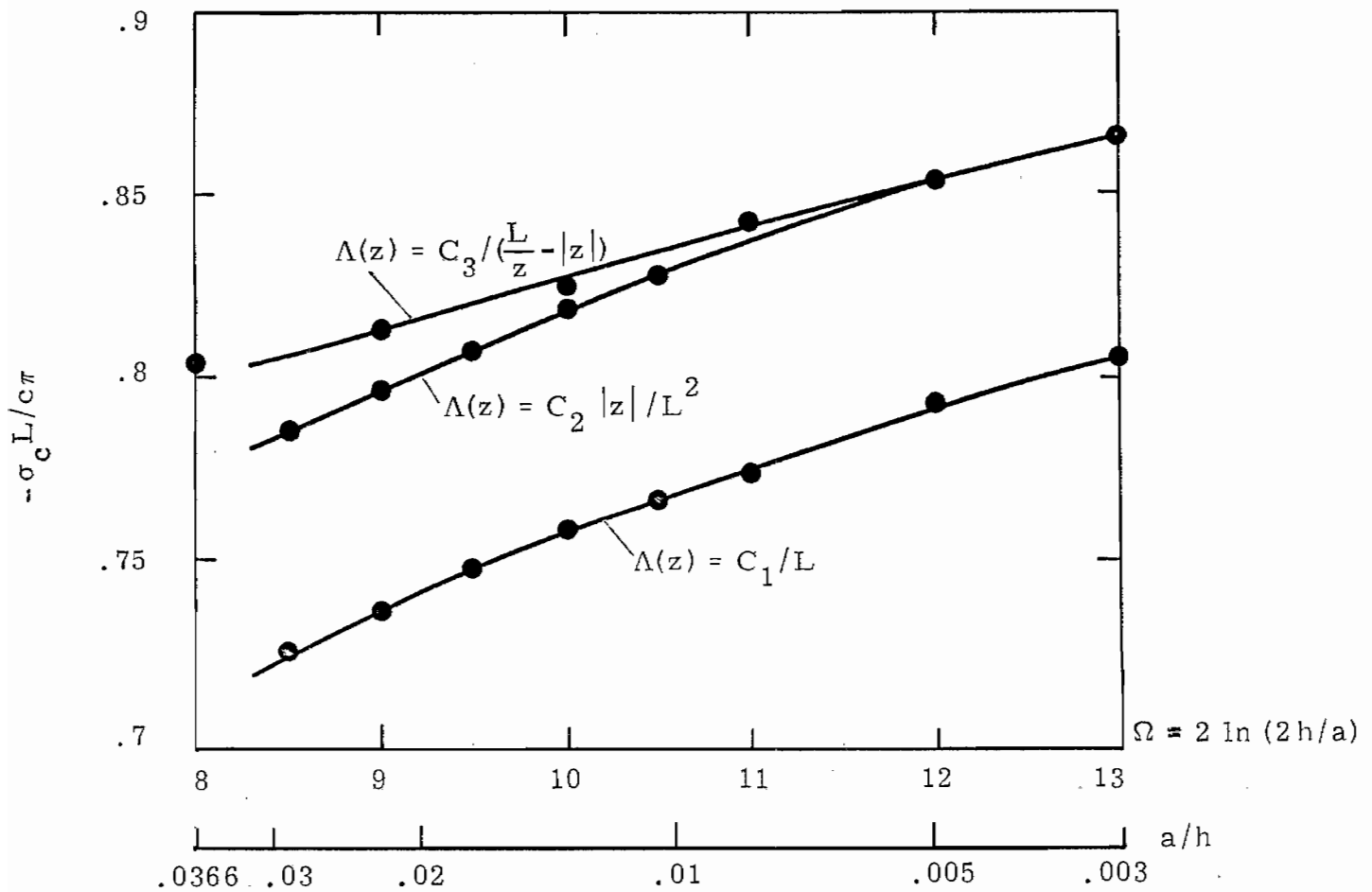
Figure 60. Plot of the damping constant σ_c for the first pole of the critically damped linear antenna as a function of Ω.

VIII. Conclusion

The analysis of a radiating antenna by using SEM has been considered in this note, with emphasis of the application to a linear EMP simulator. The extension of SEM to include impedance loaded structures was outlined, and the concept of a far-field natural mode was presented.

As an example, the center fed, linear antenna was treated in detail for three specific types of resistance loading, as well as the unloaded case. Pole locations, mode functions (current and far field) and normalizing coefficients were presented, as well as some time history curves for the input current, end charge density and radiated fields.

As is apparent from the curves, the loading function of the form $\Lambda(z) = C_3/(h - |z|)$ is such that the reflections of current at the ends of the antenna are not visible at the input of the antenna. This loading is a suitable choice for use in an EMP simulator of this type.

IX. References

1. Baum, C. E., "Resistively Loaded Radiating Dipole Based on a Transmission Line Model for the Antenna," Sensor and Simulation Notes, Note 81, April 1969.

2. Baum, C. E., "On the Singularity Expansion Method for the Solution of Electromagnetic Interaction Problems," Interaction Notes, Note 88, December 1971.

3. Baum, C. E., "On the Singularity Expansion Method for the Case of First Order Poles," Interaction Notes, Note 129, October 1972.

4. Latham, R. M., and K. S. H. Lee, "Pulse Radiation and Synthesis by an Infinite Cylindrical Antenna," Sensor and Simulation Notes, Note 73, 1969.

5. Latham, R. M., and K. S. H. Lee, "Radiation of an Infinite Cylindrical Antenna with Uniform Resistive Loading," Sensor and Simulation Notes, Note 83, 1970.

6. Latham, R. M., and K. S. H. Lee, "Transient Properties of an Infinite Cylindrical Antenna," Radio Science, Vol. 5, No. 4, pp. 715-723, 1970.

7. Lee. S. W., and B. Leung, "The Natural Resonance Frequency of a Thin Cylinder and its Application to EMP Studies," Interaction Notes, Note 96, February 1972.

8. Liu, Y. K., "Time Domain Analysis of Linear Antennas and Scattering," Ph. D. Dissertation, University of California at Berkeley, June 1972.

9. Liu, Y-P., and D. L. Sengupta, "Transient Waveforms Radiated by a Resistively Loaded Linear Antenna," presented at the 1972 Fall FULMEN Meeting, University of Michigan.

10. Liu, Y-P., D. L. Sengupta, and C-T. Tai, "On the Transient Waveforms Radiated by a Resistively Loaded Linear Antenna," Sensor and Simulation Notes, 1973.

11. Marin, Lennart, and R. W. Latham, "Analytical Properties of the Field Scattered by a Perfectly Conducting, Finite Body," Interaction Notes, Note 92, January 1972.

12. Marin, Lennart, "Application of the Singularity Expansion Method to Scattering from Imperfectly Conducting Bodies and Perfectly Conducting Bodies within a Parallel Plate Region," Interaction Notes, Note 116, June 1972.

13. Marin, Lennart, "Natural-Mode Representation of Transient Scattering From Rotationally Symmetric, Perfectly Conducting Bodies and Numerical Results for a Prolate Spheroid," Interaction Notes, Note 119, August 1972.

14. Martinez, Joe P., Zoe Lynda Pine, and F. M. Tesche, "Numerical Results of the Singularity Expansion Method as Applied to a Plane Wave Incident on a Perfectly Conducting Sphere," Interaction Notes, Note 112, May 1972.

15. Merewether, David E., "Transient Pulse Transmission Using Impedance Loaded Cylindrical Antennas," Sensor and Simulation Notes, Note 70, February 1968.

16. Merewether, D. E., "Transient Electromagnetic Fileds Near a Cylindrical Antenna Multiply-Loaded with Lumped Resistors," Sensor and Simulation Notes, Note 71, August 1968.

17. Miller, E. K., "Some Computational Aspects of Transient Electromagnetics," Lawrence Livermore Laboratory Report, UCRL-51276, 1972. (Also personal communication.)

18. Shen, L. C., and R. W. P. King, "The Cylindrical Antenna with Nonreflecting Resistive Loading," IEEE Trans. on Antennas and Propagation, AP-13, November 1965, p. 998.

19. Tesche, F. M., "On the Singularity Expansion Method as Applied to Electromagnetic Scattering from Thin Wires," Interaction Notes, Note 102, April 1972.

20. Tesche, F. M., and Zoe Lynda Pine, "Pulse Radiation by an Infinite Cylindrical Antenna with a Source Gap with a Uniform Field," Sensor and Simulation Notes, Note 159, October 1972.

21. Wright, D. L., and J. F. Prewitt, "Transmission Line Model of Radiating Dipole," presented at the 1972 Fall FULMEN Meeting, University of Michigan, November 1972. (Also subject of forthcoming Sensor and Simulation Note.)

22. Wu, T. T., and R. W. P. King, "The Cylindrical Antenna with Nonreflecting Resistive Loading," IEEE Trans. on Antennas and Propagation, AP-13, May 1965, pp. 369-373.